2023-05-01

Field Observations And Stable Isotope Analysis Of Alunite At The Sulphur Bank Mercury Mine, Clear Lake, California

David Edward Muller
University of Texas at El Paso

FIELD OBSERVATIONS AND STABLE ISOTOPE ANALYSIS OF ALUNITE AT THE SULPHUR BANK MERCURY MINE, CLEAR LAKE, CALIFORNIA

DAVID E. MULLER

Master's Program in Geological Sciences

APPROVED:

Antonio Arribas, Ph.D., Chair

Mark Engle, Ph.D.

Jason Ricketts, Ph.D.

Charles N. Alpers, Ph.D.

Stephen L. Crites, Jr., Ph.D.
Dean of the Graduate School

Dedication

I dedicate this thesis to Dr. Kurt Friehauf, and my other professors/mentors from Kutztown University who welcomed me into university and later encouraged me to pursue a graduate degree in Geology. Kurt goes far out of his way to inspire myself and many other students to seek deeper knowledge in geology and it is partly due to his enthusiasm and insistence that I apply to graduate schools that I am currently submitting a Master's thesis. Kurt Friehauf, Sarah Tindall, Laura Sherrod, and several other professors from the science department at Kutztown University created a truly unique environment that not only provided a comprehensive foundation in geological understanding, but also a community that greatly helped me on a personal level. I hope that they know how much myself and others appreciate their efforts.

FIELD OBSERVATIONS AND STABLE ISOTOPE ANALYSIS OF ALUNITE AT THE SULPHUR BANK MERCURY MINE, CLEAR LAKE, CALIFORNIA

by

DAVID E. MULLER

THESIS

Presented to the Faculty of the Graduate School of

The University of Texas at El Paso

in Partial Fulfillment

of the Requirements

for the Degree of

MASTER OF SCIENCE

Department of Earth, Environmental and Resource Sciences

THE UNIVERSITY OF TEXAS AT EL PASO

May 2023

Acknowledgements

I would like to acknowledge Dr. Charlie Alpers, Dr. Craig Johnson, and Dr. Antonio Arribas for their advice, time, and help in collecting and interpreting my data and patiently offering advice at every step of my thesis. I could not have asked for better mentors and collaborators. A special thank you to Imura Takumi for helping with the operation of the SEM and to Bill Benzel, Heather Lowers, and other scientists at the USGS federal center who offered additional tests and assistance with data collection and interpretation.

I am grateful for the Lew Teal Economic Geology Fund, the George B. McBride Graduate Fellows Endowment, the Kenneth F. and Patricia Clark Distinguished Chair Endowment, and the Michael J. Fitzgerald Fund for financially supporting my research and/or graduate training. Lastly, I would like to thank my colleagues and office mates Claudio, Hannah, Jose, and John for help and support.

Abstract

The Sulphur Bank mercury mine is a historic mine located in Lake County, California, first exploited in the 1860s. Underground mining of mercury took place from 1873 to 1906 and open-pit mining of mercury was done from 1927 to 1957. The U.S. Environmental Protection Agency listed the Sulphur Bank mine and the adjacent Clear Lake as a Superfund site in 1990 due to mercury contamination at the mine site and in the sediment and food web of Clear Lake. Previous studies have described the vein material mineralogy and wall-rock alteration at Sulphur Bank as well as the composition of water in the flooded mine pit (Herman Impoundment). This study expands on those studies by investigating the stable isotopes of alunite, kaolinite, cinnabar, amorphous silica, and native sulfur. It is hypothesized that stable isotope measurements, previous field observations, and new observations are consistent with the shallow steam-heated zone of an active geothermal system capable of precipitating precious metals within a low-sulfidation epithermal ore forming system. The research objectives of this study are: i) to better understand the steam-heated environment at Sulphur Bank by studying the stable isotope systematics of alteration minerals, and ii) to assess the gold-silver mineralization potential of the Sulphur Bank geothermal system by comparison with epithermal deposits in the Geysers-Clear Lake area of northern California.

For this study, a series of vein and wall-rock samples from the Sulphur Bank deposit were analyzed using powder X-ray diffractometry to determine mineralogy. These samples were separated into mineralogically pure concentrates for stable isotope analysis via mass spectrometry. Stable isotope analyses have yielded $\delta^{34}S$ values showing small differences between sulfate minerals (averaging +1.0 ±1.3 permil on the Vienna-Canyon Diablo troilite, or VCDT, scale) compared with native sulfur and cinnabar (averaging 0.0 ±1.2 permil VCDT); these values are

consistent with S-isotopes being derived from a mafic magmatic source. Standard fractionation of measured δD, and $\delta^{18}O$ values from alunite, kaolinite, and silica samples suggest parental fluids that are primarily meteoric in origin with calculated temperatures of 20 to 127 °C, indicating a range of temperatures consistent with the supergene and steam-heated environments of acid-sulfate alteration. Differences between $\delta^{18}O_{OH}$ and $\delta^{18}O_{SO4}$ within alunite-group minerals show both isotopic equilibrium and disequilibrium suggesting low temperature re-equilibration of the sulfate hydroxide site to a range of temperatures as low as 20 °C after initial deposition at typical steam-heated environment temperature of 110-130 °C.

Data collected for this study is consistent with previous stable isotope studies of fluids at Sulphur Bank and confirm a primarily meteoric source of fluids. Other studies of springs and deposits in the Clear Lake region show similar fluid sources although notably gold-bearing systems display more isotopically enriched fluid values. This work was done in parallel with ongoing studies that are investigating active weathering processes and current groundwater and surface-water geochemistry of mercury and sulfur at Sulphur Bank. This study provides insights into the past hydrothermal activity that formed the alteration assemblages present at Sulphur Bank and help to provide more comprehensive geochemical characterization of the site and its evolution.

Table of Contents

List of Tables

List of Figures

Chapter 1: Introduction and Previous Studies

1.1. INTRODUCTION

The Sulphur Bank mercury mine represents a well-studied example of epithermal mineralization with relevance to economic geology, mineralogy, and more recently, environmental studies. Sulphur Bank has been described as "probably the outstanding example in the world of a major ore deposit that is clearly related to hot springs," (White and Roberson, 1962) and it is among the very first examples of deposits to be studied as a direct result of hot springs. Since the initial discovery of borax and sulfur by American prospectors in 1856, many researchers have studied the deposit and reached a similar conclusion (Everhart, 1946). Because of active hot-spring activity and the economic significance of the mine, this hot-spring system has long been a reference in the exploration and interpretation of many historic deposits in northern California and elsewhere (Gustafson, 1991).

Analytical methods and geologic understanding have greatly improved over the years allowing a periodic assessment and reinterpretation of the site and surrounding mineral districts, which includes several other mercury mines along with a few notable gold deposits (Studemeister, 1984; Enderlin,1993; Rytuba, 1993). Environmental concerns related to historic mining and natural mercury contamination have introduced new relevance to understanding the depositional mechanisms at work at Sulphur Bank and surrounding deposits (Hammack & Mabie, 2002; Suchanek et al., 2008).

1.2. STATEMENT OF PROBLEM: RESEARCH QUESTIONS AND OBJECTIVES

While many interpretations of the source and nature of geothermal/hydrothermal fluids at Sulphur Bank mercury mine exist, the exact nature and evolution of these fluids remains to be constrained. Most of these previous studies sample local waters and waters emanating directly

from the hot springs or collecting in the impoundment (Engle et al., 2008). These studies provide an understanding of the current fluids but do not necessarily represent the historical fluid that initially formed the deposit due to the evolving nature of hydrothermal systems. Measuring the stable isotope values of the alteration minerals can determine the composition of parental fluids and temperatures of deposition to better understand the steam-heated environment at Sulphur Bank. This provides further insights about the evolution and source of mineralizing hydrothermal fluids.

Classification and understanding of the epithermal environment has evolved since the bulk of previous studies were performed. While traditionally Sulphur Bank has been classified as a "hot-spring style Hg-deposit", literature review and field observations show that a more updated low-sulfidation epithermal deposit model (e. g. Hedenquist & Arribas, 2000) may provide further insights for assessing the gold-silver mineralization potential of the Sulphur Bank geothermal system by comparison with other epithermal deposits in the Geysers-Clear Lake area of northern California.

1.3. PREVIOUS WORK AND BACKGROUND INFORMATION

1.3.1 The Sulphur Bank mercury mine Mining History

Sulphur Bank was originally discovered in 1856 and described as a bleached powdery hill with boric hot springs and sulfurous fumes (Leconte and Rising, 1882). Mining began in 1865 initially for borax and sulfur (MacGowan, 1867) which lasted until 1868 when sulfur prices plummeted, and ore grade dropped. Mining resumed in 1873 when a significant amount of mercury ore was discovered just ~5 to 8 m below the surface (Everhart, 1946).

Trench and open-pit mining with underground shafts exploiting high-grade zones mainly in the faulted and brecciated feeder zones was employed to extract mercury. This initial period

lasted from 1873 to 1897 and saw the bulk of mercury production. Several shafts were sunk reaching a maximum depth of 127 m below the surface with 7 levels of drifts into the high-grade zone below the main pit (Everhart, 1946). Underground working conditions were abysmal for the predominately Chinese miners who had to endure boiling temperatures and increasingly noxious H_2S fumes at depth. Open pit mining resumed from 1899-1906, and 1915-1918 (Figs. 1.1 and 1.2). Mechanized mining from 1927-1947, and finally 1955-1957, greatly increased the scale of the pit and the volume of tailings dumped into the surroundings (White and Roberson, 1962). Over this long history of intermittent mining, SBMM produced roughly 7 million kg of mercury making it one of the largest producers in the USA at the time (White and Roberson, 1962).

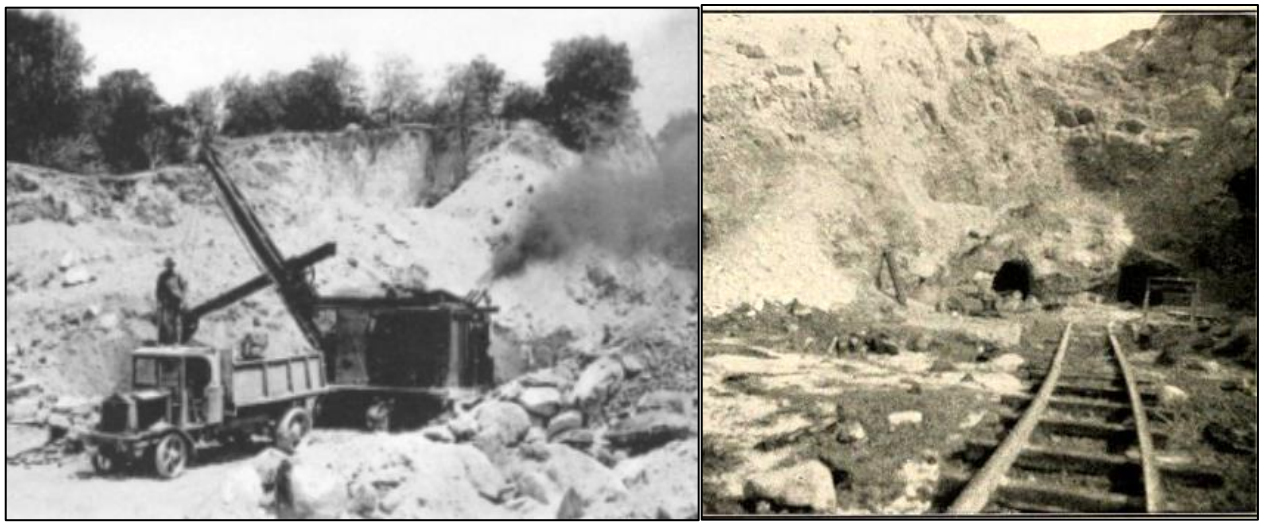

Figure 1.1: Historic photos from SBMM showing the start of mechanized mining in the early 20th century (left) and a 1903 photo of old tunnels now collapsed and presumably under the current Herman Impoundment (right). Public domain photos from https://californiawaterblog.com/2020/11/22/getting-to-the-bottom-of-what-fuels-algal-blooms-in-clear-lake/, "William Forstner - California State Mining Bureau "Quicksilver Resources of California", and https://resources.ca.gov/CNRALegacyFiles/wp-content/uploads/2019/06/2-EPA-Sulphur-Bank-Presentation.pdf

Figure 1.2: View of the mid-20th century open pit looking southwest with Mt. Konocti in background. See Figure 1.1 for photo sources.

1.3.2 Site Description and Geology

The Sulphur Bank mercury mine study area is about 0.65 km^2 (160 acres) and is located directly at the end of the Oaks Arm of Clear Lake in Lake County, California (Figure 1.3). In the center of the property is the Herman impoundment which is an open pit with roughly 30 m (100') of water with active degassing and upwelling hydrothermal fluids (Fig. 1.3). Much of the area of the mine visible at the surface is composed of highly altered andesite or piles of waste rock. To the south of the Herman Impoundment lies waste-rock dumps near the remains of the mercury

smelter. Separating the Herman Impoundment from Clear Lake is a dam constructed from mine tailings (Figs. 1.3 and 1.4). North of the impoundment is the Northwest Pit and various trenches and mine benches. The whole property is dotted with monitoring wells and surrounded by fencing (Engle at al., 2008).

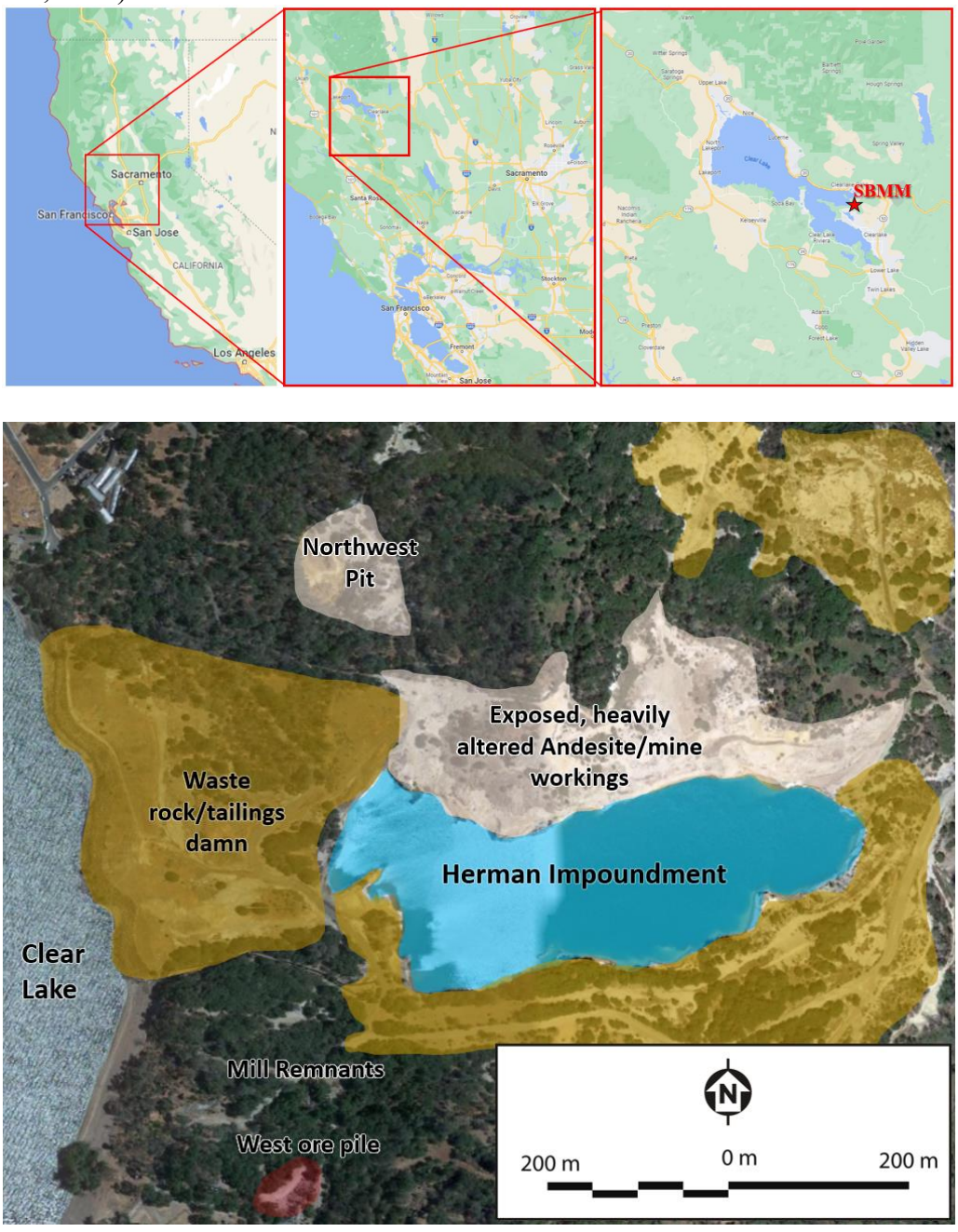

Figure 1.3: Location of Sulphur Bank mercury mine in Lake County, California, and generalized map of the mine site (from Google Maps).

Figure 1.4: Photo of SBMM looking west towards Mt. Konocti with Herman impoundment in foreground. Note the stark bleached appearance of the north wall of the impoundment.

Previous studies have classified the alteration assemblages into 3-5 distinct horizontal zones. First observed at the surface was abundant sulfur crystals and white powdery remains of acid-attacked basalt. This zone is referred to as the steam-heated zone and is interpreted as the unsaturated area above highest extent of the pre-mining water table. The steam-heated zone extends down 1-5 meters where a stark transition to the lower zone is encountered occasionally with opaline silica blankets (White and Roberson, 1962). It is important to note that while this top zone represents the most intense steam-heated alteration, steam-heated acid-sulfate alteration occurs in lower zones as well since the water table shifts with time and was much lower during certain periods.

The second zone encountered is comprised of large spheres or blocks of lightly to strongly altered basalt with clays, silica, and sulfate forming “veins” and exfoliations around and between

blocks (Fig. 1.5). These veins consist of altered zones between less altered basalt "boulders" and are decimeter to meter across, often presenting a lateral zonation of kaolinite, alunite, and amorphous silica with moderate amounts of native sulfur and cinnabar (Wells and Ghiorso, 1988). Most of the mineral samples discussed later in this study are from these veins. Because these veins and exfoliation shells of alteration form blocky to rounded boulders of less altered basalt, several previous studies refer to this zone as the "boulder zone" although it should be noted that this is a strictly visual description since the boulders are formed from alteration and not erosion (Fig. 1.5; White and Roberson, 1962, Wells and Ghiorso, 1988). This zone is roughly 3-25 meters in vertical extent and is sometimes subdivided into "basal" and "intermediate" units depending on the extent of argillic alteration and andesite replacement. The base of this zone is the bottom of the andesite flow (White and Roberson 1962). This altered andesite unit of the Clear Lake volcanics is referred to as Sulphur Bank andesite and is dated to 44,500 ± 800 years BP (Donnelly-Nolan et al., 1981, Hearn et al., 1995).

The third zone is an unconsolidated unit called the Cache Creek sediments (Fig. 1.5; sometimes called lake sediments) and has the appearance of a clay to sand-cemented breccia or conglomerate with sand, silt, mud, and course sandstone and shale cobbles in places. This zone hosted cinnabar mineralization as "globules", disseminations, and clast coatings (LeConte and Rising, 1882; Everhart, 1946).

Below this unconsolidated unit lies the fourth and final zone which consists of shales and blueschists of the Franciscan Formation (Fig. 1.4). Unlike the unconsolidated zone, this unit has a much lower permeability except around faults and shear zones which also underly the most intensely altered zone above. A series of faults observed by multiple studies host rich-cinnabar mineralization along with other sulfides, carbonates, kaolinite, silica and sulphates at depth

contained mainly within fault planes and associated breccias (Everhart, 1946). Older articles written during the late 19th century observe enriched parts of breccia around fault conduits with rock containing up to 50% cinnabar by weight. This unit was the target of early mine workings in trenches and underground drifts (LeConte and Rising, 1882). Historic studies have mapped various faults and shear zones and recent studies have used airborne geophysical methods to highlight and confirm these now mostly covered fault traces that underly the system (Hammack and Mabie, 2002, Hammack et al., 2003).

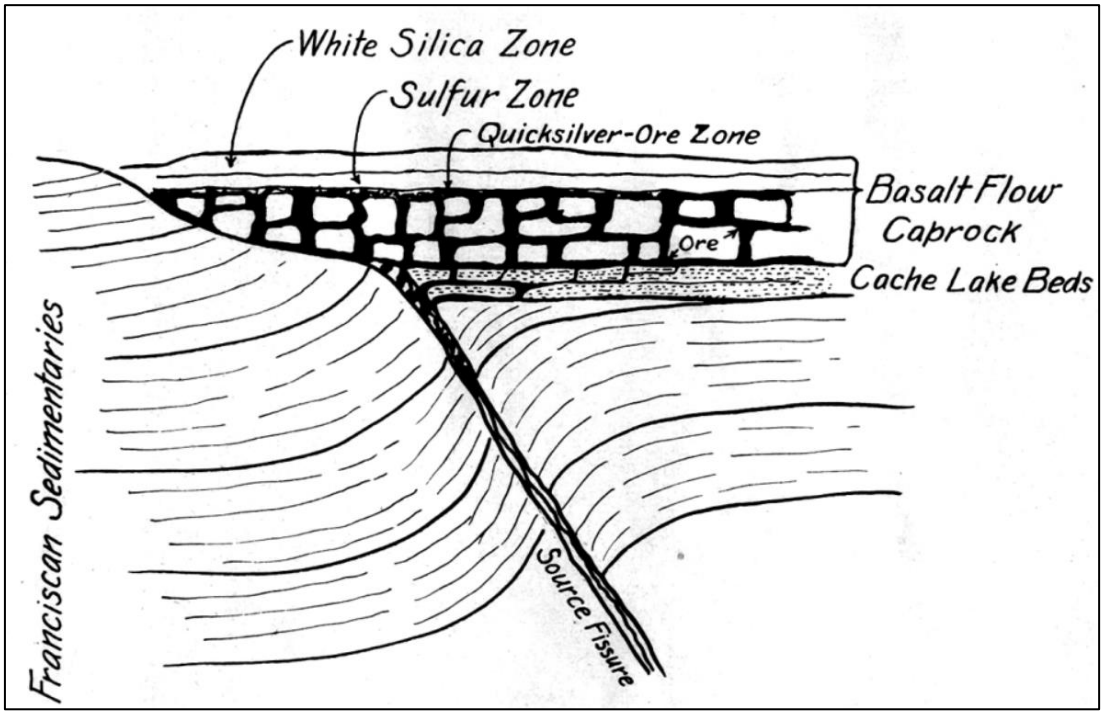

Figure 1.5: Idealized cross-section showing alteration and mineralization zones and major lithologic units at the Sulphur Bank mercury mine, note that this figure shows zones labeled by alteration and sulfur/mercury content while later studies rename the "quicksilver-ore zone" as the "boulder zone" and the "White Silica/Sulfur Zone" as the "Steam heated zone"(Schuette, 1931).

1.3.3 Environmental context

Problems with eutrophication and water quality have plagued Clear Lake for decades prompting environmental studies. In 1986, elevated levels of mercury were found in fish and

subsequent studies found elevated levels of mercury in local watersheds (Suchanek et al., 2008). In 1990, both the Sulphur Bank mine site and the entirety of Clear Lake were listed as superfund sites due to mercury contamination (Hammack and Mabie, 2002; US EPA, 2019). The Bradley Mining Corporation fought a legal battle contesting the role of the Sulphur Bank mine tailings and other related mine waste in contamination. Ultimately the D.C. Circuit Court ruled against the mining corporation citing that the large amounts of waste rock and tailings on the mine site and adjacent to it under the waters of the Oaks arm are directly responsible for Hg contamination (D.C. Circuit Court 1992, Suchanek et al., 2008).

More recent studies have investigated further into the environmental impact of this contamination and the amount of mercury introduced from natural, historic mercury-bearing fluids and modern mining practices. One study into sediment cores from Clear Lake found 5-7 episodic enrichments near the Sulphur Bank deposit with ages spread out over 34,000 years before present (Sims and White, 1981) causing some to speculate that mercury is enriched mainly through natural processes as opposed to anthropogenic activity (Varekamp and Waibel, 1987). Regardless, mining activity has been shown to facilitate methylation of mercury from cinnabar in waste rock and tailings and this is shown through increased methylmercury detected in sediments, waters, biota, and aquatic life in the watershed that includes the Sulphur Bank mine. Several projects detailing and quantifying the speciation of mercury in mine wastes and surrounding areas have been completed (Jew et al., 2011; Kim et al., 2003; Lowry et al., 2004) along with other studies currently underway. The environmental project now focuses on ongoing mercury studies at Clear Lake and the Sulphur Bank mercury mine and is led by the U.S. Geological Survey (USGS) and the Environmental Protection Agency (EPA) with the intent of additional remediation efforts to take place in the near future to remedy the issue of continued mercury speciation into local watersheds.

This study was initiated and has been partially funded by the USGS as an additional research component of the environmental project underway at the Sulphur Bank.

1.3.4 Previous Isotope and Fluid Studies and Comparison to Regional Fluids

Ongoing hydrothermal deposition and its obvious association to mineralization has resulted in water and gas analyses for a host of variables including temperature, Cl, B, Na, H_2S, HCO_3, NH_4, and CO_2 observed roughly every decade since 1863 as proxies for hydrothermal input and dilution from meteoric water (LeConte and Rising, 1883; White and Roberson, 1962; White et al., 1973; Engle et. al., 2008). Water and gas compositions have historically been compared with other hydrothermal springs notably other springs local to the Northern Coast Ranges as well as springs at Yellowstone National Park. By the 1970s, isotopic analyses of δD, and $\delta^{18}O$ were included along with current and historic B/Cl and other ratios showing isotopic enrichment and a unique B/Cl signature of 1:1 (Goff et al., 1995).

Previous researchers have generally concluded that, although the hydrothermal waters show isotopic enrichment and non-meteoric chemical compositions, they are most likely metamorphic fluids from hydrolytic dewatering or formational fluids owing shifts to water-rock interactions of deep circulating fluids flowing through organics-enriched marine sedimentary rocks (Studemeister, 1984; Goff et al., 1995). Regional trends of isotopic ratios and ionic content were created to compare Sulphur Bank hydrothermal waters to other local springs showing similar isotopic shifts speculated to be related to temperature fractionation, evaporation from boiling, and various levels of mixing with meteoric fluids (Donnelly-Nolan et al., 1993).

Analyses of gases at Sulphur Bank similarly show relations to organic-rich and sedimentary source rocks rather than magmatic gases with attention paid to isotopically light $\delta^{13}C$ from CO_2 (Goff et al., 1995). Analyses of mercury isotopes also suggest that they are derived

from sedimentary host rocks but the local difference between magmatic mercury and sedimentary mercury is too small to be conclusive which is a common problem with stable Hg isotopes (Smith, 2010, Smith et al., 2008). Although the gases are not indicative of a magmatic source, there is evidence of mantle derived volatiles in the form of high R/R_A values for ^3He of 7.9 compared to local values of 0.4 (Goff et al. 1995).

Deep drill holes investigating geothermal potential reached a maximum of 637-m depth and encountered fluid temperatures in excess of 200 °C, while near surface hydrothermal waters have a range of temperatures from 10-186 °C (Engle et al., 2008). Historic temperature measurements starting from 1863 to present and regional hot-springs and historic mines show similar warm temperatures within this range (White et al., 1973).

1.3.5 Clear Lake area ore deposits and hot springs

Hydrothermal fluids around the Clear Lake region are associated with various hot springs, mercury and mercury-gold deposits, and geothermal fields around the region (Fig. 1.6; Sherlock, 2005). The Geysers Steam field is host to the largest operating geothermal power plant in the world. Steam at The Geysers is related to geothermal fluids at depth encountering steeply dipping faults related to district scale faulting. The steam field is proximal to historic mercury mines and represents a vapor-dominated system (opposed to fluid-dominated hot springs which form most of the deposits) (Stimac et al., 2001).

Various mercury districts occur in the region and are divided into silica-carbonate-type or hot-spring type (like Sulphur Bank). Several authors speculate that silica-carbonate types are slightly deeper analogues of hot-spring-style mercury deposits forming from altered serpentinite zone within metasedimentary host rocks. Both styles are associated with gold-bearing springs and geothermal steam fields (Pickthorn, 1993).

Gold mines in this area have also been exploited since the mid-19th century to the present and include various small mines such as Silverado, Palisades, Manzanita/Cherry Hill, and (most notably) the McLaughlin gold deposit (Fig. 1.6). Isotopic analyses of historic fluids from McLaughlin show evidence of meteoric waters, oilfield/metamorphic waters, and magmatic waters which are speculated to provide the gold that is missing from other hydrothermal systems. Sherlock (2005) suggests that while waters from McLaughlin, Cherry Hill, and Sulphur Bank are similarly isotopically enriched, they display different chemistries and thus different sources and enrichment

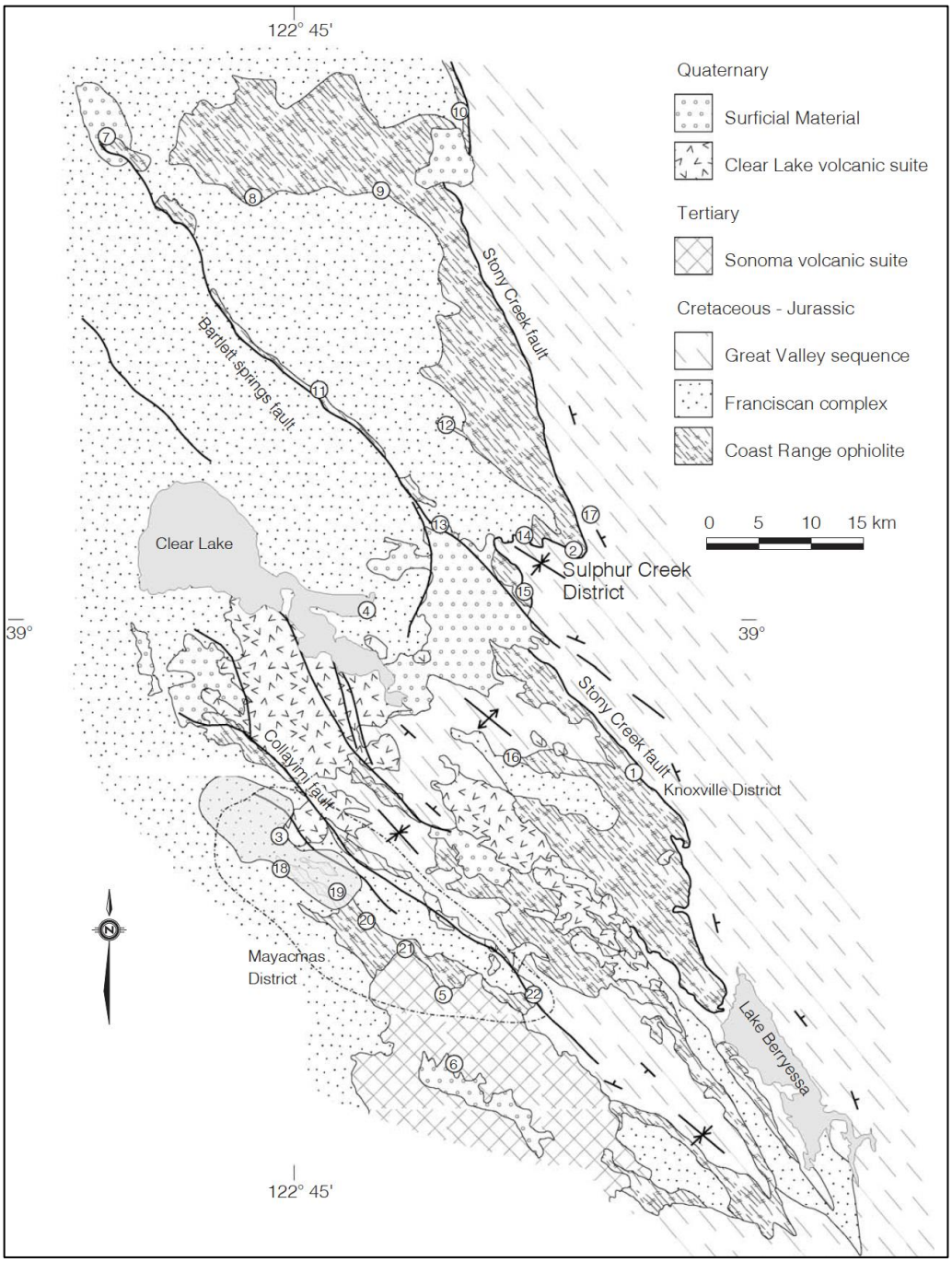

Figure 1.6. Geologic map and location of geothermal systems and ore deposits of the Clear Lake Area. 1: McLaughlin deposit, 2: Sulphur Creek District, 3: The Geysers steam field, 4: Sulphur Bank, 5: Silverado, 6: Palisades, 7: Soda Springs Lake Pilsbury, 8: Crab Tree hot springs, 9: Foutes Red Eye, 10: Salt Spring, 11: Bartlett Springs, 12: Allen Springs, 13: Chalk Hill, 14: Elgin Hg deposit and spring, 15: Abott and Turkey Run Hg deposit and springs, 16: Barker Hg deposit and spring, 17: Terhel-1 oil well, 18: Culver–Baer, 19: Socrates and Eureka, 20: Chicago and Helna, 21: Great Western, 22: Aetna (Fig. 1 in Sherlock, 2005).

mechanisms. Furthermore, measured and estimated temperatures from Cherry Hill ores and McLaughlin ores show values of slightly higher temperatures, although this is consistent with the mineralization occurring at greater depths (Sherlock et al, 1995; Rytuba et al., 2009). Hydrocarbons assumed to be from Great Valley Sediments are present at McLaughlin and are correlated with Au mineralization prompting several studies concluding that they act as a mechanism for trapping gold. Silverado and Palisades mines also feature silver and gold mineralization associated with mercury and hydrocarbons but have ores that deposited at a greater estimated depth with slightly greater depositional temperatures of 200-300 °C and a dominantly meteoric isotopic origin significantly less isotopic enrichment (Enderlin, 1993).

Gold ore associated with mercury and the major discovery of large reserves at McLaughlin created a new deposit model of mercury-hot-spring style deposit which has been used successfully in other exploration campaigns (Gustafson, 1991; Pickthorn, 1993). Gold-bearing deposits are almost exclusively hosted in structures within more Easterly Great Valley Sequence rocks. Differences between these deposits and Sulphur Bank will be discussed later in this paper.

1.4. SUMMARY AND DEPOSIT MODEL

The alteration and mineralization of SBMM has been studied for over 150 years and the general formational processes are understood and summarized here. Local circulating meteoric and fluids gain heat and mix with CO_2 and H_2S that is currently degassing from shallow magmatic systems. To some extent, these fluids interact with oceanic metasedimentary rocks of the Franciscan formation picking up hydrocarbons and volatilizing mercury which was slightly enriched from shallow marine processes during initial deposition of the formation. Isotopic enrichment of the hydrothermal fluids occurs due to fluid-rock exchange with these sedimentary rocks (Donnelly-Nolan et. al., 1993; Crede et. al., 2020; Stimac et. al., 2001). When the fluid

encounters permeable zones it ascends along local faults present around Clear Lake causing boiling as depth and pressure decrease which releases the volatiles. Once the volatiles reach the water table, H_2S combines with oxygen to form sulfuric acid (H_2SO_4) creating acid-sulfate conditions that aggressively leach the host rocks in the vadose zone (Studemeister, 1984; White and Roberson, 1962) creating what is referred to as the "steam-heated zone" (Wells and Ghiorso, 1988). Ascending Hg^0 vapors are oxidized below the water table to Hg^{2+} which in turn reacts with H_2S (Smith, 2010) to deposit cinnabar (Hg sulfide) in the brecciated feeder faults and shear zones. These alteration mineral assemblages belong to the 'steam-heated acid-sulfate condensate environment' (Fig. 1.7; Hedenquist and Arribas, 2022).

The steam heated zone is the bleached-white sulfur-bearing zone while the lower zone referred to as the "boulder zone" is found below the paleo-water table. Both of these zones are hosted in a moderately to heavily altered Pleistocene andesitic unit. Underlying this unit is an unconsolidated sedimentary layer which in turn overlies metamorphic rocks formally known as the Franciscan Complex which are locally brecciated around steeply dipping faults serving as the feeder systems that both deliver the hydrothermal fluids and gasses as while hosting the richest mercury ore.

Traditionally, the Sulphur Bank mercury deposit was classified as a "mercury hot-spring deposit" (White and Roberson, 1962; Wells and Ghiorso, 1988). This type of deposits fits well within the current, broader context of epithermal mineralization under the 'low-sulfidation epithermal gold-silver deposit model (Fig. 1.7; Hedenquist et al., 2000). Further insights can be learned through comparison with other low-sulfidation deposits such as McLaughlin, among others.

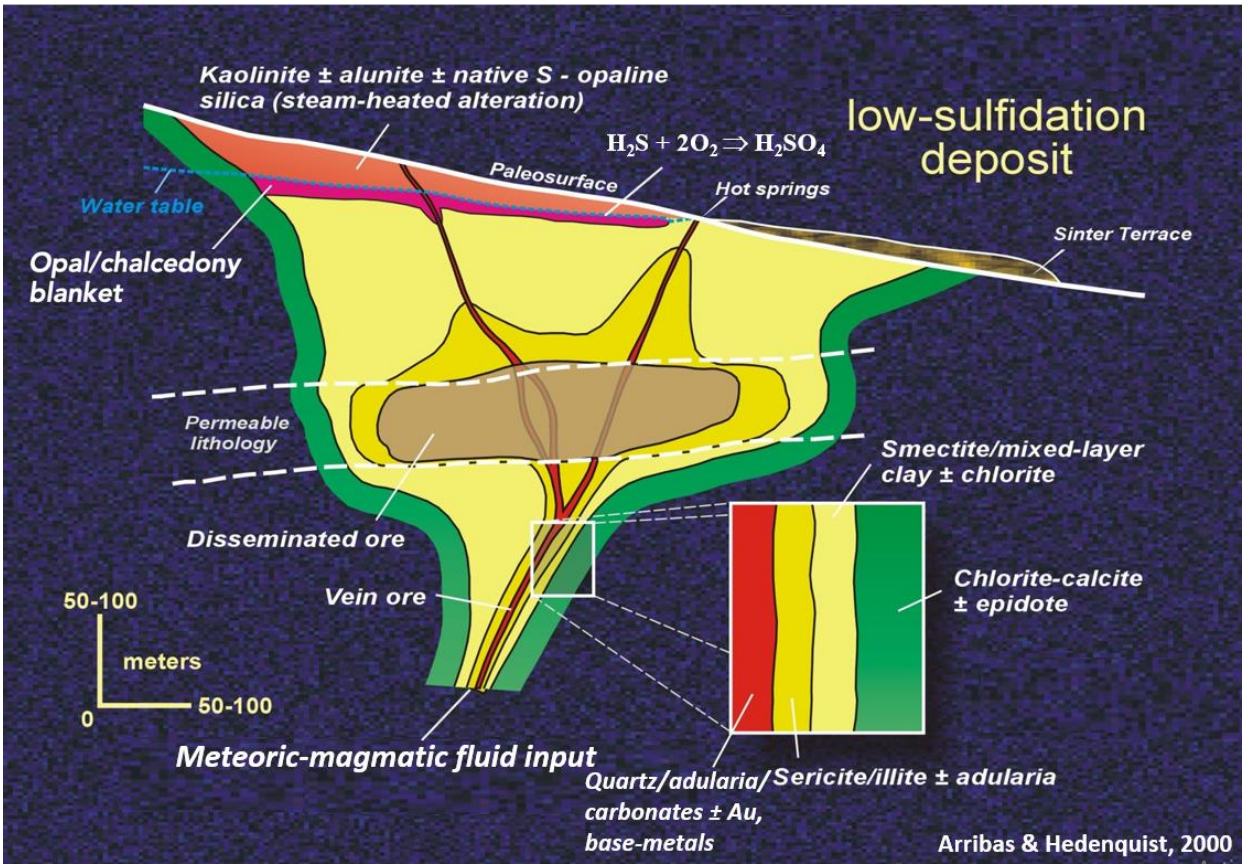

Figure 1.7: Model for epithermal low-sulfidation gold-silver deposit (modified from Hedenquist et al., 2000).

Previous studies have employed various methods to constrain the source of the mineralizing fluids. Waters at SBMM and other deposits are derived from multiple sources interpreted to be a mixture of meteoric waters with metamorphic and rock-exchanged hydrothermal fluids. Magmatic water input has been speculated but has not been definitively shown through chemical analysis, although the presence of volatiles and He^3 enrichment prove that mantle/magma derived sources are present (Goff et al., 1995; Engle et al., 2008; Fig. 1.8).

Stable isotope analyses have been employed in various other settings to help describe ore deposits and zonation. Sulfur, hydrogen and/or oxygen isotope analyses on sulfides, alunite and other alteration minerals provide insights into the source of the H_2S and other fluids that are the

source of alteration (Rye, 2005; Seal et. al., 2000) and will complement the many previous studies performed on fluids at Sulphur Bank and other deposits/springs with similar features.

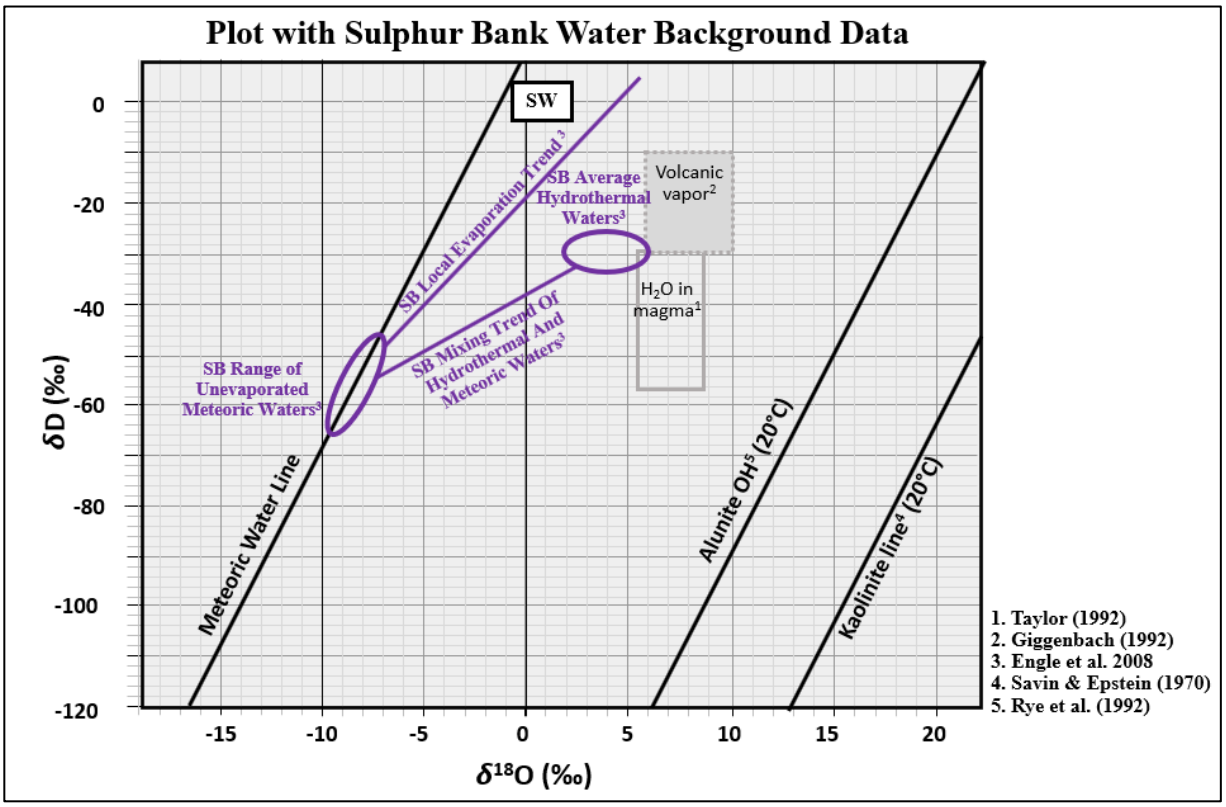

Figure 1.8: Plot showing known stable isotope data trends and average values for Sulphur Bank fluids (in purple, from Engle et al., 2008). The δD-δ^{18}O values for reference crustal fluids (e.g., meteoric water line, SW = seawater; volcanic vapor, etc.) and minerals (e.g., kaolinite and alunite OH in isotopic equilibrium with meteoric water at 20°C) are shown in black and gray (1 to 5 = data sources).

Chapter 2: Geologic Setting and Regional Tectonic History

2.1. STRATIGRAPHIC UNITS

The area around Clear Lake can generally be grouped into four major formations (Figs. 2.1 and 2.2) consisting of the Franciscan Complex, the Great Valley Sequence, the Coast Range ophiolite, and Quaternary volcanics referred to as the Clear Lake and Sonoma Volcanics.

The Franciscan Complex is a highly heterogenous assemblage with low permeability mainly composed of lithic wackes and shales with areas of blueschist and serpentinite in areas of high shear (McLaughlin, 1981; Irwin, 1990). This assemblage is interpreted as an accretionary wedge that formed during the Mesozoic era during the subduction of the Farallon plate under North America (Furlong and Schwartz, 2004).

Structurally above the Franciscan rocks is the Great Valley Sequence with the Coast Range ophiolite serving as its base. The Coast Range Ophiolite is interpreted as oceanic crust formed in a forearc environment during the Late Jurassic consisting of mafic to ultramafic rocks that are locally sheared and serpentinized (McLaughlin, 1981).

Above the Coast Range Ophiolite lies the Great Valley Sequence comprised of interbedded marine mudstones, sandstones, and conglomerates which are much less deformed and dismembered when juxtaposed with the Franciscan rocks (Irwin, 1990). The Great Valley sequence is thought to be the forearc deposition of the rapidly eroding Klamath and Sierra Nevada ranges to the North and East during the Jurassic to Cretaceous periods (Furlong and Schwartz, 2004).

Finally, the volcanic suites are quaternary mafic to intermediate extrusive rocks directly related to recent magmatism from shallowly emplaced magma chambers. Other rocks/sediments in the area primarily consist of unconsolidated sediments referred to as Clear Lake sediments or

Cache Creek sediments. In the case of Sulphur Bank deposit, these sediments are present as a thin to thick layer separating the altered andesite from the Franciscan rocks below and they play a role in distributing mineralizing fluids from the fault conduits (Wells and Ghiorso, 1988).

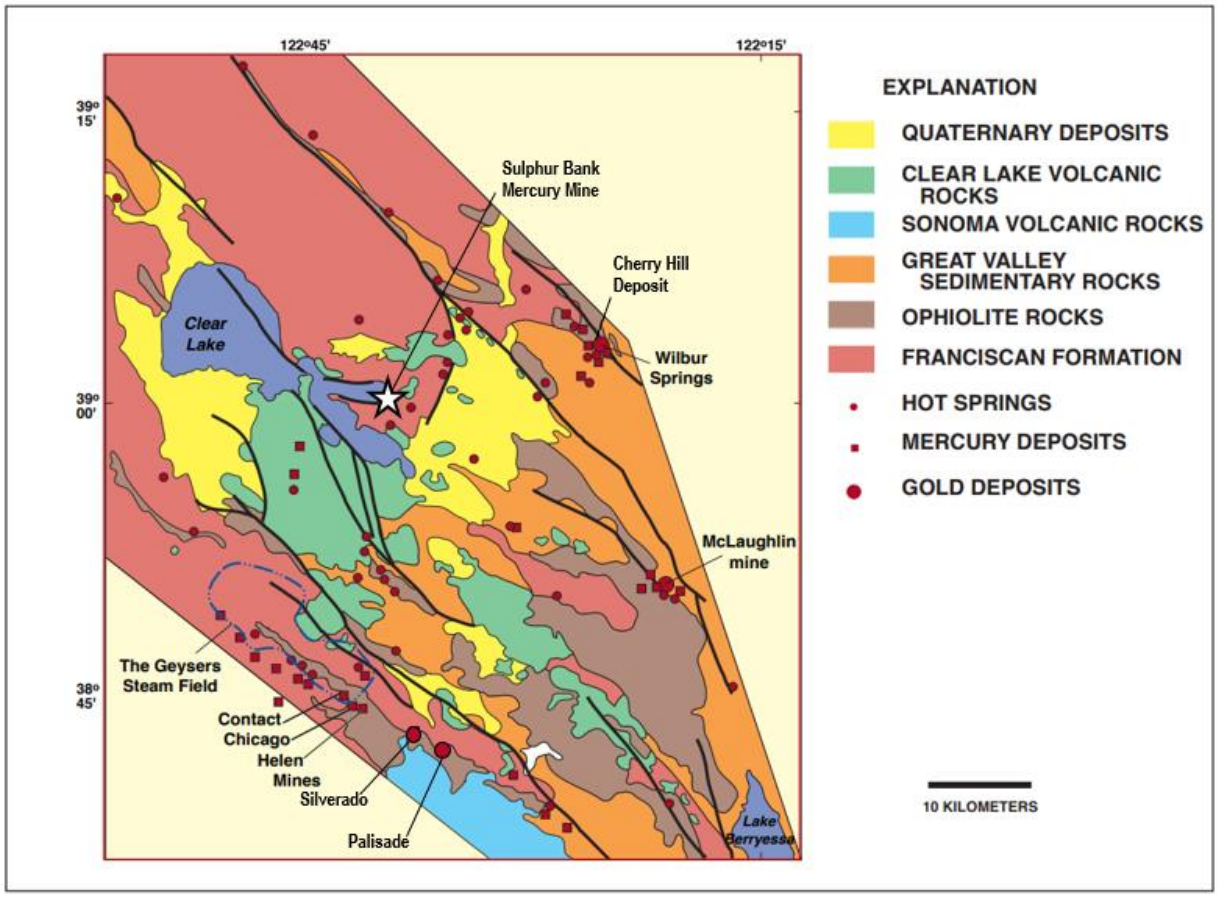

Figure 2.1: Geologic map of the Clear Lake area showing the major geologic units and faults. Note the relation of hot springs and ore deposits with major fault systems (modified from Rytuba et al., 2009).

2.2 REGIONAL TECTONIC HISTORY

The tectonic emplacement and interleaving of these units reflect a complex process involving various thrust faults and later strike-slip faults coupled with erosion and volcanic activity that serve to juxtapose the different major stratigraphic units (Sherlock et al., 1995). The process begins with the formation of the primary sedimentary packages during the mid to late Mesozoic.

First, the Franciscan formation forms as an accretionary prism in the trench formed from the subducting Farallon plate under the North American plate creating the highly dismembered and locally sheared and metamorphosed sequence (Dickinson et al., 1982). Coeval to this is the formation of the Coast Range ophiolite in the forearc environment with Great Valley Sediments deposited on top. The Franciscan Complex was then thrusted underneath the Coast Range Ophiolite and Great Valley Sequence with the Coast Range thrust serving as the contact (Hearn et al., 1988). The Franciscan Complex and the Great Valley Sequence are often referred to as the underplate and the upper plate respectively in reference to this event. The exact nature of this thrusting event is uncertain since the majority of the upper plate has been lost to erosion leaving various windows of Coast Range Ophiolite and Great Valley sediments preserved (Hearn et al., 1988). These processes and general sequence are summarized in Figure 2.2 from Dickinson et al. (1982).

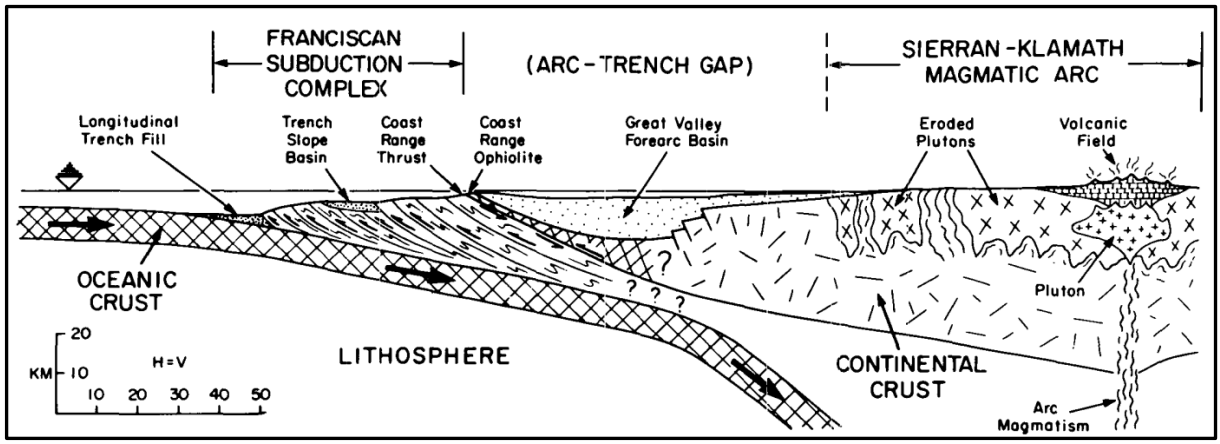

Figure 2.2: Idealized diagram of the Mesozoic setting of the primary stratigraphic units of northern California (Dickinson et al., 1982).

The Miocene saw the formation of the Mendocino Triple Junction and the Riviera Triple Junction from the subduction of a spreading center that subsequently changed the convergent regime into a transform regime between the triple junctions (Irwin, 1990; Furlong and Schwartz,

2004) (Fig. 2.3). After formation, the Mendocino Triple Junction migrated northward with time. This event effectively split the Farallon Plate into the current Juan de Fuca Plate in the north (with the southern most part sometimes called the Gorda Plate just above the Mendocino Triple Junction), and the Cocos Plate in the south. The newly created and ongoing transform zone eventually became the modern San Andreas Fault system with the opening of the Gulf of California about 4 Ma (Irwin, 1990). The San Andreas Fault System plays the largest role in ongoing tectonic controls creating episodic dextral translation and therefore significant northward migration of different sections around Sulphur Bank (Irwin, 1990). Accompanying this dextral translation is the expression of numerous transpressional and transtensional features including the pull-apart basin where Clear Lake and its immediate surroundings now reside.

The general trend of the San Andreas Fault System is dextral shear trending N35-45W while the local trend for the Clear Lake basin is N25W with evidence of a gradual clockwise rotation of the basin (Hearn et al., 1988). Two regional fault zones trending NW define a pull-apart regime and the local transtensional forces that work to create the basin of Clear Lake. The frequent Quaternary volcanism stemming from shallowly emplaced magma chambers is speculated to be a source of subsidence. About one million years ago, Clear Lake itself first appeared in roughly the same location as the older (2-3 Ma) Cache Creek basin. The basin is defined by fluvial to lacustrine sediments periodically intruded by or layered with volcanics and pyroclastics (Hearn et al., 1988). After about 0.6 Ma, lake sediment thicknesses show an average sedimentation and subsidence of about 1.7 mm/year implying a long-lived lacustrine system of relatively consistent size (Hearn et al., 1988). The basin history can be summarized as a volcano-tectonic depression with constant lacustrine deposition from about 0.6 Ma to the present.

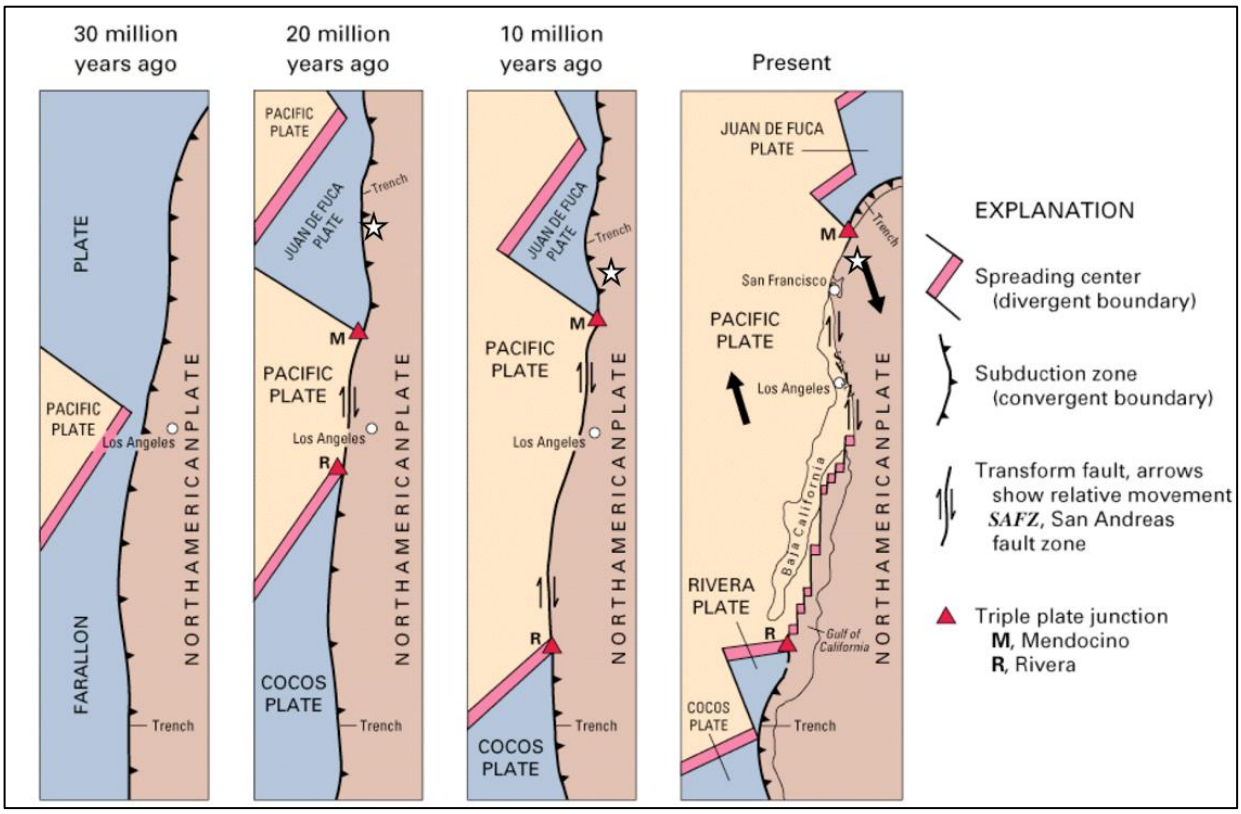

Figure 2.3: Schematic diagrams showing the formation and movement of the Mendocino Triple Junction, a white star added in this study represents the approximate location of the Sulphur Bank mercury mine (Irwin, 1990).

2.3. EMPLACEMENT OF MAGMATISM

The formation of a transform fault boundary between the triple junctions saw the local termination of subduction and thus arc magmatism on the western coast of North America above the newly formed slab-less window. Around 4-3 Ma, the Mendocino Triple Junction was approximately adjacent to present-day Clear Lake. Just after the passage of the Mendocino Triple Junction the Clear Lake Volcanic field was emplaced. The azimuth of shear changed as the Mendocino Triple Junction migrated northward creating multiple extensional basins in the northern Coast Ranges which allowed pressure release and subsequent emplacement of mantle material into the shallow crustal chambers. This formed the chamber that spawned the Sonoma and Clear Lake Volcanics around 2-3 Ma (Stimac et al., 2001). There exists a gap of .5-1 Ma

between younger Clear Lake and older Sonoma volcanism. Dating of discrete volcanic units in the last 130 ka has shown frequent eruptions with an average eruption interval of 2-5 ka from this magma chamber. Volcanic rocks range from basaltic to rhyolitic and show evidence of both mantle-derived melts and intermediate melts that assimilate sedimentary units (Hearn et al., 1981). The magma chambers are interpreted to be slowly migrating northward with time following the northward migration of the Mendocino Triple Junction (Stimac et al., 2001). This process is recorded in the dating of the volcanics shown in figure 2.4.

The shallow crustal magma chambers are key to the formation of the Sulphur Bank mercury and surrounding deposits since they are temporally linked with the chambers providing the source of intrusions and probably associated magmatic fluids as well as the heat source for hydrothermal fluids and the local high heat flow anomalies in the Clear Lake region. Steeply dipping faults related to the San Andreas Fault system provide pathways for steam and hydrothermal fluids to travel to the surface and more efficiently advect this heat (Stimac et al., 2001).

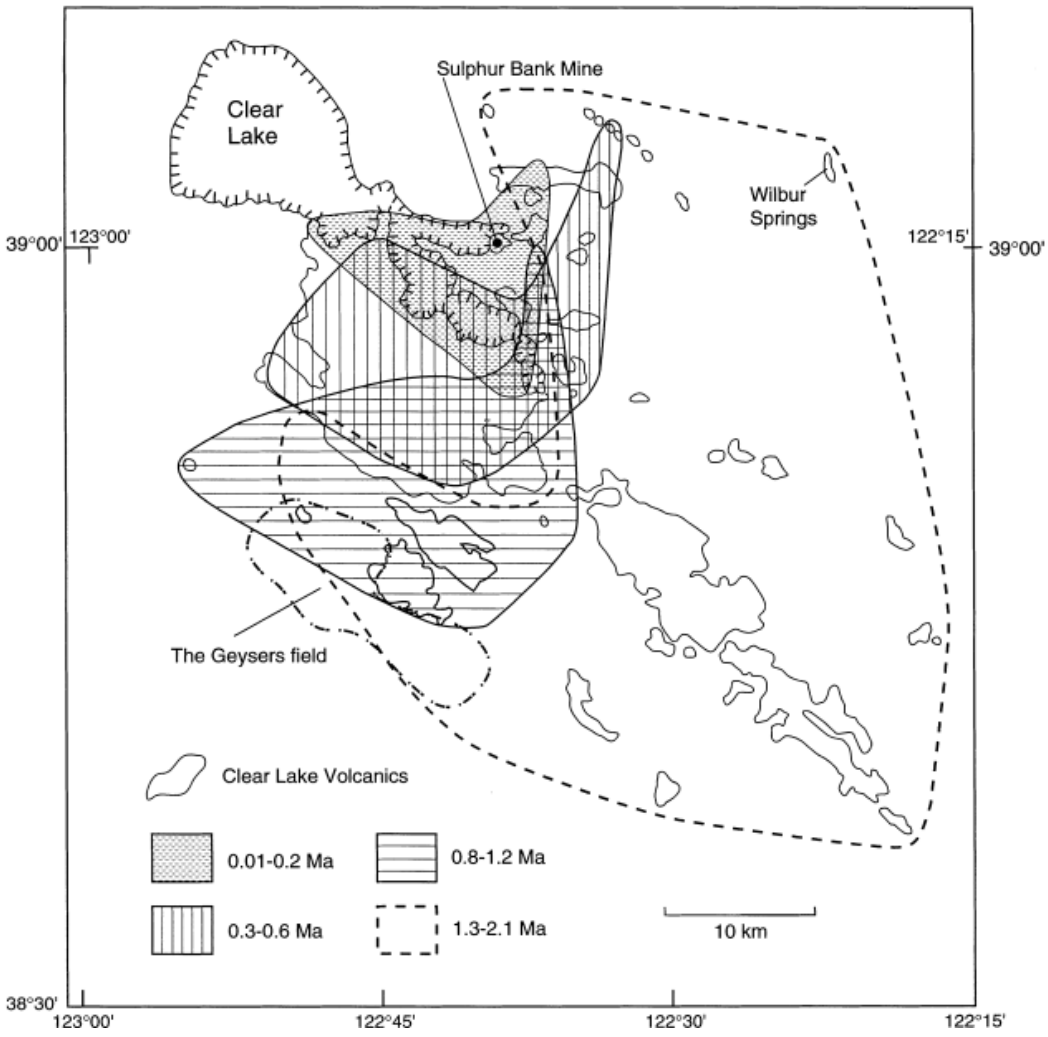

Figure 2.4: Map showing spatial and temporal distribution of volcanics. Note the Northward migration and shrinking with time (Stimac et al., 2001).

2.4. GEOLOGIC SETTING SUMMARY

Key insights can be made about the nature and genesis of the formation of Sulphur Bank mercury deposit and the surrounding precious-metal district which are different in nature from the orogenic gold districts in the Sierra Nevada to the east. Central and Northern California host the most significant mercury district in North America, from the New Almaden mine to the South to Sulphur Bank in the north, with a series of precious metal deposits proximal to the study areas that share a similar genetic setting/source (Studemeister, 1984).

High heat flow from shallow magmatism resulting from cessation of subduction and asthenospheric upwelling from the slab-less window created long-lived hydrothermal systems in the Coast Ranges. Pliocene to Quaternary transform faulting created permeable pathways for these hydrothermal fluids to mineralize favorable lithologies and structural contacts. These fault zones are mostly sub-parallel to the San Andreas Fault Zone (centered roughly 50 km to the SW of Clear Lake) and they typically represent areas of weakness related to rheological differences in terranes or lithologies within the Mesozoic rocks that comprise the bulk of this region (Donnelly-Nolan et al., 1993). Furthermore, some faults are speculated to be high-angle reactivations of thrust faults that formed from the accretionary wedging of the units themselves such as the Coast Range Thrust. Thus, the structure of the region plays an intrinsic role in the channeling and focusing of mineralizing fluids (Donnelly-Nolan et al., 1993).

Chapter 3: Methods

3.1. Field Methods

Hand samples and photographs were taken during two field visits to the Sulphur Bank mine with special attention paid to minerals found within veins from the boulder zone as described in Wells and Ghiorso (1988). To simplify the preparation of mineral separates, samples were taken where 1) minerals were coarse enough to identify visually and to remove by hand picking, or 2) the rocks appeared on visual inspection to be monomineralic. Isolating individual minerals by hand was only possible for native sulfur. Hand samples are wrapped, labelled, and brought back to El Paso for further analysis. Sample location is shown in Figure 3.1 and detailed sample information is included in Appendices I and II.

3.2. X-ray diffraction and scanning electron microscopy

Since most steam-heated minerals are white to tan and microcrystalline, it is not possible tell samples apart visually. The primary tool for analysis in the initial identification of minerals present was the X-ray diffractometer (XRD) which is particularly useful for determining the crystal structure of minerals like clays and sulfates.

Small fragments taken from hand samples were ground to a fine powder using an agate or steel mortar and pestle and sieved using a 200-mesh sieve to remove coarse fragments and fine particle size for cleaner measurements. The powdered sample was then carefully packed into a puck for XRD analysis.

X-ray diffraction patterns were obtained in the X-ray laboratory of the Department of Earth, Environmental and Resource Sciences of The University of Texas at El Paso using a Bruker D2 Phaser instrument and Cu K alpha radiation (see Appendix II). Scans covered a two-theta range of 5°-60° 2θ and a time/step of 0.02-.2 seconds depending on the complexity of the sample.

Minerals were identified using DIFFRAC.EVA, the system software which compared the scans to reference scans for individual minerals contained in the software library. A more detailed description of the operation of the XRD is found in Appendix III (XRD User Manual Notes).

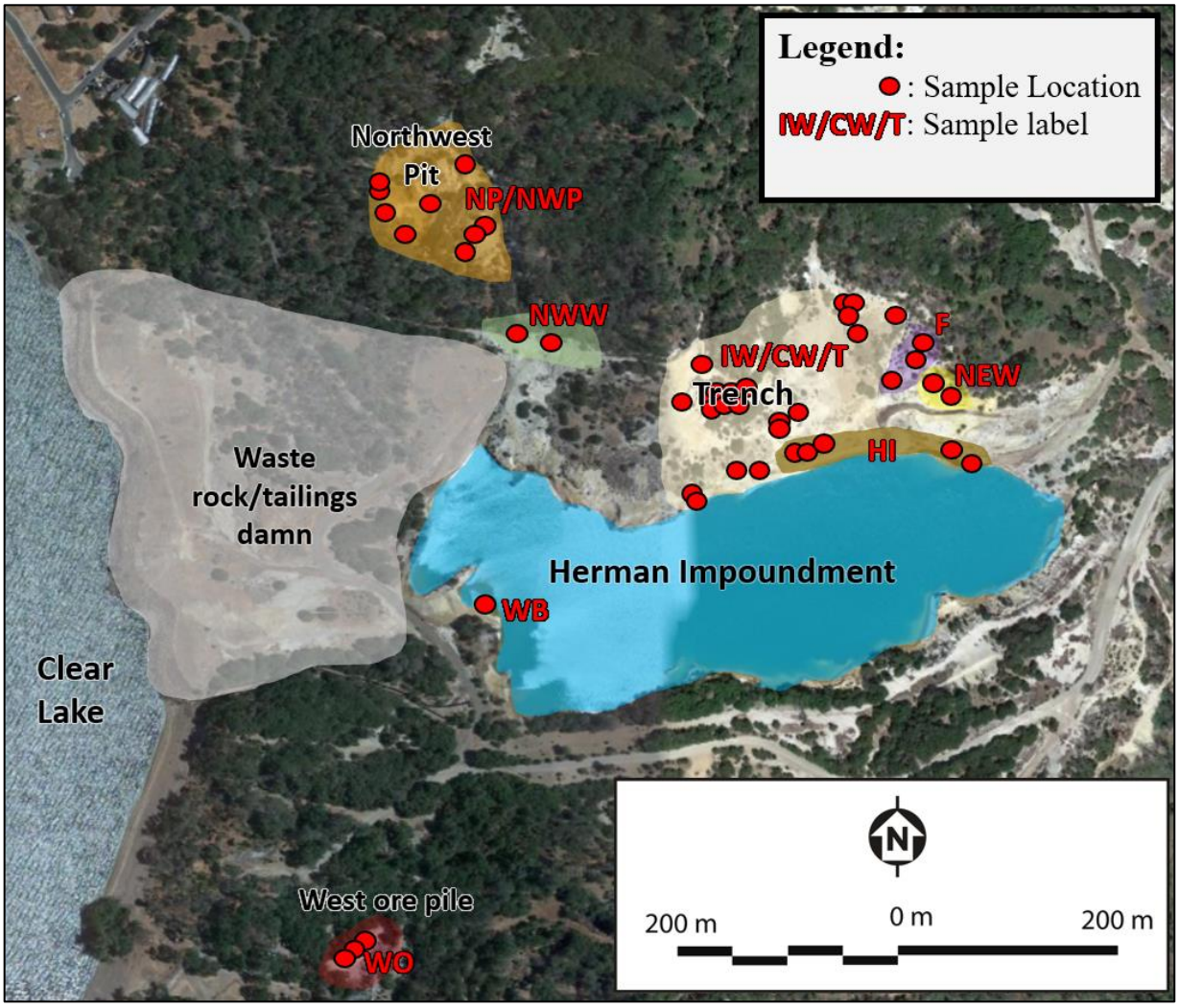

Figure 3.1: Map of the study area with approximate locations of sample collection and sample name labels.

Unit-cell values were determined from completed XRD scans of relatively pure alunite samples using JADE software which calculated cell dimensions a, b, and c using the Rietveld method (Young, 1993).

Representative rock samples were also examined by a scanning electron microscope to provide information on grain size, texture, and habit of the minerals. Images were obtained using a Hitachi SU1000 FlexSEM 1000II. Secondary electron images were obtained at accelerating voltages ranging from 5 to 15 kV whereas backscattered electron images were obtained at an accelerating voltage of 15 kV. Magnification varied among the acquired images; scale bars are shown at the bottoms of individual images.

3.3. ISOTOPIC ANALYSES

Isotopic analyses were performed in the laboratories of the U. S. Geological Survey (Geophysics, and Geochemistry Science Center), Denver Federal Center, Denver, Colorado. Analytical procedures are described in detail in Johnson et al. (2023) and summarized below.

Alunite separates were dissolved in 0.5M sodium hydroxide solution and the liberated sulfate was then recovered by precipitating it as $BaSO_4$. This was performed in accordance with the procedure in Wasserman et al., 1992.

For hydrogen isotopes, aliquots of alunite or kaolinite weighing about 0.5 milligrams were placed in silver capsules for analysis using a ThermoQuest high temperature conversion elemental analyzer (TCEA) coupled to a Thermo Scientific Delta V Plus isotope-ratio mass spectrometer (IRMS). Results were normalized so that results obtained for the USGS 57 and USGS 58 hydrogen isotope standards in the same autorun gave the delta (δD) values recommended by Brand and others (2014), -91.5 and -28.4 permil, respectively. Aliquots of USGS 58 analyzed as unknowns gave -28.3+/- 1.6 permil (n = 2) in good agreement with the recommended value.

For sulfur isotopes, aliquots of native sulfur, cinnabar, or precipitated $BaSO_4$ weighing about 0.5 milligrams were placed in tin capsules for analysis using a Thermo Scientific Flash 2000 elemental analyzer (EA) coupled to a Thermo Delta XP IRMS. For $BaSO_4$, results were

normalized so that results for NBS 127 and IAEA-SO-6 standards in the same autorun gave the delta ($\delta^{34}S$) values recommended by Brand et al. (2014), 21.12 and -34.05 permil, respectively. For cinnabar and native sulfur, results were normalized so that results for the IAEA-S-1 and IAEA-S-2 standards gave the delta values recommended by Brand et al. (2014), -0.3 and 22.62 permil, respectively. Aliquots of IAEA-SO-5 and IAEA-S-1 analyzed as unknowns gave 0.81 +/- 0.04 permil (n=4) and -0.14 +/- 0.01 permil (n=2), respectively, in good agreement with the recommended values. For alunite, the sulfur isotope measurement was made on the $BaSO_4$ precipitate.

For oxygen isotopes, two different methods were used. Silica and kaolinite were reacted with bromine pentafluoride in nickel vessels to produce CO_2 gas (Clayton and Mayeda, 1963) which was then analyzed for oxygen-18 using a Micromass Optima IRMS. Results were normalized so that results obtained for the NBS 28 silica standard gave the delta ($\delta^{18}O$) value recommended by Brand et al. (2014), 9.58 permil. Aliquots of NBS 28 analyzed as unknowns gave 9.6 +/- 0.4 permil (n=2), in good agreement with the recommended value.

Oxygen isotopes in alunite, $BaSO_4$ from alunite, and $BaSO_4$ from sulfate in mine waste were analyzed using a ThermoQuest TCEA coupled to a Thermo Delta XP IRMS. Results for total alunite oxygen and alunite sulfate oxygen were normalized so that results for the $BaSO_4$ standards used by Wasserman et al. (1992) give the $\delta^{18}O$ values determined by them: LSO-1, -16.2 permil, JM: -6.1 permil, JC: 0.1 permil, SG: 9.0 permil; HB: 16.9 permil. Normalized in this way the values are consistent with the alunite-H_2O fractionation factors reported by Stoffregen et al. (1994) which were determined in the U. S. Geological Survey Denver Federal Center laboratory using the same alunite dissolution procedure (Wasserman et al., 1992) and the same Denver Federal Center tap water (deionized).

For calculation of the $\delta^{18}O$ and δD values of the fluids in equilibrium with the minerals analyzed, the fractionation factors of Gilg and Sheppard (1996) were used for $\delta^{18}O_{kaolinite} - H_2O$; Marumo et al. (1980), Gilg and Sheppard (1996) and Sheppard and Gilg (1996) for $\delta D_{kaolinite} - H_2O$; Kita et al. (1984) for $\delta^{18}O_{amorphous\ silica} - H_2O$, and Stroffregen et al. (1994) for $\delta^{18}O_{alunite(OH)} - H_2O$, $\delta^{18}O_{alunite(SO4)} - H_2O$ and $\delta D_{alunite} - H_2O$. These equations were accessed using the AlphaDelta Stable Isotope Fractionation Calculator of Beaudoin and Therrien (2004, 2009; https://alphadelta.ggl.ulaval.ca).

Chapter 4: Results

4.1. Hand Samples and field observations

A catalogue of samples and field observations is presented in Figures 4.1 to 4.3 and Appendices I and II. Results are consistent with past mineralogical studies showing varying degrees of altered andesite with alteration zones between less altered andesite blocks referred to as "veins" comprised almost entirely of kaolinite, alunite, and amorphous silica with native sulfur and cinnabar in places. Zonation is also consistent with past literature, including a major steam-heated zone with amorphous silica and sulfur in stark contrast with a lower boulder zone comprised of altered andesite with abundant veins of kaolinite and alunite (Fig. 1.5). Closer to the more intensely altered rocks it is possible to observe evidence of ongoing active degassing and hydrothermal input as shown by venting in Figure 4.2 (h and i). Figure 4.1 (e) and (f) shows pictures of the unconsolidated sediments that underly the altered andesite flow. Outcrops of this unit do not contain the characteristic "boulders" of the altered andesite zone above although kaolinite-alunite-amorphous silica veins do appear in this layer.

Attack of rock appears to be episodic or multi-staged in nature as shown by the zonation in both veins and exfoliation shells around boulders as seen in figures 4.2 (a)-(e) and 4.1(d) respectively, implying waxing and waning or pulses of hydrothermal fluids forming this alteration over time, this will be expanded upon in the Discussion section below.

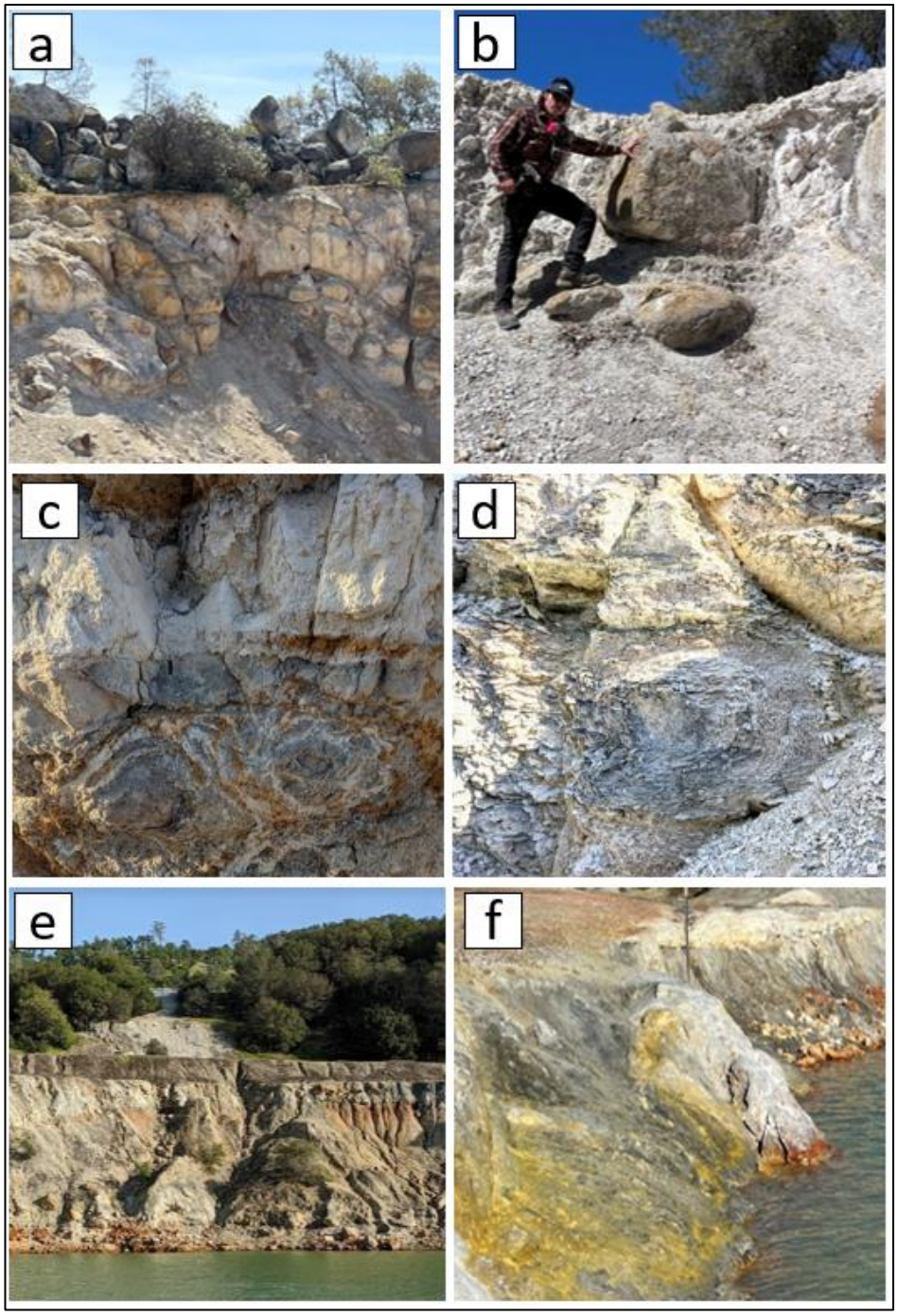

Figure 4.1: Field photographs highlighting zones and outcrop-scale features. (a) & (b) represent the 'Boulder Zone', showing altered andesite with kaolinite-alunite-amorphous silica veins between less altered 'boulders'. (c) shows the sharp transition from the boulder zone to the steam heated zone. (d) displays a "boulder" from within or near the steam-heated zone with exfoliation sphere completely penetrating the boulder which is now primarily residual silica. (e) & (f) are faces that represent Cache creek sediments exposed around the Herman Impoundment.

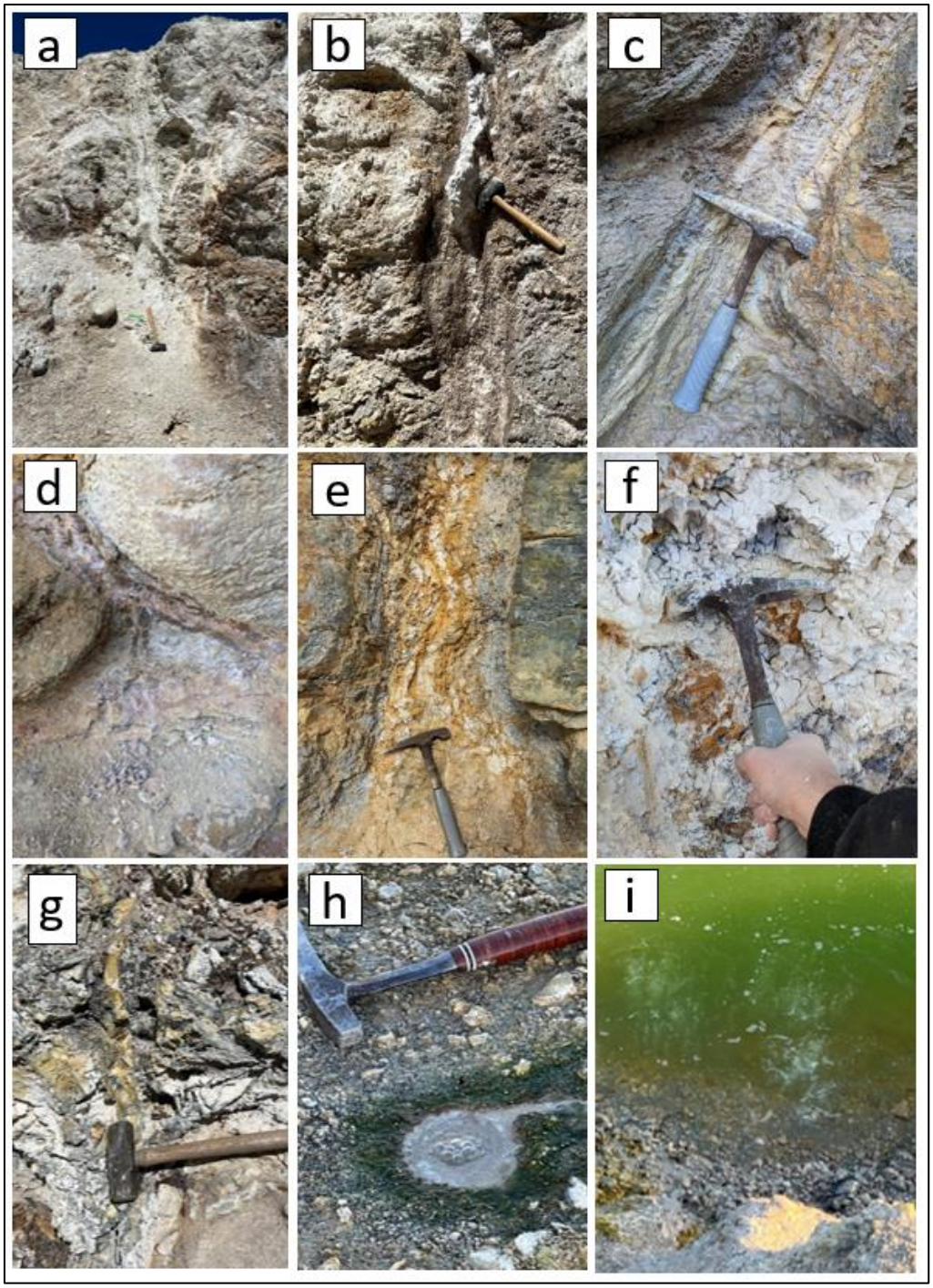

Figure 4.2: Photographs showing vein structure and smaller-scale features. (a)(b)(c) represent typical kaolinite/alunite/amorphous silica veins showing lateral zonation.(f) is residual silica from the steam-heated zone which easily crumbles away. (g) opal horizon from the wall of the Northwest Pit. (h)(i) show active degassing/venting proximal to more highly acid-sulfate attacked areas of the mine.

4.2. IDENTIFICATION AND CHARACTERIZATION OF ALTERATION MINERALS:

XRD analysis has shown the presence of dominantly kaolinite, alunite, and amorphous silica alteration minerals in the "Boulder Zone". Samples suspected to be from the lower unconsolidated sediments show these alteration minerals along with illite, zeolite, and clays. The chemical purity of alunite, kaolinite, and quartz samples was mainly determined by the peaks present in the XRD scans (Fig. 4.3). Where scans only showed peaks from one mineral, or where secondary peaks were vanishingly small compared to primary peaks, the sample was assumed to be of sufficient purity for isotopic analysis. A list of interpreted XRD scans can be found in Appendix II.

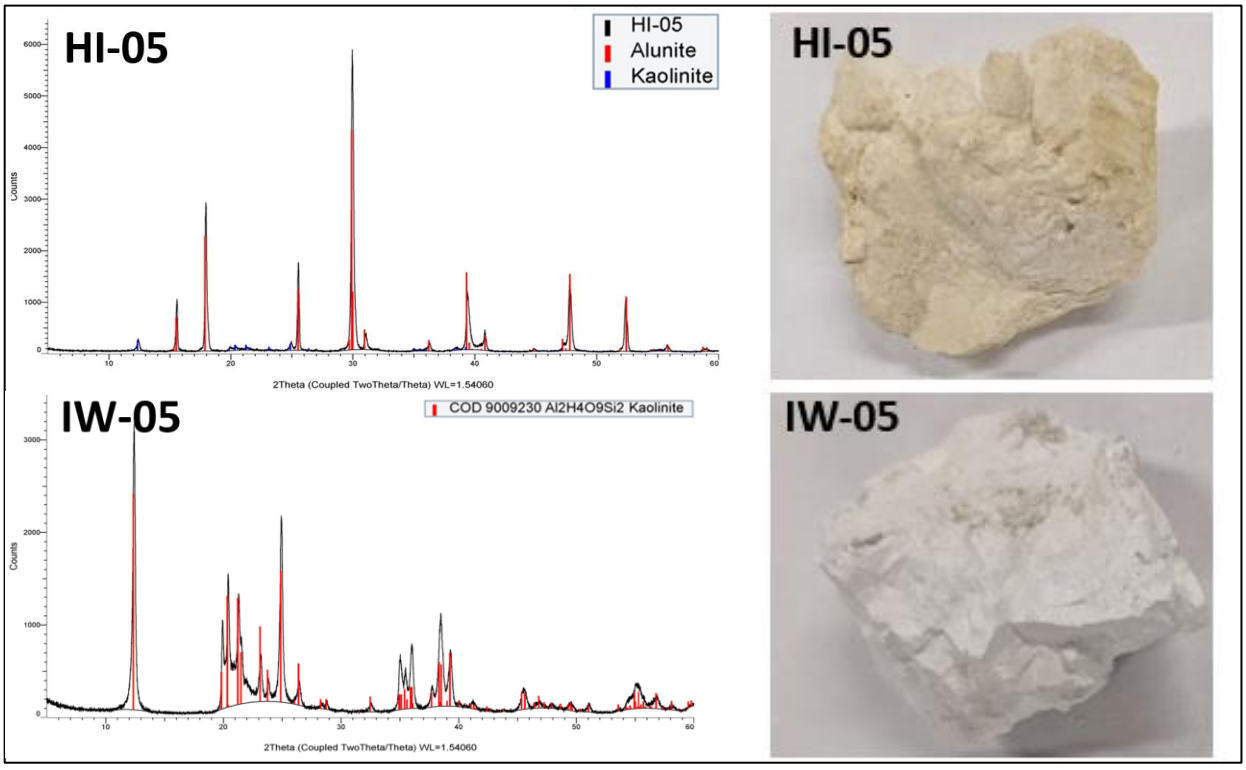

Figure 4.3: Interpreted XRD peaks for monomineralic samples used for SEM and stable isotope analyses (left). Two hand samples representing alunite and kaolinite are compared demonstrating the similarity in appearance and texture (right).

Crystal shape images from SEM confirm the presence of alunite with micro-crystalline pseudo-cubic texture typical of low temperature alunite (Arribas et. al, 1995; Itaya et al., 1996) as well as small cylinders (nanotubes) characteristic of halloysite, a low temperature member of the kaolinite group (Fig. 4.4). Thus the crystal habit of the two main alteration minerals is consistent with a low temperature (< ~120 °C) environment, either supergene or steam-heated. For the purposes of this study, halloysite is usually referred to with the more general mineral name of kaolinite.

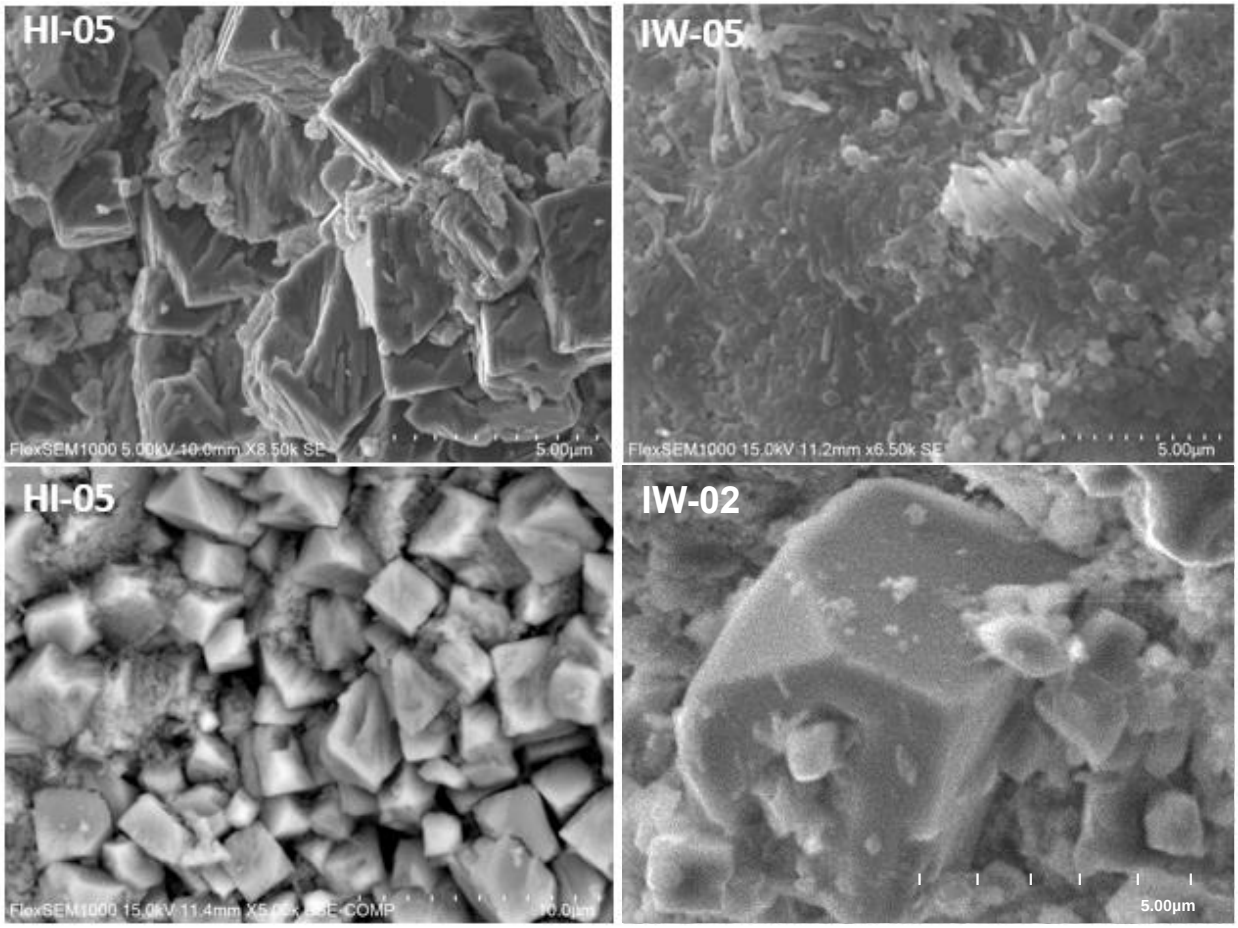

Figure 4.4: Images from the SEM show the micro-crystalline structure, habit, and size of the grains. HI-05 and IW-02 show a pseudo-cubic crystal habit, typical of low temperature alunite, while the sample IW-05 shows tube-like crystals of halloysite, the low-temperature variant of kaolinite.

Alunite XRD spectra from Sulphur Bank showed a variety of peak locations and intensities (Fig. 4.5). Alunite unit cell dimensions calculations (Fig. 4.6; with boxes drawn for unit cell dimensions found in Stoffregen, 2000) support the presence of predominately typical K-rich alunite with some of the Na-rich endmember natroalunite (See Table 4.1 for mineral formulas). These unit cell calculations do not rule out the presence of the hydronium-bearing alunite and thus the slight possibility of isotopic contamination from additional hydronium H or O atoms. For the purposes of this study, these mineral endmembers of the alunite supergroup are referred to as alunite.

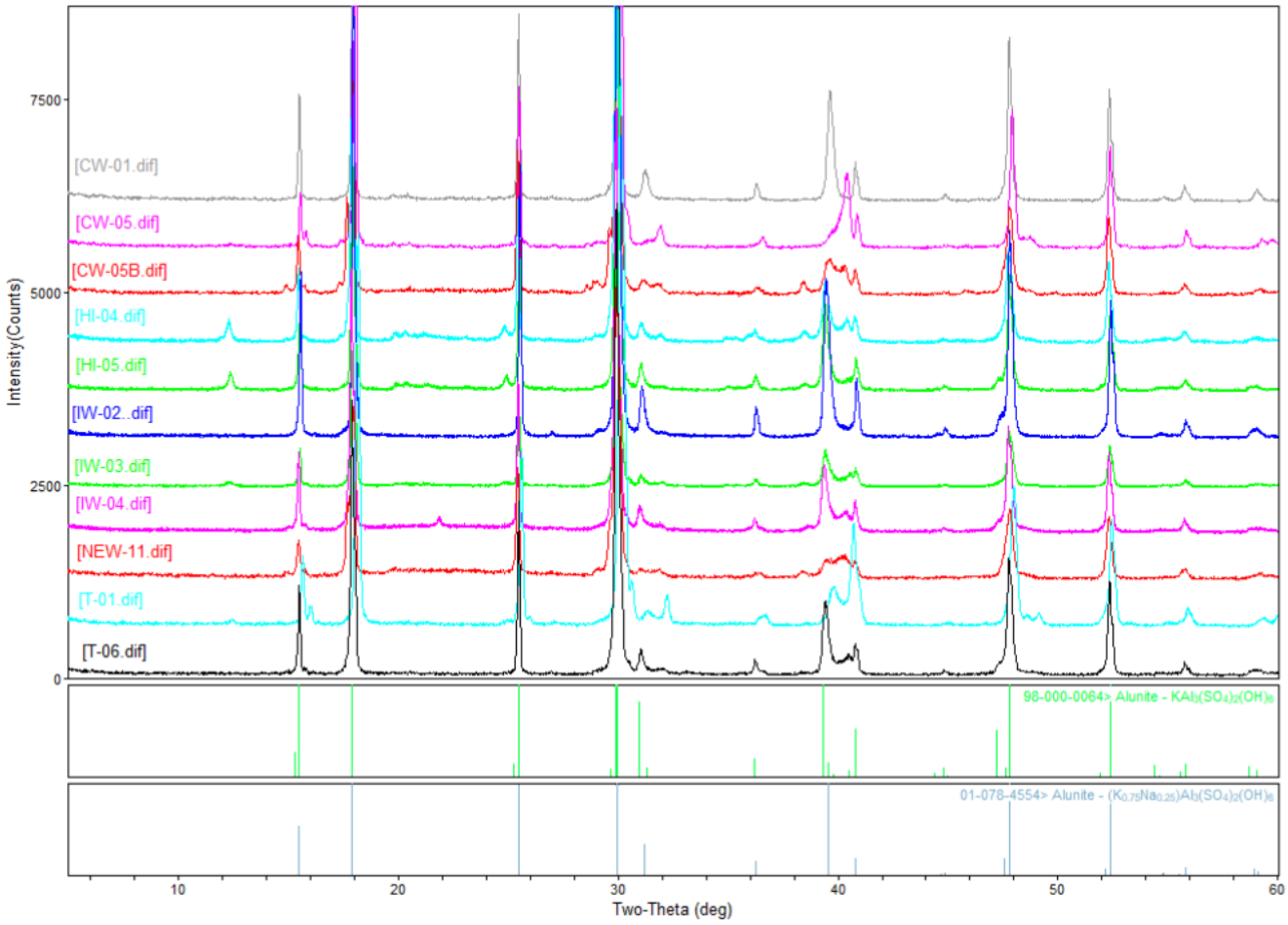

Figure 4.5: Nested XRD peaks interpreted for alunite characterization. Note the slight variations in peak locations and intensities. These peaks were analyzed for cell dimensions displayed in Figure 4.6.

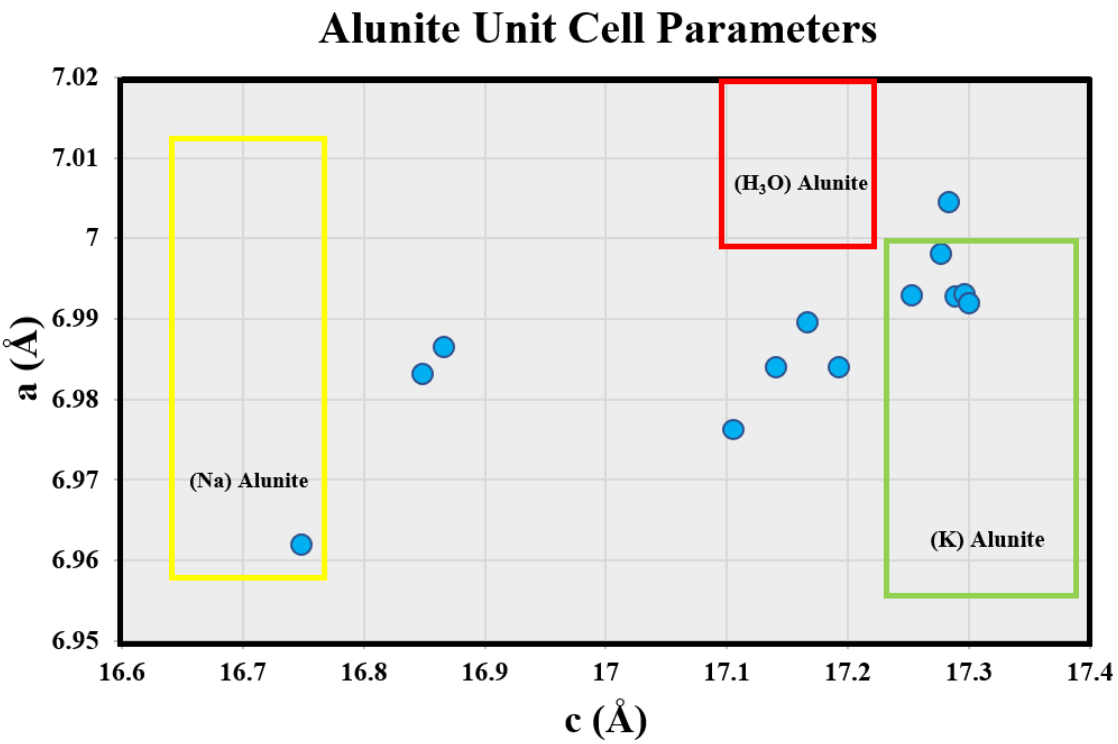

Figure 4.6: Alunite unit cell parameters with colored boxes around end-member alunite-group mineral ratios compiled by Stoffregen, 2000.

Table 4.1: Generalized formulas for some minerals mentioned in this study

Mineral	Generalized formula
Alunite	$KAl_3(SO_4)_2(OH)_6$
Natroalunite	$NaAl_3(SO_4)_2(OH)_6$
Hydronium alunite	$(H_3O)Al_3(SO_4)_2(OH)_6$
Jarosite	$KFe_3(SO_4)_2(OH)_6$
Kaolinite/Halloysite	$Al_2Si_2O_5(OH)_4$
Illite	$(K, H_3O)(Al, Mg, Fe)_2(Si, Al)_4O_{10}(OH)_2 \cdot H2O$
Amorphous Silica	SiO_2
Pyrite	FeS_2
Cinnabar	HgS

4.3. ISOTOPE RESULTS:

A list of all the stable isotope values obtained during this study is shown in Table 4.2. In total, isotopic compositions were obtained from 11 alunite, 8 kaolinite, 3 amorphous silica samples, 4 native sulfur, and 2 cinnabar samples.

Table 4.2: Stable isotope (permil) values collected during this study.

		Mineral							
Sample	**Mineral**	**$\delta^{18}O$**	**δD**	**δD replicate**	**$\delta^{34}S$**	**$\delta^{34}S$ replicate**	**$\delta^{18}O$ (SO4)**	**$\delta^{18}O$ (SO_4) replicate**	**$\delta^{18}O$ (OH) calculated**
NWW-04	Amorphous silica	24.3							
IW-11	Amorphous silica	23.3							
F2A	Amorphous silica	25.2							
NWP-01	kaolinite	10.3	-104						
NWP-04	kaolinite	11.6	-101	-103					
NWW-03	kaolinite	12.7	-120	-126					
NEW-01	kaolinite	12.3	-100						
IW-05	kaolinite	10.2	-101	-99					
T-05	kaolinite	10.1	-100	-98					
T-12	kaolinite	10.5	-101	-101					
WB-01	kaolinite	12.7	-90	-90					
CW-01	alunite		-50	-52	2.8	2.8	7.7		14.1
CW-05	alunite		-44	-44	2.8		7.0		11.6
CW-05B	alunite		-42	-41	2.7		7.0		7.8
HI-04	alunite		-56	-58	0.8		6.4		3.3
HI-05	alunite		-58	-56	1.5		7.3		3.6
IW-02	alunite		-54	-54	0.6		8.3		2.2
IW-03	alunite		-55	-53	0.5		8.9		2.5
IW-04	alunite		-48	-50	0.2		10.7		7.1
NEW-11	alunite		-37	-37	1.9	1.9	8.7		9.4
T-01	alunite		-38	-38	-1.8		4.3		11.7
T-06	alunite		-49	-48	0.6		7.7	6.8	6.5
IW-20 NS	native S				0.9	1.1			
NEW-07 NS	native S				-0.1				
NEW-08 NS	native S				1.3				
IW-18 NS	native S				-2.2				
F3B CIN	Cinnabar				0.9	0.2			
W-O1 CIN	Cinnabar				-0.5	-0.1			

For alunite samples, δD, and $\delta^{18}O_{OH}$ range from -37‰ to -58‰ and 2.2‰ to 14.1‰ respectively. For the alunite SO_4, $\delta^{34}S$ and $\delta^{18}O_{SO4}$ range from -1.8‰ to 2.8‰ and 4.3‰ to 10.7‰ respectively (Figs. 4.7 and 4.8). While $\delta^{18}O_{SO4}$, and $\delta^{34}S$ appear to be relatively tightly clustered

and consistent with equilibration with fluids, there appears to be a spread of $\delta^{18}O_{OH}$ values that suggests disequilibrium or later re-equilibration (Figs. 4.9, 4.10 and 4.11).

Kaolinite hydroxide values show a tight clustering with one outlier with δD and $\delta^{18}O$ values of roughly -90‰ to -110‰ (outlier at -120‰), and 9‰ to 13‰ (Fig. 4.7). Similarly, while there is a small sample size of three, $\delta^{18}O$ values for amorphous silica are consistent with each other at about 23‰ to 25‰ (Fig. 4.7).

$\delta^{34}S$ values show small differences between sulfate minerals averaging +1.0 ±1.3‰ Vienna-Canyon Diablo troilite (VCDT) compared with native sulfur and cinnabar which average around 0.0 ±1.2‰ VCDT (Fig. 4.8).

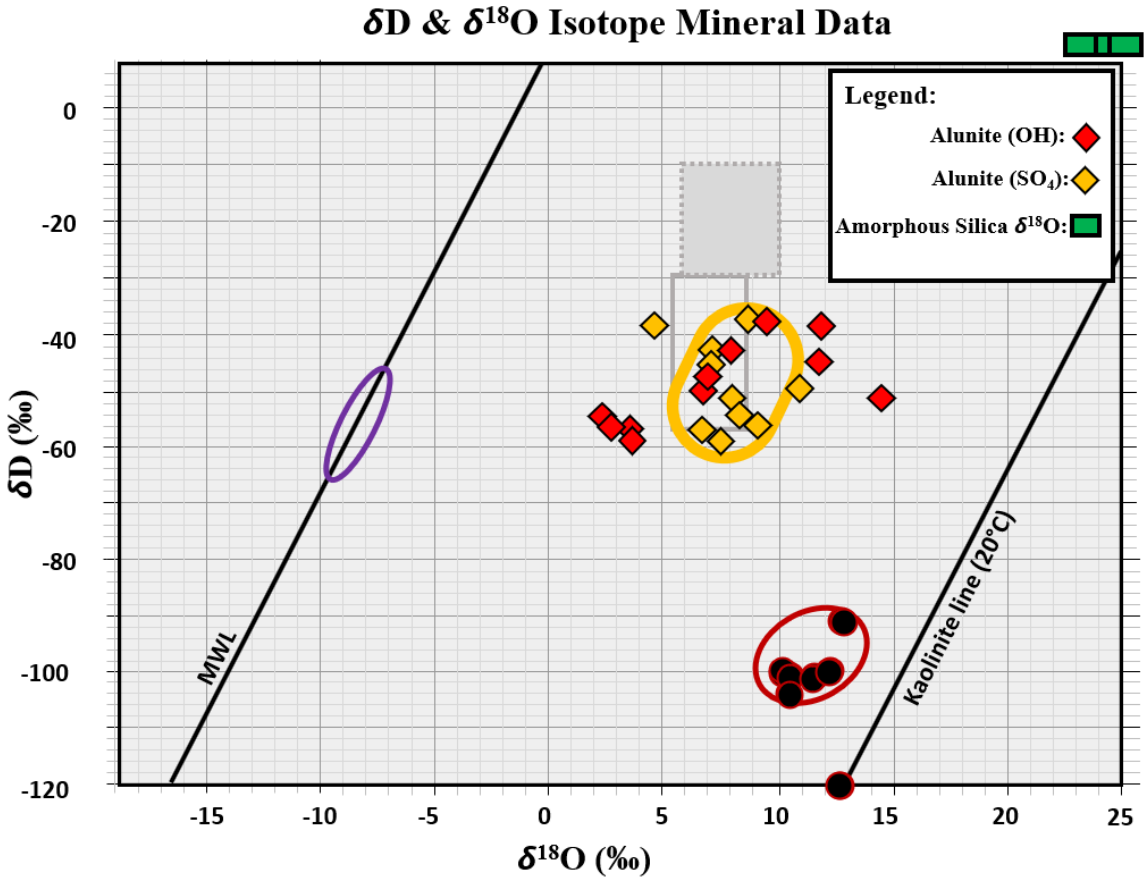

Figure 4.7: Plot of mineral δD-$\delta^{18}O$ measurements from this study (diamonds = alunite, circles = kaolinite, rectangles = opal. Colored circles represent clustering of isotopes. Note that $\delta^{18}O$ for opal samples are shown outside of the δD-$\delta^{18}O$ graph because they do not have a δD value.

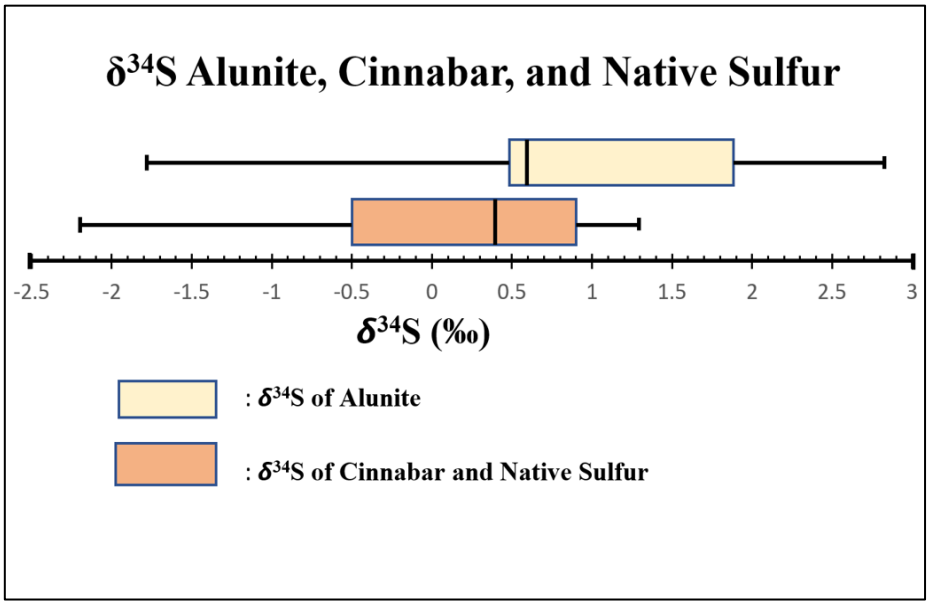

Figure 4.8: Box and whisker plots for $\delta^{34}S$ values comparing those of sulfates to cinnabar and native S.

4.4. ISOTOPIC COMPOSITION OF FLUIDS AND TEMPERATURE CALCULATIONS:

This study used the fractionation factors of Kita et al., (1984), Gilg and Sheppard (1996), Sheppard and Gilg (1996), and Stoffregen et al. (1994) to estimate the isotopic composition of the waters in equilibrium with the different minerals analyzed, alunite, kaolinite and amorphous silica. As shown in Figure 4.9, the $\delta^{18}O$ values of kaolinite waters at roughly ~40 °C plot close to the meteoric water line.

The calculated alunite $\Delta^{18}O_{SO4\text{-}OH}$ fractionation temperatures are shown in Figures 4.10 and 4.11. Only two samples (IW-02 and IW-03; highlighted in green in Figs. 4.10 and 4.11) yield reasonable temperatures of 112 and 127 °C supporting the hypothesis that the $\delta^{18}O_{OH}$ values have been reset in the other nine samples by re-equilibration with ambient waters at lower temperatures. The two

reasonable temperatures obtained from these samples can be used to calculate the parental H_2O shift from standard fractionation factors which also plots the waters along the meteoric water line at the same location as the unevaporated Sulphur Bank meteoric waters reported by Engle et al. (2008). From this calculated $\delta^{18}O$ (H_2O) value of about -8.5‰ (Fig. 4.12; orange oval), a temperature of formation was calculated for the remaining nine using $\Delta^{18}O_{SO4\text{-}OH}$ fractionation factors from Stoffregen et al. (1994). These calculations yield temperatures a series of cooler temperatures from 110 °C down to 20 °C (Fig. 4.13 and Table 4.3).

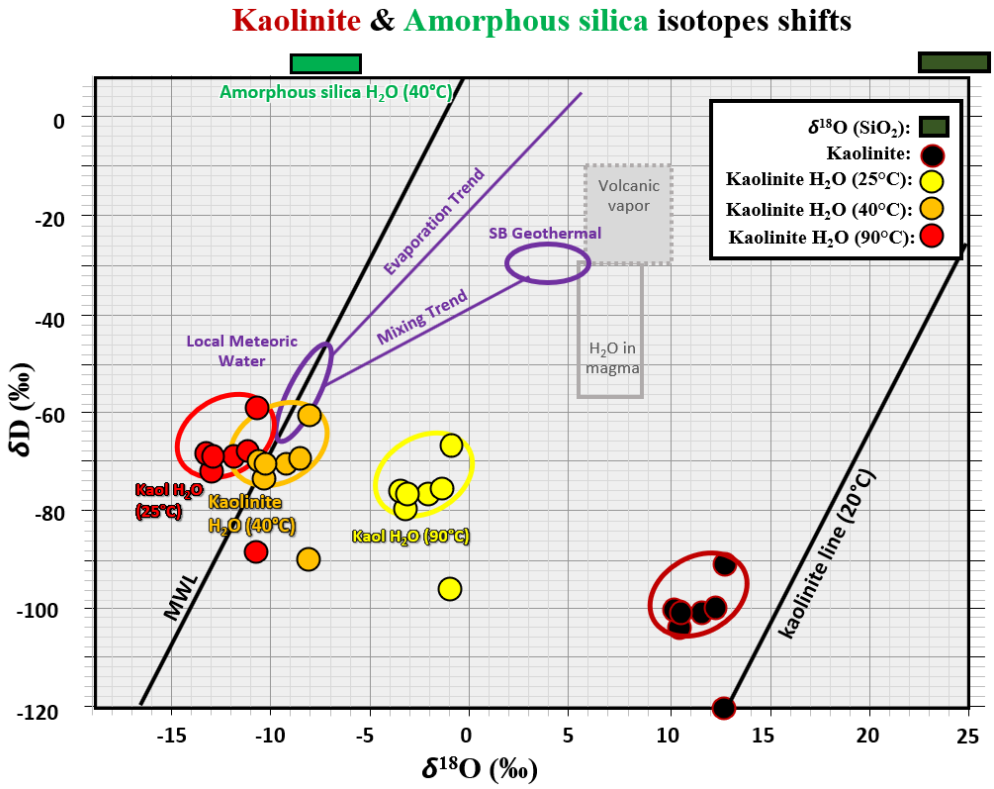

Figure 4.9: Calculated isotope fractionations from kaolinite at several temperatures and amorphous silica at 40° C. Both plot right on the meteoric water line at 40°C.

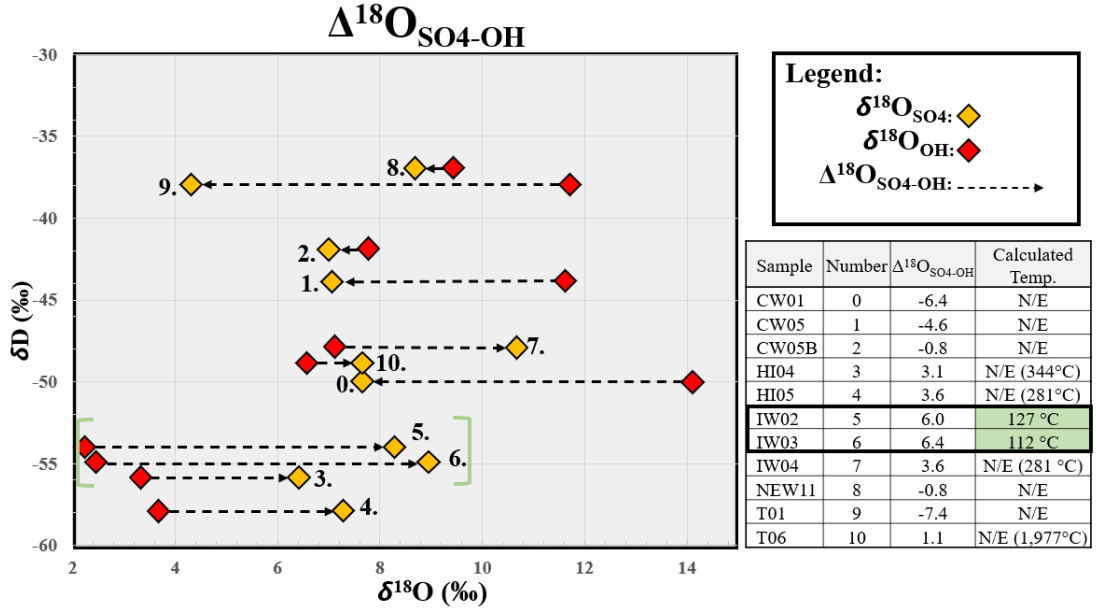

Sample	Number	$\Delta^{18}O_{SO4-OH}$	Calculated Temp.
CW01	0	-6.4	N/E
CW05	1	-4.6	N/E
CW05B	2	-0.8	N/E
HI04	3	3.1	N/E (344°C)
HI05	4	3.6	N/E (281°C)
IW02	5	6.0	127 °C
IW03	6	6.4	112 °C
IW04	7	3.6	N/E (281 °C)
NEW11	8	-0.8	N/E
T01	9	-7.4	N/E
T06	10	1.1	N/E (1,977°C)

Figure 4.10: δD vs $\Delta^{18}O_{SO4-OH}$ plot highlighting $\delta^{18}O$ variation between values from sulfate and hydroxide of the same sample. With the exception of two samples (highlighted in green), the calculated temperatures yield no results or unreasonably hot temperatures and are thus interpreted to be in isotopic disequilibrium with the fluids that initially deposited them. Temperature calculations are shown in table inset.

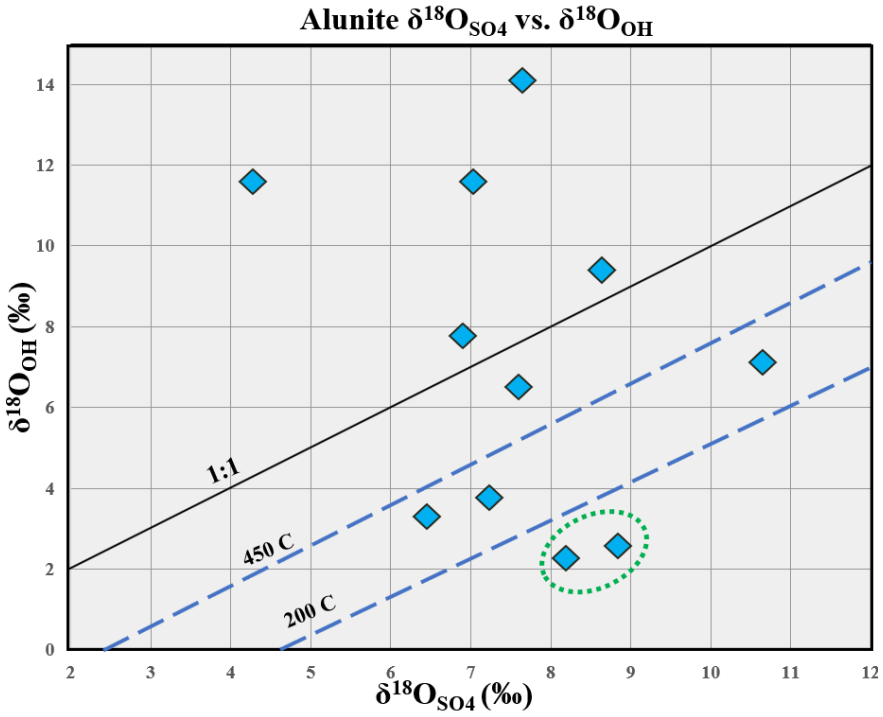

Figure 4.11: Alunite $\delta^{18}O_{SO4}$ vs $\delta^{18}O_{OH}$ plot highlighting variation between values from sulfate and hydroxide of the same sample. See Fig. 4.10 figure caption.

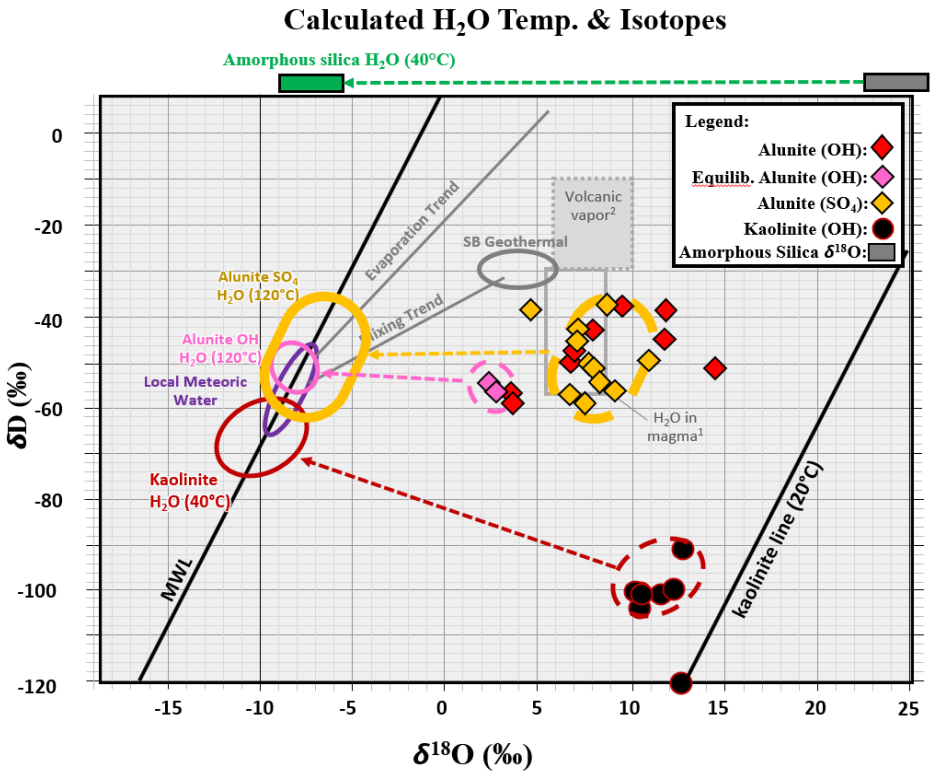

Figure 4.12: Plot with arrows pointing towards the calculated fluid isotopic compositions. For alunite OH, only the values from two samples interpreted to be in equilibrium with their fluids (highlighted in pink) were shifted using proper fractionation factors.

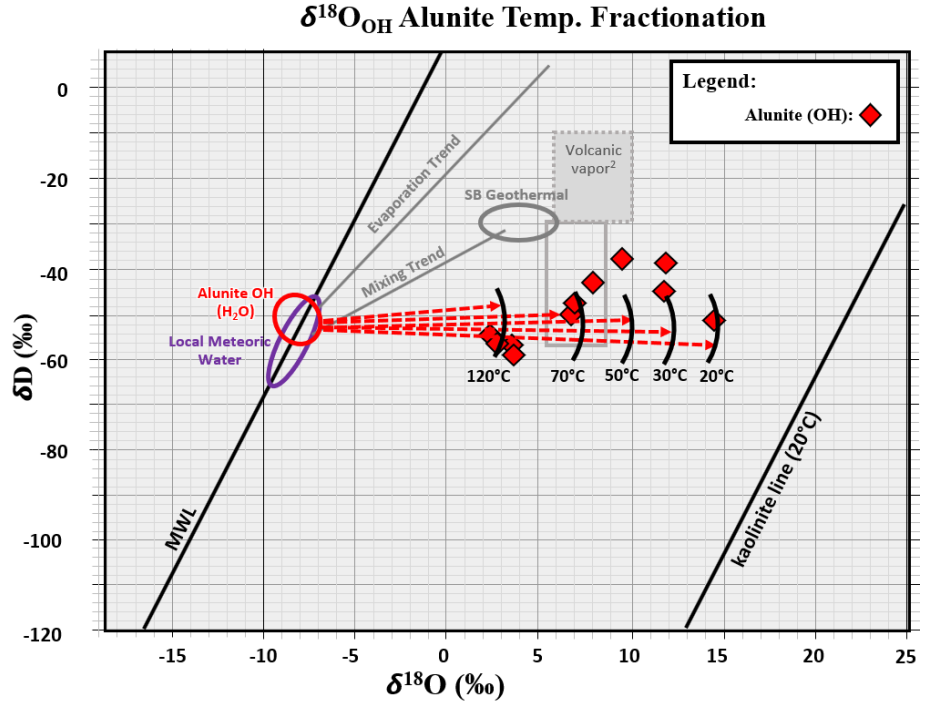

Figure 4.13: In this figure, fraction of the $^{18}O_{alunite}$ values in disequilibrium were measured from the fluid ^{18}O value of the two samples that were in equilibrium to calculate temps. Isotherms were added at regular intervals to aid in the easy understanding of the new values.

Table 4.3: Calculated parental fluid temperatures in this study.

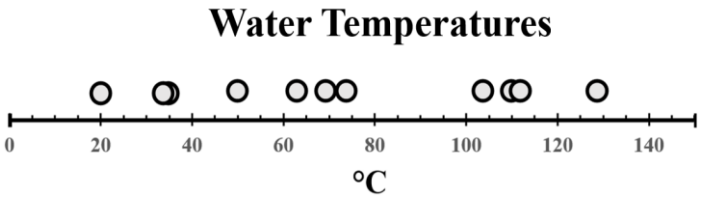

Alunite H_2O Temperature Calculations		
Sample	Direct $\Delta^{18}O_{SO4\text{-}OH}$	Measured $\Delta^{18}O_{SO4\text{-}OH}$
CW-01	N/E	20 °C
CW-05	N/E	35 °C
CW-05B	N/E	63 °C
HI-04	N/E (344 °C)	110 °C
HI-05	N/E (281 °C)	104 °C
IW-02	127 °C	
IW-03	112 °C	
IW-04	N/E (281 °C)	69 °C
NEW-11	N/E	50 °C
T-01	N/E	34 °C
T-06	N/E (1,977 °C)	74 °C

Chapter 5: Discussion

5.1. Fluid Source and Temperature Implications

The $\delta^{34}S$ values of magmatic steam are generally close to 0‰ VCDT or slightly positive in some arcs magmas (Rye et al., 1992; Hedenquist and Arribas, 2022). The $\delta^{34}S$ values of this study from sulfate minerals averaging +1.0 ±1.3‰ and native sulfur + cinnabar around 0.0 ±1.2‰ VCDT are consistent with a magmatic source for the sulfur especially when compared to $\delta^{34}S$ values from pyrite and chalcopyrite in the metasediments of the Franciscan Formation which are significantly lower at –31 and –19 ‰, respectively (Shimizu and Marchall, 2012). The minimal fractionation between sulfates and native sulfur/HgS is also consistent previous studies which observed a similar lack of isotopic fractionation low-temperature alunite formed from oxidizing H_2S in the steam-heated environment (Rye et al., 1992; Hedenquist and Arribas, 2022).

The δD and $\delta^{18}O$ values calculated from stable isotope measurements of this study indicate a primarily meteoric source for the parental hydrothermal fluids. Like various previous studies investigating δD and $\delta^{18}O$ of the Sulphur Bank hydrothermal fluids, no conclusive evidence of magmatic waters is present. Given that most of these samples were obtained from the near surface proximal to or just below the paleowater table, this finding is not surprising and does not preclude evidence for more strongly isotopically shifted δD and $\delta^{18}O$ values from minerals deeper in the system where the Hg and H_2S gasses came from.

Temperature calculations of 20-127° C from these stable isotopes yield values that are consistent with ongoing hydrothermal fluid input currently and historically observed from Sulphur Bank hot springs and monitoring wells (Engle et al., 2008). This implies that the temporal regime of the fluid observed presently behaved similarly throughout the lifespan of this relatively young in system. Furthermore, as shown in Table 4.3, alunite sulfate values and alunite hydroxide values

appear to be deposited at equilibrium with fluids plot at the higher limit of temperatures around 120 °C. Lower temperatures recorded are interpreted to be re-equilibration of alunite hydroxides. This re-equilibration comes from the same hydrothermal fluid at a lower temperature reflecting the episodic nature of fluid/heat input. During isotopic re-equilibration from lower-temperature fluids, oxygen in the hydroxide site exchanges more readily while oxygen in the sulfate site remains unchanged (Rye et al., 1992). This apparent re-equilibration of hydroxides occurred over a nearly continuous span from 110° C to 20° C and these lower temperatures are repeated in the calculated water temperatures of the kaolinite samples. These results for parental water temperature calculations are consistent with findings from stable-isotope systematics studies of the steam-heated acid-sulfate environment by Rye et. al 1992 observed at Yellowstone, Wyoming, Waiotapu, New Zealand, Marysville, Utah, and Tolfa, Italy. However, unlike those analogous locations, the data at Sulphur Bank document the lower temperature re-equilibration of some samples.

5.2. DEPOSIT MODEL AND DISTRICT COMPARISONS

According to the low sulfidation epithermal model described by Hedenquist and Arribas (2000), precious metal mineralization mainly occurs at depths of tens to hundreds of meters below the surface in feeder zones and areas of permeability where boiling occurs over a wide subsurface interval and acts as a mechanism for depositing thio-complexed gold through release of volatiles. Since most of the mining and all of the samples described here are derived from the top 50 meters of the system, gold would not be present unless there was a significant amount of erosion and telescoping that would expose lower mineralized areas to the surface. Given that mineralization at Sulphur Bank is <~45,000 years old and shows no signs of significant erosion, this telescoping and exposure of lower parts of the system has not occurred. If gold does exist in this deposit, it

would be found at deeper levels below the surface in the faults and shear zone which comprise the most mineralized and permeable areas of the host rocks. The nearby McLaughlin mine, which is a classic low sulfidation epithermal deposit (Hedenquist et al., 2000), exhibits this concept with gold mineralization most prevalent at depths of 50-200 meters below the surface, and silver mineralization from 200 to 350 meters below the surface (Sherlock et al., 1995).

It is important to note here that along with a lack of any significant detectable gold anomalies, miners in the late 19th century who descended to the proper depths of roughly 100 to 150 meters below the surface following high-grade mercury zones with underground shafts and drifts did not observe any gold or other appreciable precious metals (Everhart, 1946). Such miners would certainly have been able to recognize any significant amount of gold as there are geological records of the underground workings along with various other historic mines in the district where small amounts of gold were found and exploited (Leconte and Rising, 1882; Enderlin 1993).

Many implications can be made from adding stable isotopes of the acid-sulfate minerals to the Sulphur Bank mercury mine research project since many gold deposits that fit the same low sulfidation epithermal model have their own respective stable isotope studies for comparison. The nearby McLaughlin mine shows a heavier isotopic enrichment with respect to $\delta^{18}O$ than Sulphur Bank and other studied thermal springs. This fluid is also similar to fluids at the gold depositing springs of the Wilbur Springs district (Rytuba, 1993; Sherlock, 2005). Isotope ratios from Sulphur Bank, McLaughlin, and deposits around Wilbur Springs, are all isotopically shifted to reflect heavier $\delta^{18}O$ when compared to non-mineralized hot springs elsewhere in the region; the reason for this is related to isotopic exchange from long travel and residence times in the host rocks. Since Great Valley Sequence host rocks have heavier isotope values than Franciscan sediments from whole-rock analysis, this could explain the isotopically heavier evolved hydrothermal fluids at

McLaughlin and other deposits compared to Sulphur Bank. Another explanation is the possibility of magmatic-sourced fluids mixing with circulating fluids and increasing the isotopic enrichment although it is difficult to prove such a connection through $\delta^{18}O$ and δD values alone, particularly when the evolved hydrothermal fluids show similar enrichments (Sherlock, 2005). Repeated subsurface-boiling has also been proposed to be the reason for isotopic enrichment at Sulphur Bank and other deposits (Donnelly-Nolan et al., 1993). I speculate that all of these factors play a role in the isotopic enrichment of fluids depositing at Sulphur Bank and other local hot-springs, and end-members from the resultant spectrum of isotope enrichment are partly responsible for different mineralization styles.

Mercury-gold deposits occurring primarily in more easterly Great Valley Sequence-hosted deposits of the Northern Coast Ranges district has led some authors to speculate that the Au is related to Great Valley Sequence rocks as a possible source or more favorable conduit (White et al., 1973; Rytuba, 1993). Franciscan-hosted deposits are primarily mercury-only deposits (Rytuba, 1993). The Calistoga district to the west of the Clake Lake area are clearly associated with Franciscan host rocks and thus provide evidence for gold-silver system not hosted in Great Valley sequence rocks. It should be noted however that the Calistoga district host very small and short-lived deposits (Enderlin, 1993). Contained within the Calistoga district are the Palisades and Silverado silver-gold deposits which interpreted to have formed at a deeper paleodepth (Enderlin, 1993) and thus may be analogous to the lower silver-dominated parts of a classic epithermal system such as the silver-dominated deeper roots of the McLaughlin mine. Their existence shows that appreciable gold systems can have formed in Franciscan hosts, albeit smaller and shorter lived when compared to McLaughlin and Cherry-Hill systems. Drilling in The Geysers steam field area

has shown areas with high gold and silver anomalies (Sherlock, 2005). This demonstrates that minor precious-metal enrichment is present in Franciscan Complex hosts.

Since there is no clear evidence of either Franciscan or Great Valley Sequence hosts themselves being a source for the gold enrichment, their ability to transport and distribute metals in long-lived hydrothermal systems (which may or may not periodically receive magmatic input) is more likely the reason for an apparent association with precious metal enrichment. Franciscan sediments are dismembered and metamorphosed often containing lithic wackes and shales making them significantly less permeable than Great Valley Sequence sediments. Units with low permeability within the Franciscan complex also have been speculated to trap fluid in reservoirs that see repeated boiling episodes releasing great amounts of steam and mercury vapor while ponding silicic and possible Au mineralization at depth. Evidence for the existence of such reservoirs has been seen in drilling around the Geysers steam field area (Sherlock, 2005). Circulating fluids in the Franciscan therefore may have a difficult time sustaining the very long-lived systems formed the McLaughlin and Cherry Hill deposits (2.2-.75 Ma and .56-present, respectively; Sherlock, 1995; Pearcy and Petersen, 1990).

The two primary sedimentary hosts can sustain long-lived hydrothermal systems that allow fluid-dominated systems (as opposed to the steam-dominated systems of the Geysers Steam Field) to form to varying degrees. This could be the reason why the Calistoga mines associated with Franciscan hosts are much smaller and shorter lived than the McLaughlin and Cherry hill systems (Enderlin, 1993). Mercury deposits are common in both units since mercury, by nature of traveling in vapor form, can still deposit if permeability causes ponding of potentially precious metal enriching fluids. Precious metal enrichment most-likely favors fluid-dominated systems (such as McLaughlin), which are more common in the Great Valley Sequence units since they are less

complicated mineralogically and structurally and are therefore more permeable. Such sediments are more conducive to sustaining robust long-lived hydrothermal input in the same location over time with favorable channeling locations formed from the base of the Great Valley Sequence near the Coast Range Thrust forming the upper and lower plate which is in contact with the rheologically different coast range ophiolite and increased locally permeability from San Andreas Fault system faults. This long lifespan of hydrothermal systems coupled with dilatant zones related to faults may be the necessary factor for low grade gold-enrichment, and it may be another major reason why gold is not present in the very young Sulphur Bank system.

5.3. TEMPORAL EVOLUTION OF FLUID INPUT

Evidence in this study that points towards the episodic nature of hydrothermal input includes laterally-zoned replacement zones of alteration with more intense development of alteration in the middle of the structure (often referred to as "veins" by Wells & Ghiorso 1988 due to appearance), and dramatic exfoliation shell textures in the boulder zone at Sulphur Bank. Sims and White (1981) showed evidence for at least 6 prior peaks of mercury in Clear Lake sediments from Oaks Arm adjacent to Sulphur Bank at 34, 23.3, 18, 9.5, 7.4, and 3.6 thousand years before the present. These spikes demonstrate that natural mercury deposition dramatically increases periodically. These increases are most likely due to temporary increases in permeability along local faults related to seismic activity with the natural assumption that there is little change in major fluid source or heat regime over the short lifespan of the Sulphur Bank mercury mine hydrothermal system. Varekamp and Waibel have speculated that these mercury spikes in the sediments are promising paleoseismic indicators due to the association of seismic activity and increased permeability along local faults. This phenomenon is also noted to affect the behavior of geysers such as the Calistoga geyser during local seismic activity (Enderlin, 1993).

The episodic nature of epithermal input and mineralization is also recorded in the multi-stage veining at McLaughlin hosting ore in a sheeted vein complex Cherry Hill ore in 13 stages of veining. In the case of Cherry Hill, only three of these stages are observed to have gold mineralization (Pearcy and Peterson, 1990). Pearcy also demonstrates the evolution temporal and chemical evolution of the Cherry Hill fluids over time, pointing out a gradual decrease in temperature and increase in gold content. This observation shows that while hydrothermal fluid mineralization is frequent, gold mineralization only occurs intermittently. A possible cause for this is periodic gold-bearing magmatic fluids joining the hydrothermal fluid. Seismic events occasionally changing permeability could temporarily and periodically introduce such magmatic fluids. Extending this concept to Sulphur Bank, the fluid pulses recorded in the local rocks may only represent an early gold-free stage that could evolve into a gold-mineralizing system with enough time and possibly magmatic input or evolution of fluid regime or gradual shift to fluids with a greater capacity to complex and transport dilute gold. Alternatively, past seismic events increasing permeability and thus fluid flow could create short-lived pulses of increased fluid flow with resultant higher temperatures and increased ability to concentrate minor amounts of gold from surroundings to deposit in favorable settings.

While previous studies have failed to show definitive isotopic and compositional evidence of magmatic input, $\delta^{34}S$ values from this study show that there is a high probability of magma-sourced volatiles as opposed to S being sourced from the local rock formations where the mercury and bulk of the fluid isotopes are believed to be sourced from. This magmatically-source sulfur would greatly increase the fluids' ability to complex dilute gold from the surroundings and thus periods of more active degassing from shallow magma chambers may be a cause for periodic gold-enrichment seen in other more mature systems, although this process is hindered by Franciscan

rocks hosting less favorable conduits to the surface causing possibly gold-enriching fluids to pond and boil at depth releasing only steam with H_2S, CO_2, and Hg^0 permitting only mercury-enrichment in the near surface.

Chapter 6: Conclusions

6.1. SUMMARY AND CONCLUSIONS

Stable isotopes values and associated fluid calculations and temperature calculations from this study provide new insights into the evolution and nature of fluids at Sulphur Bank. $\delta^{34}S$ values near 0 VCDT strongly point towards a magmatic, rather than sedimentary source for the H_2S gasses that formed the alunites, cinnabar, and native sulfur. This along with previously observed He^3 anomalies is strong evidence that magmatic or mantle-derived volatiles are being present at the Sulphur Bank mercury mine.

Alunite samples have intramineral $\delta^{18}O$ values in equilibrium and disequilibrium with depositing fluid indicating the fluid evolved into a lower-temperature fluid that overprinted alteration minerals and re-equilibrated the hydroxide values thus recording the lower temperatures in calculations from observed fractionation. This is recorded calculated depositional temperatures ranging from 110-120° C to 20° C. I interpret that sulfate alteration minerals (all) formed within a steam-heated environment at a typical T ~120° C, then, as the system cooled, the O in OH re-equilibrated with essentially the same (meteoric) that had cooled down with time. The re-equilibration happened over the entire temperature interval of 120° C and 20° C, with more samples in the 40-60° C range, demonstrating a gradual shift from initial hotter temperatures to cooler overprinting temperatures of the same fluid possibly indicating zonation and/or waxing and waning of hydrothermal fluid conduits. The δD and $\delta^{18}O$ values calculated for parental fluids are consistent with a primarily meteoric water source which is consistent with the steam-heated zone and near surface setting observed and expected in the acid-sulfate deposit model. Fluids depositing alunite in equilibrium is consistent with isotopes recorded in similar steam-heated acid sulfate environments around the world reported by Rye et al. 1992, although this study expands on these

observations by showing the presence of alunites both in equilibrium and disequilibrium with evidence of re-equilibration of the hydroxide site at lower temperatures.

Field observations are both consistent with past mineralogical studies at the site and the steam-heated acid-sulfate condensate environment described by Hedenquist and Arribas (2022). If Au is present in this system, it would therefore be located below the current workings of the abandoned mine where the ascending fluids begin to boil at depths of roughly 50-300 meters as is seen in nearby gold deposits like McLaughlin. Within the region there exists evidence for impermeable reservoirs ponding fluids in Franciscan rocks causing subsurface boiling while trapping hydrothermal fluids releasing the volatiles that permit alteration, isotopic enrichment, and mercury-enrichment, but not gold deposition in the near surface environment. This is a possible explanation for the rich Hg deposition but lack of gold at Sulphur Bank. Another possibility is the fact the young hydrothermal system needs more time to evolve fluid conditions which more effectively transport gold to the feeder system along with favorable magmatic and seismic conditions to create episodes of Au input.

6.2 FUTURE WORK:

Future studies could investigate stable isotopes further by sourcing alteration minerals from deeper in the system where values might be more indicative of the isotopically shifted hydrothermal waters observed from wells and springs. More complete isotopic studies could also be performed on other mercury deposits near Clear Lake for further comparison to epithermal gold-bearing systems and hot-springs in other districts to better understand fluid sourcing implications from stable-isotope analysis. While there are multiple studies comparing δD and $\delta^{18}O$ values in the area, there could be a more comprehensive look into $\delta^{34}S$ in other systems.

It is possible to use Ar-Ar dating to date the young alunites at Sulphur Bank and possibly link alunite formation to historic mercury spikes in Clear Lake sediments as well as derive paleoclimate implications from the associated δD and $\delta^{18}O$ isotope value. Due to the very microcrystalline nature of the alunite however, refractory losses of potassium and argon from traditional techniques (Stoffregen et al., 1994b) would be too great requiring a difficult and time-consuming encapsulation process that has not been performed before, preventing the use of this method in this study. It is possible that future studies could explore this process further.

References

Arribas, A., Cunningham, C., Rytuba, J., Rye, R., Kelly, W. 1995, Geology, geochronology, fluid inclusions, and isotope geochemistry of the Rodalquilar Au- alunite deposit, Spain. Economic Geology, 90, 795-822.

Beaudoin, G. and Therrien, P., 2004. The web stable isotope fractionation calculator. Handbook of stable isotope analytical techniques, 1, pp.1045-1047

Brand WA, Coplen TB, Vogl J, Rosner M, and Prohaska T, 2014, Assessment of international reference materials for isotope-ratio analysis (IUPAC Technical Report): Pure and Applied Chemistry 86, 425-467.

Clayton RN and Mayeda TK, 1963, The use of bromine pentafluoride in the extraction of oxygen from oxides and silicates for isotopic analysis: Geochimica et Cosmochimica Acta 27, 43-52.

Crede, L.S., Evans, K.A., Rempel, K.U., Brugger, J., Etschmann, B., Bourdet, J. and Reith, F., 2020, Revisiting hydrocarbon phase mobilization of Au in the Au–Hg McLaughlin Mine, Geysers/Clear Lake area, California: Ore Geology Reviews, v. 117, 103218.

D.C. Circuit Court, 1992. Bradley Mining Company v. Environmental Protection Agency 938 F.2d 1299, 1302-05. p.1

Donnelly-Nolan, J.M., Burns, M.G., Goff, F.E., Peters, E.K., Thompson, J.M., 1993, The Geysers-Clear Lake, California; Thermal waters, mineralization, volcanism, and geothermal potential: Economic Geology, v. 88, p. 301-316.

Enderlin, D. A., 1993, Epithermal precious metal deposits of the Calistoga mining district Napa County, California, in Rytuba, J. J., ed., Active geothermal systems and gold-mercury deposits in the Sonoma-Clear Lake volcanic fields, California: Soc. Econ. Geol. Guidebook Series

Engle, M.A., Goff, F., Jewett, D.G., Reller, G.J. and Bauman, J.B., 2008, Application of environmental groundwater tracers at the Sulphur Bank Mercury Mine, California, USA. Hydrogeology Journal, 16(3), pp.559-573.

Everhart, D.L., 1946. Quicksilver Deposits at the Sulphur Bank Mine, Lake County, California. California Journal of Mines and Geology, v. 42, p. 125-153.

Giggenbach, W.F., 1992. Isotopic shifts in waters from geothermal and volcanic systems along convergent plate boundaries and their origin. Earth and planetary science letters, 113(4), pp.495-510.

Gilg, H.A., and Sheppard, S.M.F., 1996, Hydrogen isotope fraction between kaolinite and water revisited: Geochimica et Cosmochimica Acta, v. 60, p. 529-533.

Goff F, Janik C.J., Stimac, J.A., 1995, Sulphur Bank Mine, California: an example of a magmatic rather than metamorphic hydrothermal system?: In Proceedings at the World Geothermal Conference, Florence, Italy, v. 2m p. 1105-1110.

Gustafson, D.L., 1991. Anatomy of a discovery: the McLaughlin gold mine, Napa, Yolo, and Lake counties, California. Economic Geology, Monograph 8, p. 350–359.

Hammack, R.W., and Mabie, J.S., 2002, Airborne EM and magnetic surveys find fault(s) with Sulphur Bank Mercury Mine Superfund site: The Leading Edge, v. 21, p. 1092–

1095.

Hammack, R.W., Sams, J.I., Veloski, G.A. and Mabie, J.S., 2003. Geophysical Investigation of the Sulphur Bank Mercury Mine Superfund Site, Lake County, California. Mine Water and the Environment, 22(2), p.69.

Hearn Jr., B.C., Donnelly, J.M., Goff, F.E., 1995. Geologic map and structure sections of the Clear Lake volcanics, northern California. US Geological Survey Miscellaneous Investigation Series Map I-2362

Hearn Jr, B.C., Donnelly-Nolan, J.M. and Goff, F.E., 1981. The Clear Lake volcanics: Tectonic setting and magma sources. US Geol. Surv. Prof. Pap, 1141, p.25-45.

Hearn Jr., B.C., McLaughlin, R.J., Donnelly-Nolan, J.M., 1988, Tectonic framework of the Clear Lake Basin, *in* Sims, J.D. (Ed.), Late Quaternary Climate, Tectonism, and Sedimentation in Clear Lake, Northern California Coast Ranges: Geological Society of America Special Paper 214, p. 9–20.

Hedenquist, J.W., Arribas, A., 2022, Exploration Implications of Multiple Formation Environments of Advanced Argillic Minerals, Economic Geology, v. 117, no. 3, pp. 609–643.

Itaya, T., Arribas, A., Okada, T., 1996, Argon release systematics of alunite based on stepwise heating experiments from 100 to 1000°C. Geochimica et Cosmochimica Acta, 22, 4525-4535.

Jew, A.D., Kim, C.S., Rytuba, J.J., Gustin, M.S. and Brown Jr, G.E., 2011. New technique for quantification of elemental Hg in mine wastes and its implications for mercury evasion into the atmosphere. Environmental science & technology, 45(2), p.412-417.

Johnson, C.A., Muller, D.E., Alpers, C.N., and Arribas, A., in preparation, Stable isotope analyses of minerals and mine waste at Sulphur Bank mercury mine, Lake County, California: U.S. Geological Survey data release.

Kim, C.S., Bloom, N.S., Rytuba, J.J. and Brown, G.E., 2003. Mercury speciation by X-ray absorption fine structure spectroscopy and sequential chemical extractions: a comparison of speciation methods. Environmental science & technology, 37(22), p.5102-5108.

Kita, I., Taguchi, S. & Matsubaya, O. Oxygen isotope fractionation between amorphous silica and water at 34–93°C. Nature 314, 83–84 (1985).

LeConte, J. and Rising, W.B., 1882. The phenomena of metalliferous vein formation now in progress at Sulphur Bank, California. American Journal of Science, 3(139), p.23-33.

Lowry, G.V., Shaw, S., Kim, C.S., Rytuba, J.J. and Brown, G.E., 2004. Macroscopic and microscopic observations of particle-facilitated mercury transport from New Idria and Sulphur Bank mercury mine tailings. Environmental Science & Technology, 38(19), p.5101-5111.

MacGowan, D.J., 1867, The Borax Lake and Sulphur Banks in Napa Valley, California: American Journal of Pharmacy (1835-1907), p. 155

Marumo, K., 1989, Genesis of kaolin minerals and pyrophyllite in Kuroko deposits of Japan: Implications for the origin of the hydrothermal fluids from mineralogical and stable isotope data: Geochimica et Cosmochimica Acta, v. 53, p. 2915-2924.

Pearcy, E.C. and Petersen, U., 1990, Mineralogy, geochemistry and alteration of the Cherry Hill, California hot-spring gold deposit: Journal of Geochemical Exploration, v. 36,

p.143-169.

Pickthorn, W.J., 1993. Relation of hot-spring gold mineralization to silica-carbonate mercury mineralization in the Coast Ranges, California. Eureka, 122, p.00.

Rye, R.O., Bethke, P.M. and Wasserman, M.D., 1992. The stable isotope geochemistry of acid sulfate alteration. Economic Geology, 87(2), pp.225-262.

Rye, R.O., 2005, A review of the stable-isotope geochemistry of sulfate minerals in selected igneous environments and related hydrothermal systems: Chemical Geology, v. 215(1-4), p. 5-36.

Rytuba, J.J., 1993. Epithermal precious-metal and mercury deposits in the Sonoma and Clear Lake volcanic fields, California. Guidebook. S. 16, p. 38–51.

Rytuba, J.J., Hothem, R.L., May, J.T., Kim, C.S., Lawler, David, and Goldstein, D., 2009, Environmental impact of the Contact and Sonoma mercury mines on water, sediment, and biota in Anna Belcher and Little Sulphur Creek watersheds, Sonoma County, California: U.S. Geological Survey Open-File Report 2008-1381, 76 p. [https://pubs.usgs.gov/of/2008-1381/].

Savin, S.M. and Epstein, S., 1970. The oxygen isotopic compositions of coarse grained sedimentary rocks and minerals. Geochimica et Cosmochimica Acta, 34(3), pp.323-329.

Schuette, C.N., 1931. Quicksilver (No. 335). US Government Printing Office. V. 331-340, p. 86-88

Seal, R.R., Alpers, C.N., Rye, R.O., 2000, Stable isotope systematics of sulfate

minerals: Reviews in Mineralogy and Geochemistry, v. 1, 40(1), p. 541-602.

Sheppard, S.M. and Gilg, H.A. and 1996. Hydrogen isotope fractionation between kaolinite and water revisited. Geochimica et Cosmochimica Acta, 60(3), p.529-533.

Sherlock, R.L., 2005. The relationship between the McLaughlin gold–mercury deposit and active hydrothermal systems in the Geysers–Clear Lake area, northern Coast Ranges, California. Ore Geology Reviews, 26(3-4), p.349-382.

Sherlock, R.L., Tosdal, R.M., Lehrman, N.J., Graney, J.R., Losh, S., Jowett, E.C., Kesler, S.E., 1995, Origin of the McLaughlin mine sheeted vein complex: metal zoning, fluid inclusion and isotopic evidence: Economic Geology, v. 90, p. 2156 – 2181.

Shimizu and Marchall, 2012, Sulfur isotopes in subduction systems and the global sulfur cycle, DOEI project #15140, "Global Sulfur Cycle"

Sims, J.D., and White, D.E., 1981, Mercury in the sediments of Clear Lake, in McLaughlin, R.J., and Donnelly-Nolan, J.M., eds., Research in The Geysers-Clear Lake geothermal area, northern California: U.S. Geological Survey Professional Paper 1141, p. 237-241.

Smith, C.N., 2010. Isotopic geochemistry of mercury in active and fossil hydrothermal systems. PhD thesis, University of Michigan.

Smith, C.N., Kesler, S.E., Blum, J.D. and Rytuba, J.J., 2008. Isotope geochemistry of mercury in source rocks, mineral deposits and spring deposits of the California Coast Ranges, USA. Earth and Planetary Science Letters, 269(3-4), pp.399-407.

Stimac, J.A., Goff, F., Wohletz, K., 2001, Thermal modeling of the Clear Lake magmatic hydrothermal system, California, USA: Geothermics, v. 30, p. 349–390.

Stoffregen RE, Rye RO, and Wasserman MD, 1994, Experimental studies of alunite: I. 18O-16O and D-H fractionation factors between alunite and water at 250-450 degrees C: Geochimica et Cosmochimica Acta, 58, 903-916.

Stoffregen, R.E., Rye, R.O. and Wasserman, M.D., 1994. Experimental studies of alunite: II. Rates of alunite-water alkali and isotope exchange. Geochimica et Cosmochimica Acta, 58(2), p.917-929

Studemeister, P.A., 1984, Mercury deposits of western California: An overview. Mineralium Deposita, v. 19, p.202-207.

Suchanek, T.H., Eagles-Smith, C.A., Slotton, D.G., Harner, E.J. and Adam, D.P., 2008. Mercury in abiotic matrices of Clear Lake, California: human health and ecotoxicological implications. Ecological Applications, 18(8) Supplement, 2008, p. A128–A157

Taylor, B., 1992. Degassing of H2O from rhyolite magma during eruption and shallow intrusion, and the isotopic composition of magmatic water in hydrothermal systems. Chishitsu Chosajo Hokoku (Report, Geological Survey of Japan), 279.

The Rietveld method: Edited by R. A. Young. Oxford University Press, Oxford/New York (1993), 298 pp./ Young, R.A., 1993. The Rietveld method (Vol. 5, p. 1-38). International union of crystallography.

United States Environmental Protection Agency, 2019 United States Environmental Protection Agency, 2019, Sulphur Bank Mercury Mine Superfund Site, Retrieved: retrieved

April 20, 2023 https://resources.ca.gov/CNRALegacyFiles/wp-content/uploads/2019/06/2-EPA-Sulphur-Bank-Presentation.pdf

Varekamp, J.C. and Waibel, A.F., 1987. Natural cause for mercury pollution at Clear Lake, California, and paleotectonic inferences. Geology, 15(11), p.1018-1021.

Wasserman MD, Rye RO, Bethke PM, and Arribas A, Jr., 1992, Methods for separation and total stable isotope analysis of alunite: US Geological Survey Open-File Report 92-9, 20 p.

White and Roberson 1962 White, D.E., and Roberson, C.E., 1962. Sulphur Bank, California: a major hot-spring quicksilver deposit, in Engel, A.E.J., James, H.L., and Leonard, B.F., (Eds) Petrologic studies: a volume to honor AF Buddington: Geological Society of America, p. 397–428

White, D.E., Barnes, I. and O'Neil, J.R., 1973. Thermal and mineral waters of nonmeteoric origin, California Coast Ranges. Geological Society of America Bulletin, 84(2), p.547-560.

Appendix I: Samples

Catalog of hand samples with sample name, minerals identified through XRD analysis, and a physical description. Mineral abbreviations: Alg = alunogen, Alm = alum, Aln.= alunite, Bud = buddingtonite, Cop = copiapite, Ctb = cristobalite, Gyp = gypsum, Hg = cinnabar, Ill = illite, Mes = mesolite, Nat = natrolite, Qtz = quartz, S = sulfur

Sample label	Location	Date collected	Analysis type	XRD identified peaks	Stable isotopes	Description
20220401 NP1	Northwest Pit	3/31/22				gray/tan opal
20220401 NP1	Northwest Pit	3/31/22				gray/tan opal
20220401 NP1	Northwest Pit	3/31/22				gray/tan opal
20220401 NP2	Northwest Pit	3/31/22	XRD	Hg-Kao-S-Ctb		gray/brown clay w/ yellow,red,black
20220401 NP3	Northwest Pit	3/31/22	XRD	Aln-Kao-S-Ctb		yellow/white friable
20220401 WO1	West Ore Pile	3/31/22				opal/cristobalite
20220401 WO1	West Ore Pile	3/31/22				opal/cristobalite
20220401 WO1	West Ore Pile	3/31/22	XRD	Hg-Ctb	yes	Vein with Cinnabar
20220401 WO2	West Ore Pile	3/31/22	XRD	Ctb-Hg		opal/kaolinite with red stain
22SBM-HI-01	Herman Impoundment north Bank	3/31/22	XRD	Alm-Ill-S-Qtz-Mes-Cop		yellow Sulfur crust
22SBM-HI-02	Herman Impoundment north Bank	3/31/22	XRD	Qtz-Ill-S-Kao-Ctb		crumbly black rock
22SBM-HI-02	Herman Impoundment north Bank	3/31/22	XRD	Qtz-Ill-Alm-S		crumbly black rock from smoker
22SBM-HI-03	Herman Impoundment north Bank	3/31/22	XRD	Kao-Mon-Aln		friable white/tan rock, and andesite
22SBM-HI-04	Herman Impoundment north Bank	3/31/22	XRD, SEM	Aln-Kao	yes	tan friable rocks
22SBM-HI-05	Herman Impoundment north Bank	3/31/22	XRD, SEM	Aln-Kao	yes	tan friable rocks
22SBM-HI-06	Herman Impoundment north Bank	3/31/22	XRD	Qtz-S-Ill-Nat		black crumbly rocks
22SBMM-IW-01	Impoundment Wall Trench Area	4/1/22	XRD	Kao-Aln		Alunite/Kaolinite Vein
22SBM-IW-02	Impoundment Wall Trench Area	4/1/22	XRD, SEM	Aln	yes	Alunite vein center
22SBM-IW-03	Impoundment Wall Trench Area	4/1/22	XRD	Aln-Kao	yes	Alunite vein center
22SBM-IW-04	Impoundment Wall Trench Area	4/1/22	XRD	Aln-Ctb	yes	Alunite vein center
22SBM-IW-05	Impoundment Wall Trench Area	4/1/22	XRD, SEM	Kao	yes	Kaolinite vein center
22SBM-HIW-06	Herman Impoundment north Bank	4/1/22	XRD	Alg-Aln-Kao		tan/white with red specs
22SBM-IW-07	Impoundment Wall Trench Area	4/1/22	XRD	Gyp		coarse gypsum crystals
22SBM-IW-08	Impoundment Wall Trench Area	4/1/22	XRD	Kao-Gyp-Aln		Vein center and Andesite from side
22SBM-IW-09	Impoundment Wall Trench Area	4/1/22	XRD	Kao-Aln-Gyp		Kaolinite/Alunite Vein
22SBM-IW-10	North of Impoundment bank	4/1/22	XRD	Aln-Kao-Alg		vein with green spots
22SBM-IW-11	North of Impoundment bank	4/1/22	XRD	Ctb-S		Cristobalite vein
22SBM-IW-12	North of Impoundment bank	4/1/22	XRD	Ctb-S		Cristobalite vein
22SBM-IW-12	North of Impoundment bank	4/1/22	XRD	Ctb-S		Cristobalite vein
22SBM-IW-13c	North of Impoundment bank	4/1/22				Andesite Blocks
22SBM-IW-14	North of Impoundment bank	4/1/22				yellow fract coating, Jarosite?
22SBM-IW-15	North of Impoundment bank	4/1/22				andesite block
22SBM-IW-16	North of Impoundment bank	4/1/22	XRD	Ctb-Hg-S		friable tan rock w/ cinnabar
22SBM-IW-17	North of Impoundment bank	4/1/22				Andesite
22SBM-IW-18	North of Impoundment bank	4/1/22			yes	native S w/ clay
22SBM-IW-19s	North of Impoundment bank	4/1/22				Cristobalite vein side
22SBM-IW-19c	North of Impoundment bank	4/1/22	XRD	Ctb		Cristobalite vein
22SBM-IW-20	North of Impoundment bank	4/1/22	XRD	S		sulfur on tan matrix
22SBM-IW-20	North of Impoundment bank	4/1/22	XRD	S		sulfur on tan matrix
22SBM-IW-20	North of Impoundment bank	4/1/22	XRD	S		sulfur on tan matrix
22SBM-IW-20a	North of Impoundment bank	4/1/22	XRD	S-Hg-Qtz	yes	sulfur on tan matrix w/ Cinnabar
NEW-01	NE wall in boulder zone	11/8/22			yes	veins w/ orange/brown clay like material
NEW-02	NE wall in boulder zone	11/8/22				veins w/ orange/brown clay like material
NEW-03	NE wall in boulder zone	11/8/22				Efflorescent salts
NEW-04	NE wall in boulder zone	11/8/22				Efflorescent salts
NEW-05	NE wall in boulder zone	11/8/22				Andesite w/ gypsum and pyrite in vugs
NEW-06	NE wall in boulder zone	11/8/22	XRD	Gyp-Ctb-Claudetite?		white chalky vein w/ sulfur
NEW-07	NE wall in boulder zone	11/8/22			yes	white chalky vein w/ sulfur
NEW-08	NE wall in boulder zone	11/8/22			yes	white chalky vein w/ sulfur
NEW-09	NE wall in boulder zone	11/8/22				clay vein

Sample label	Location	Date collected	Analysis type	XRD identified peaks	Stable isotopes	Description
NEW-10	NE wall in boulder zone	11/8/22				Black conglomerate (former vent?)
NEW-11	NE wall in boulder zone	11/8/22	XRD	Aln	yes	white/buff chalky vein
NEW-12	NE wall in boulder zone	11/8/22				tan vein surrounded by black bank
NEW-13	NE wall in boulder zone	11/8/22				Black ppt
NEW-14	NE wall in boulder zone	11/8/22	XRD	Ctb-S		vein center, chalky tan
CW-01	Center wall (Previously called Herman Impoundment north Bank)	11/9/22	XRD	Aln	yes	white vein w/ green (arsenate?)
CW-02	Center Wall	11/9/22	XRD	Aln-Ctb-Gyp		white vein w/ red streaks
CW-03	Center Wall	11/9/22	XRD	Buddingtonite-Kao-Jar-Ctb-Dimorphite?		orange vein, surrounded by flowering salts
CW-04	Center Wall	11/9/22	XRD	Aln-Kaol		white/tan veins
CW-05	Center Wall	11/9/22	XRD	Aln	yes	white/tan veins
CW-05B	Center Wall	11/9/22	XRD	Aln	yes	white/tan veins
WB-01	West bank	11/9/22	XRD	Kaol (pure)	yes	clay vein from bank
NWW-01	Northwest Wall (near NW pit)	11/9/22				crumbly white/tan veins
NWW-02	Northwest Wall (near NW pit)	11/9/22				crumbly white/tan veins
NWW-03	Northwest Wall (near NW pit)	11/9/22			yes	crumbly white/tan veins
NWW-04	Northwest Wall (near NW pit)	11/9/22	XRD	Ctb	yes	crumbly white/tan veins
NWP-01	Northwest Pit	11/9/22	XRD	Kaol (pure)	yes	clay vein
NWP-02	Northwest Pit	11/9/22				thick clay vein with cinnabar
NWP-03	Northwest Pit	11/9/22	XRD	Kao-Aln-Ctb-		pink clay vein
NWP-04	Northwest Pit	11/9/22			yes	clay vein
NWP-05	Northwest Pit	11/9/22				peach/orange exfoliation shells of boulder
T-01	Trench Area	11/9/22	XRD	Aln	yes	white kaol/alun veins
T-02	Trench Area	11/9/22				white kaol/alun veins
T-03	Trench Area	11/9/22	XRD	Kao-Aln		white kaol/alun veins
T-04	Trench Area	11/9/22	XRD	Kao-Aln		white kaol/alun veins
T-05	Trench Area	11/9/22	XRD	Kao (pure)	yes	white kaol/alun veins
T-06	Trench Area	11/9/22			yes	white vein w/ red and black rim
T-07	Trench Area	11/9/22	XRD	Kao-Aln-Alu		brown/tan vein
T-08	Trench Area	11/9/22	XRD	Kao-Aln-Alu		brown/tan vein
T-09	Trench Area	11/9/22				gypsum cluster
T-10	Trench Area	11/9/22				sulfate salts
T-11	Trench Area	11/9/22				friable cristobalite
T-12	Trench Area	11/9/22			yes	steam-heated zone?
F-1	Final Location	11/9/22	XRD	Jar-And-Ctb-Mont		beige vein
F-2A	Final Location	11/9/22	XRD	ctb		dgray vein w/ opal
F-2B	Final Location	11/9/22				vein sides
F-3A	Final Location	11/9/22				bright green material in gray vein
F-3B	Final Location	11/9/22	XRD	gyp-ctb-jar-anh	yes	bright green material in gray vein with cinnabar
NEW-03	NE wall in boulder zone	11/9/22				efflorescent salts
NEW-05	NE wall	11/9/22				very hard volcanic rock w disseminated FeS2?
NEW-08	NE wall	11/9/22				native S
NEW-13	NE wall	11/9/22				black precipitate - recent H2S vent?
NP-02	NW pit, fractured boulder zone	11/10/22				fine-grained HgS, abundant clay altered veins
NWP-03A	Northwest pit	11/10/22				alunite?
NWP-03B	Northwest pit	11/10/22				white salt on mud/moss, vertical face
NWP-5 (2 of 2)	Northwest pit	11/10/22				unknown orange mineral - orpiment?
CW-01	Center wall	11/10/22				unknown green mineral with white clay
CW-01C	Center wall	11/10/22				unknown green mineral with white clay
T-13	Trench	11/10/22				yellow crust - alunite?

Appendix II: Sample XRD scans and sample photos

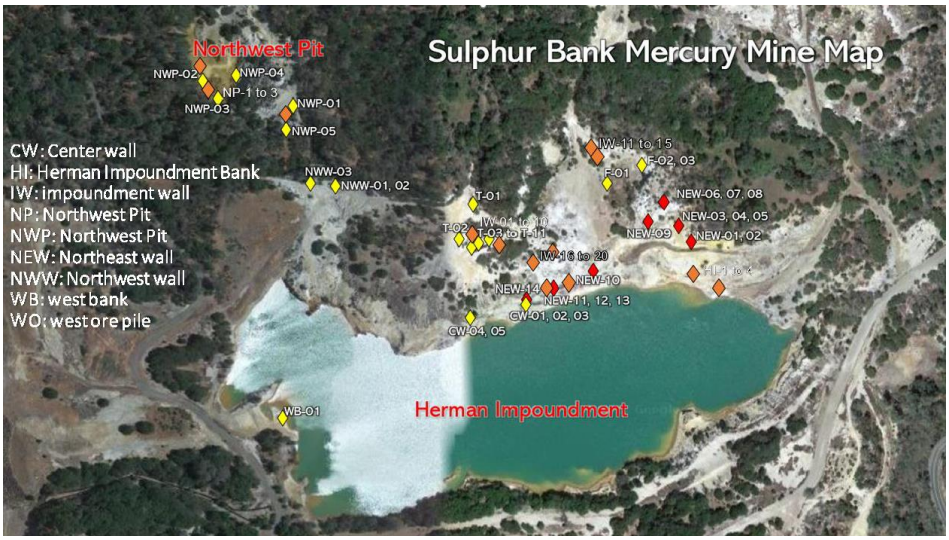

Samples With Isotope Analysis

Alunite (SOH):
- CW-01
- CW-05
- CW-05B
- HI-04
- HI-05
- IW-02
- IW-03
- IW-04
- NEW-11
- T-01
- T-06

Kaolinite (OH):
- NWP-01
- NWP-04
- NWW-03
- NEW-01
- IW-05
- T-05
- T-12
- WB-01

Cinnabar & Native S:
- F3B
- WO1
- IW-20
- NEW-07
- NEW-08
- IW-18

			Mineral				
Sample		Mineral	δ18O	δD	δ34S	δ18O (SO4)	δ18O (OH) calculated
NWW-04		quartz	24.3				
IW-11		quartz	23.3				
F2A		quartz	25.2				
NWP-01		kaolinite	10.3	-104			
NWP-04		kaolinite	11.6	-101			
NWW-03		kaolinite	12.7	-120			
NEW-01		kaolinite	12.3	-100			
IW-05		kaolinite	10.2	-101			
T-05		kaolinite	10.1	-100			
T-12		kaolinite	10.5	-101			
WB-01		kaolinite	12.7	-90			
CW01	0	alunite		-50	2.8	7.7	14.1
CW05	1	alunite		-44	2.8	7.0	11.6
CW05B	2	alunite		-42	2.7	7.0	7.8
HI04	3	alunite		-56	0.8	6.4	3.3
HI05	4	alunite		-58	1.5	7.3	3.6
IW02	5	alunite		-54	0.6	8.3	2.2
IW03	6	alunite		-55	0.5	8.9	2.5
IW04	7	alunite		-48	0.2	10.7	7.1
NEW11	8	alunite		-37	1.9	8.7	9.4
T01	9	alunite		-38	-1.8	4.3	11.7
T06	10	alunite		-49	0.6	7.7	6.5
IW20 NS		native S			0.9		
NEW07 NS		native S			-0.1		
NEW08 NS		native S			1.3		
IW18 NS		native S			-2.2		
F3B CIN		Cinnabar			0.9		
WO1 CIN		Cinnabar			-0.5		

CW-01

- white vein w/ green
- SOH isotopes

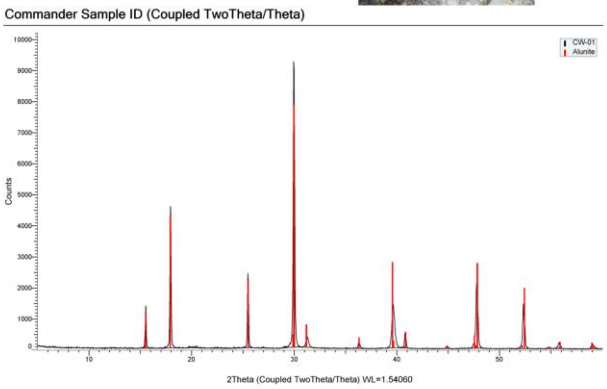

CW-02

- white vein w/ red streaks

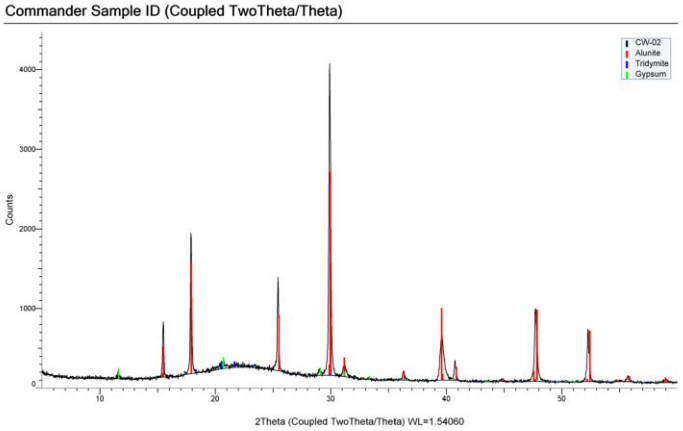

CW-03

- Buddingtonite-Kao-Jar-Ctb-Dimorphite?

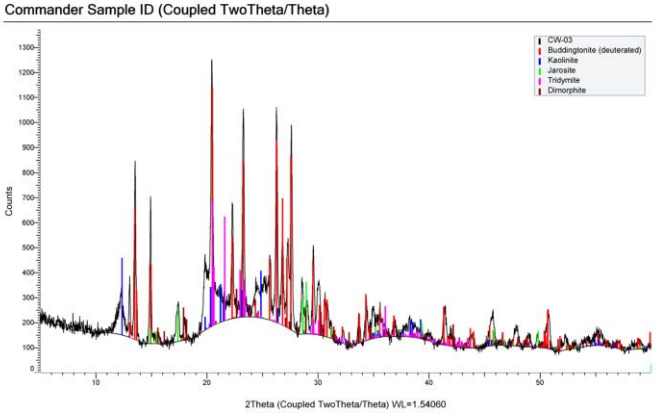

CW-04

- Vein center

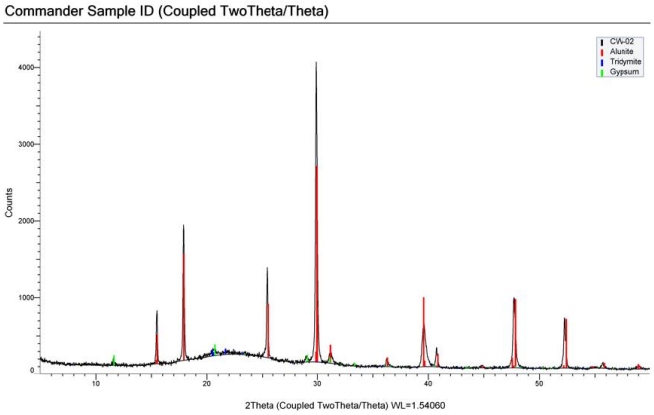

CW-05

- SOH isotopes

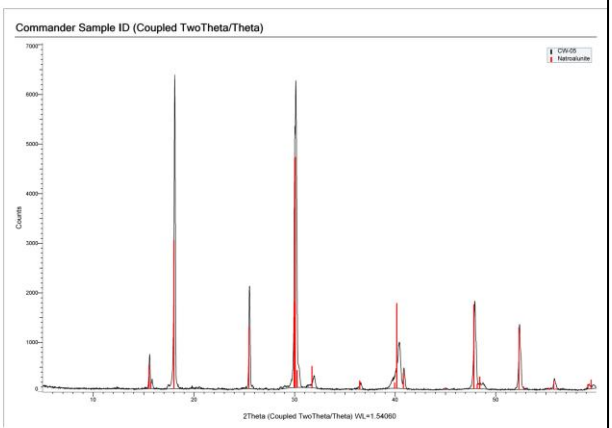

CW-05B

- SOH isotopes

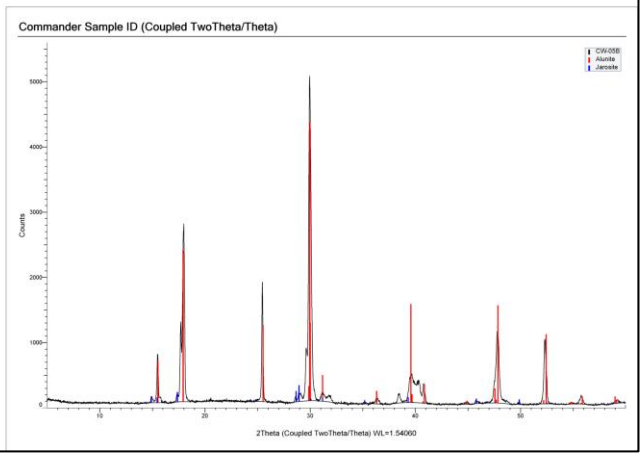

F-1

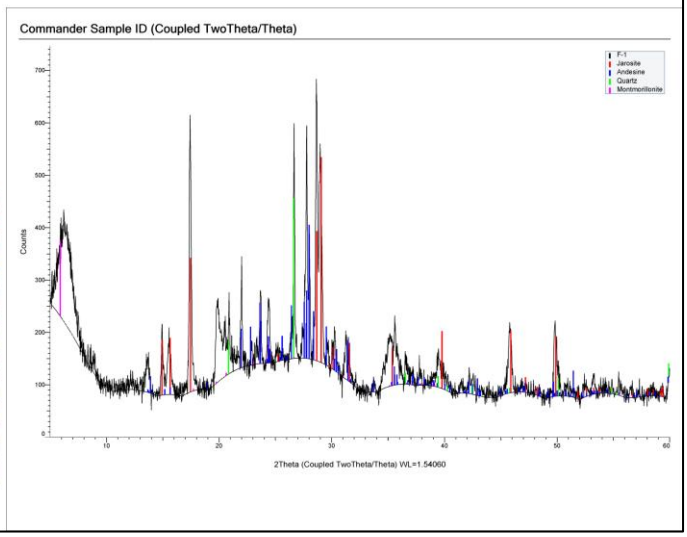

F-2A

- O isotope

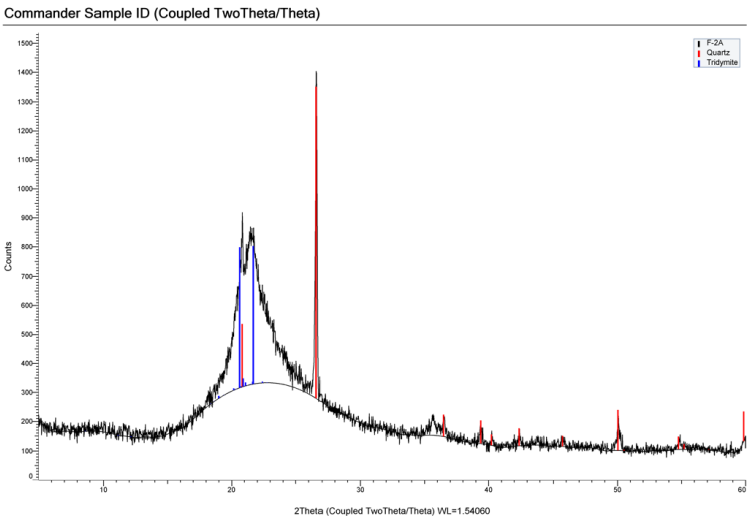

F-3A

- GREEN CONC

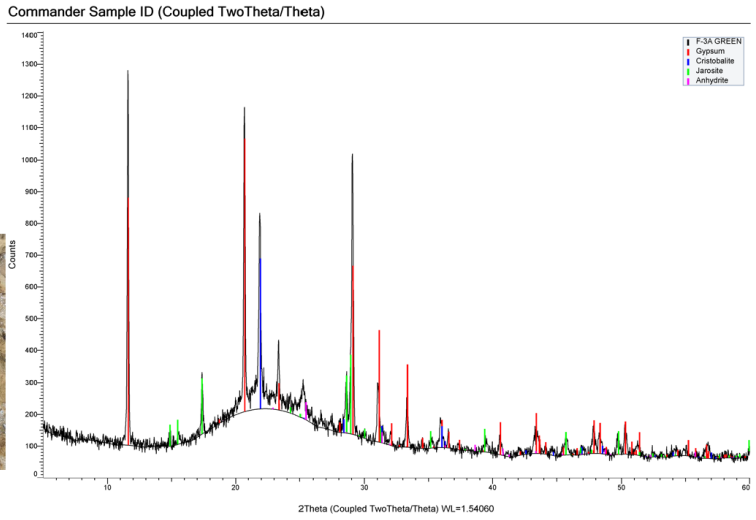

F-3B

- S isotope

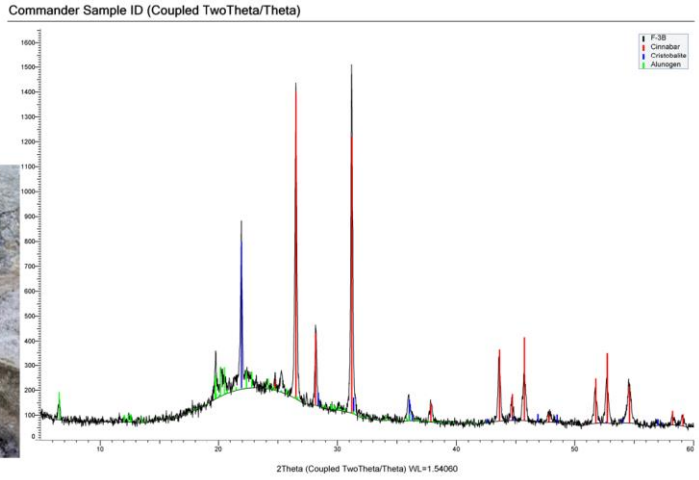

HI-01

- Location: banks of impoundment
- "yellow crust" black and yellow with mica, sulfur-smelling

HI-01 XRD

- Most difficult xrd scan with several peaks still unmatched
- Best matches include quartz, illite, Alum, sulfur
- Mesolite: in zeolite group
- Copiapite: hydrated iron sulfate

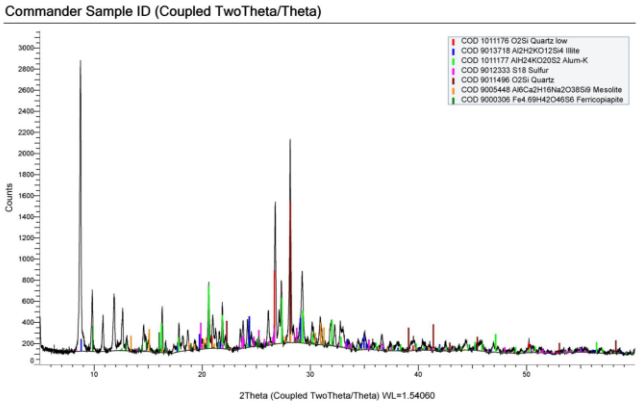

HI-02

- Location: banks of impoundment
- Strong sulfur smell and visible yellow sulfur

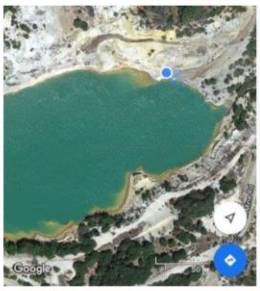

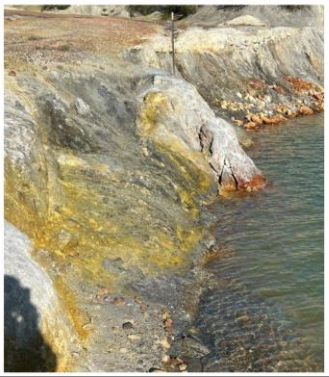

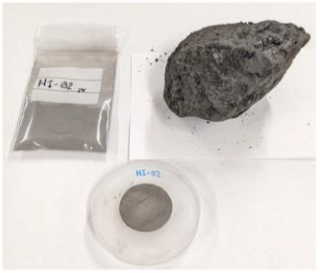

HI-02

- Sulfur peaks match
- Illite and kaolinite peaks present
- Most evident peaks are quartz and cristobalite

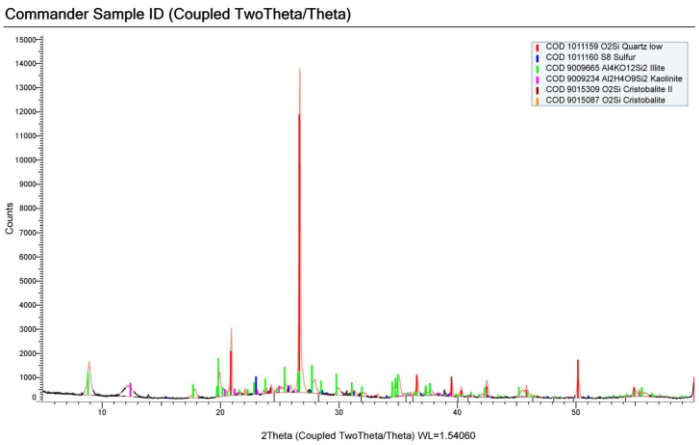

HI-03

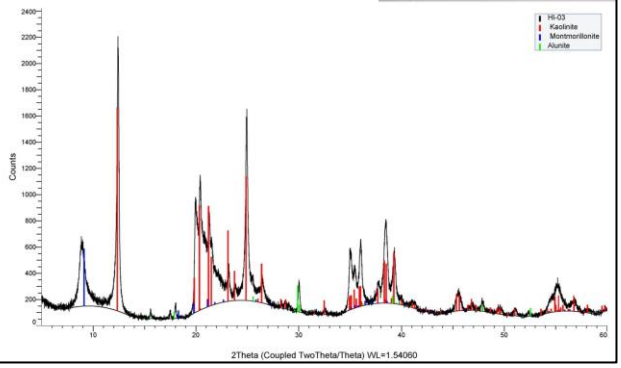

HI-04

- F

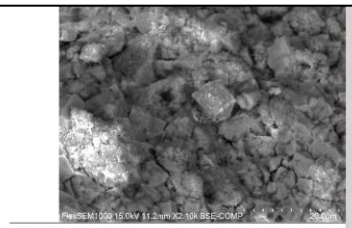

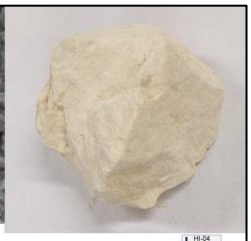

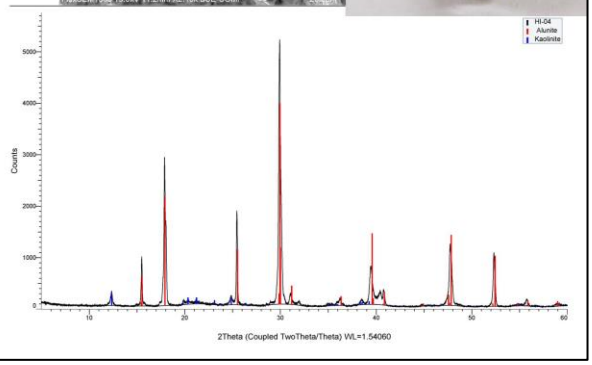

HI-04

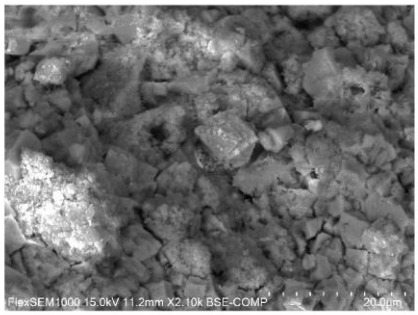

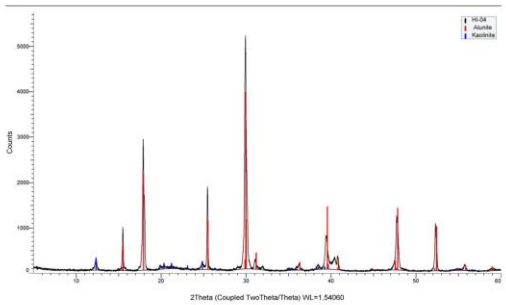

HI-05

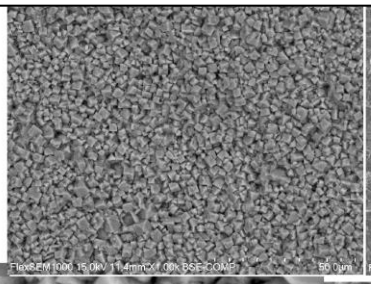

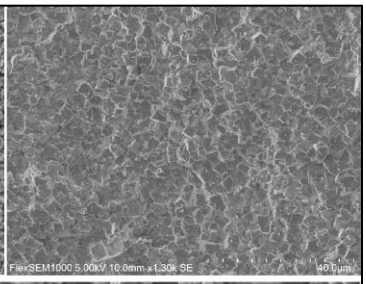

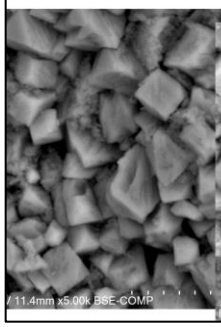

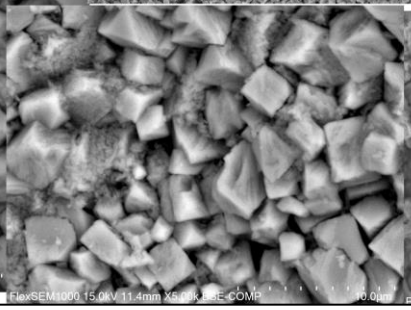

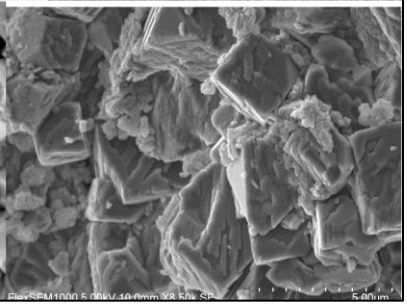

HI-05

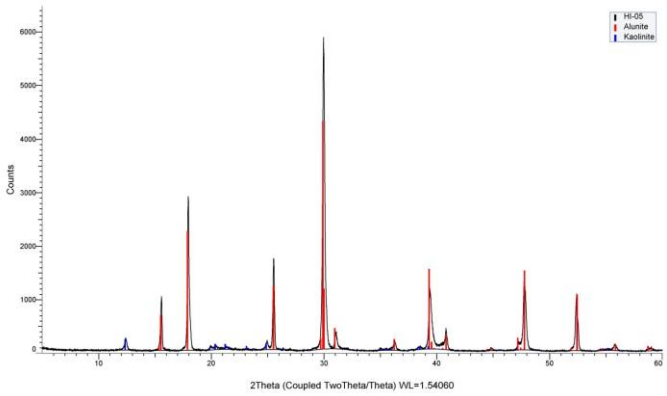

HI-06

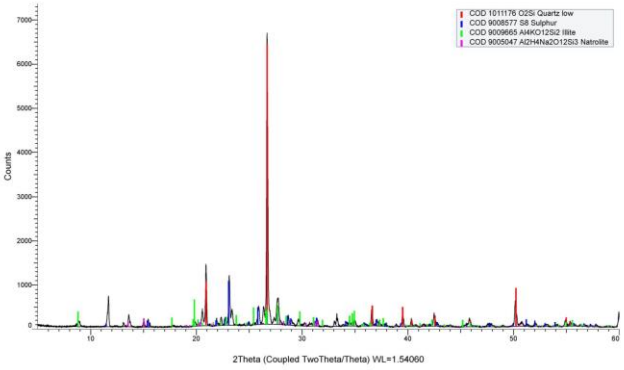

IW-1-C/S/O

- Impoundment wall "trench"
- C/S/O stands for center of vein, side of vein, and less altered andesite proximal to vein sides
- Field notes: "C: sample from vein center (bag of powder), S: between vein and "fresh" andesite (bag of powder and bleached and., O: fresh and. "boulders", vuggy"

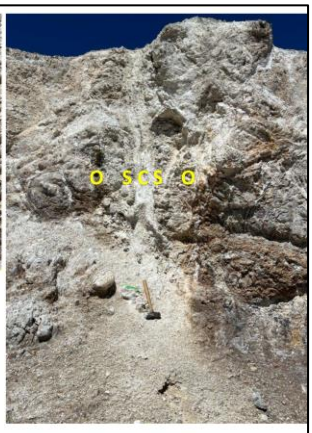

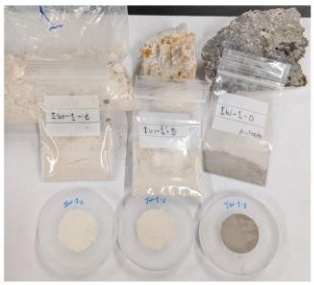

IW-1-C

- Alunite and kaolinite confirmed
- Very little appears unmatched in these scans

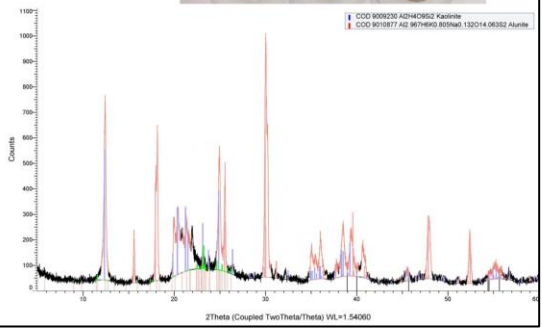

IW-1-S

- Alunite and kaolinite confirmed
- Gypsum not found in this analysis, although cm-sized crystals appeared present in field, perhaps gypsum should have been selected in custom search

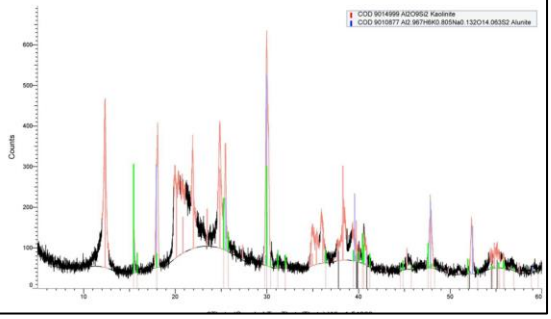

IW-1-O

- Typical minerals for an andesite with minor alteration minerals (smectite)
- Plagioclase, pyroxenes, magnetite

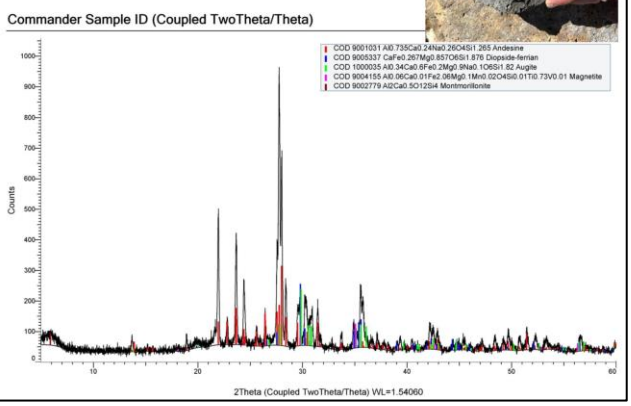

IW-02

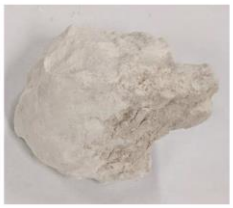

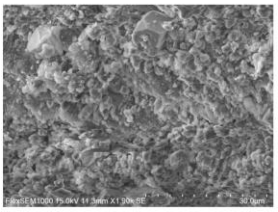

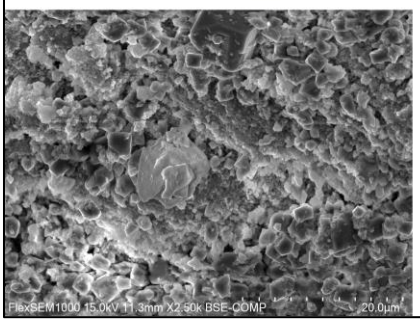

Commander Sample ID (Coupled TwoTheta/Theta)

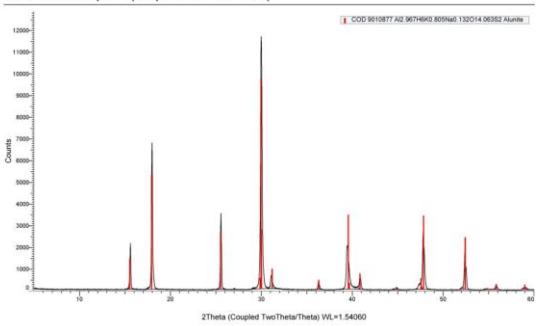

IW-03

- Location: Impoundment wall "Trench"
- Field notes: "white chalky lump from vein center, Kaol/alu?"

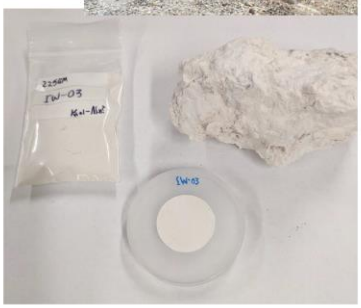

IW-03 XRD

- Alunite confirmed, near perfect match
- Minor Kaolinite peak
- Ferrihydrite peak probably from recent surface oxidation

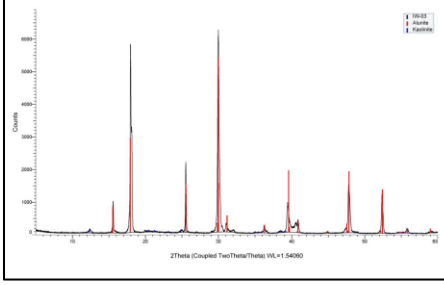

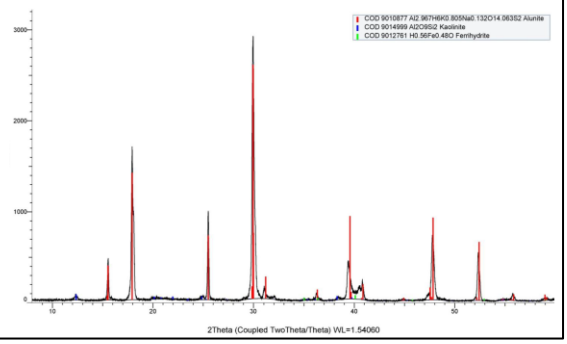

IW-04

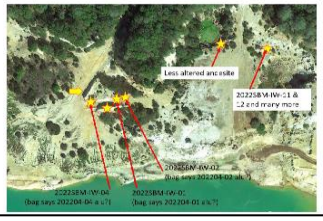

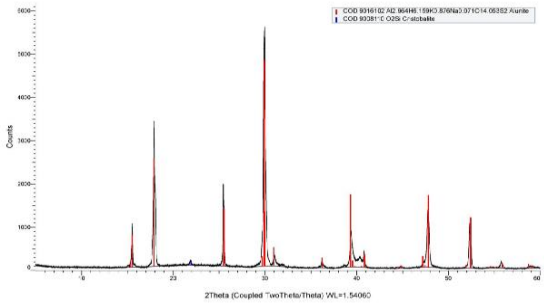

IW-05

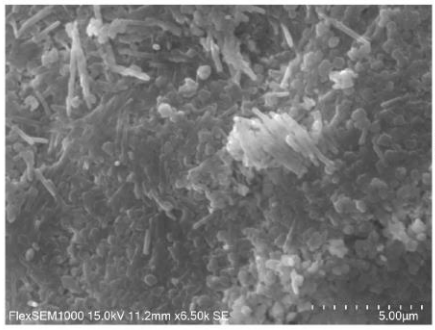

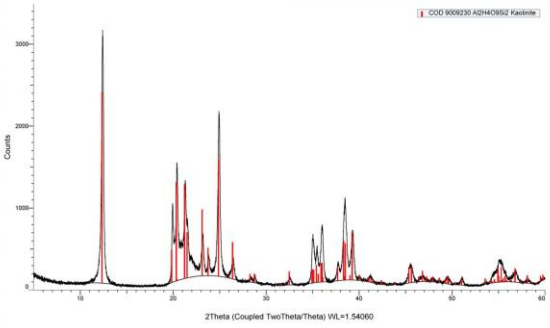

IW-06

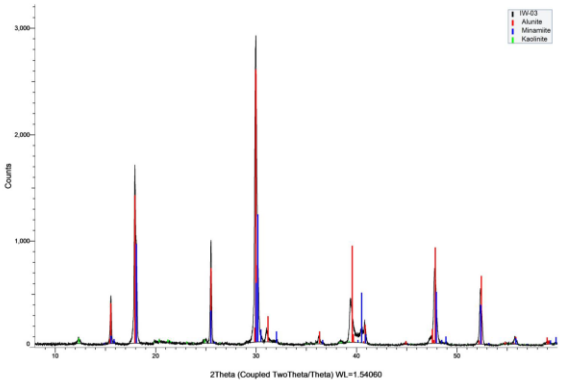

IW-07

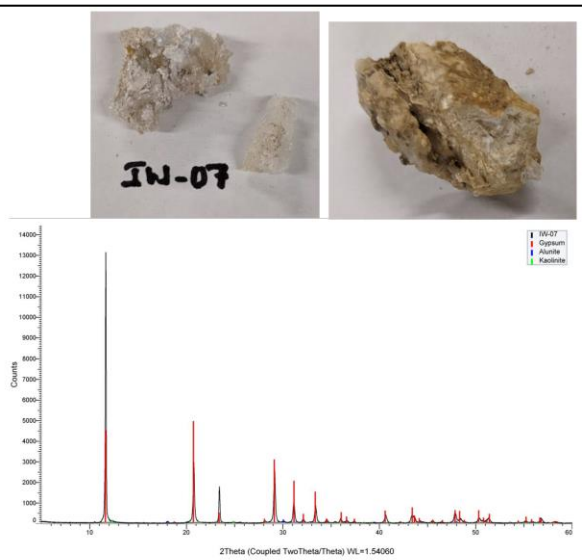

IW-08

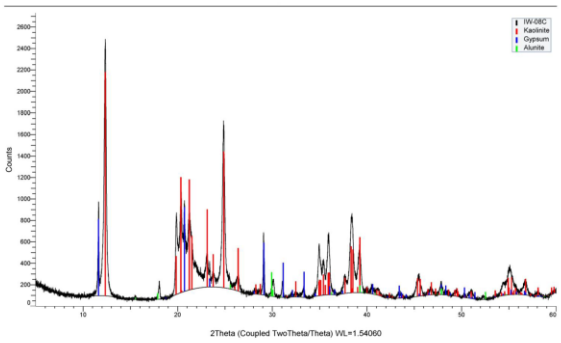

IW-09

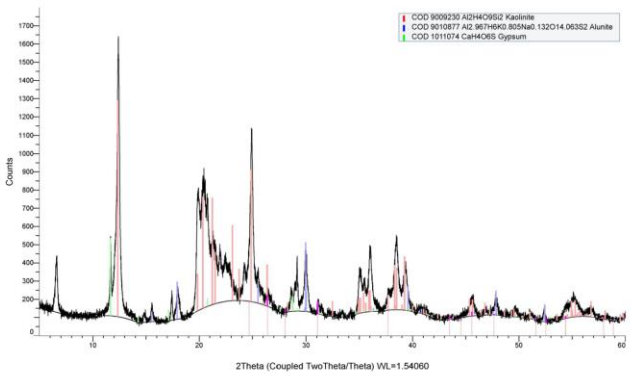

IW-10

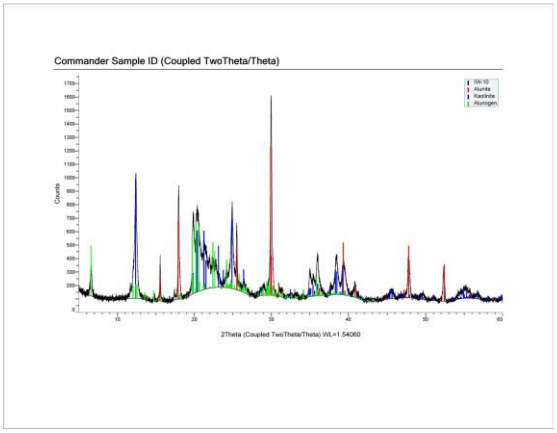

IW-11&12

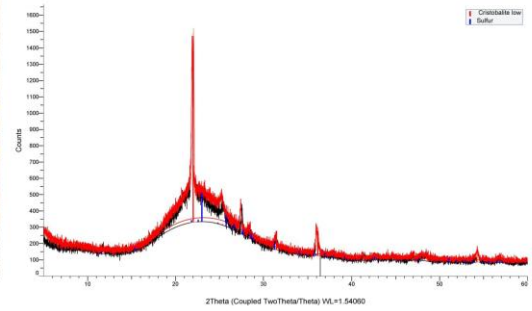

IW-16

- d

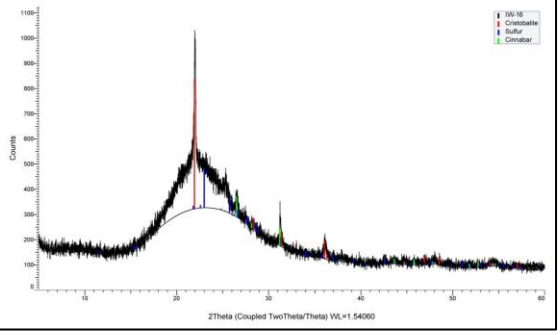

IW-17

- Location: Impoundment wall, final location near sulfur float
- Field notes: "chalky/vuggy altered andesite with amorph silica in void?"




IW-17

- Mainly quartz and cristobalite
- Sulfur peaks present

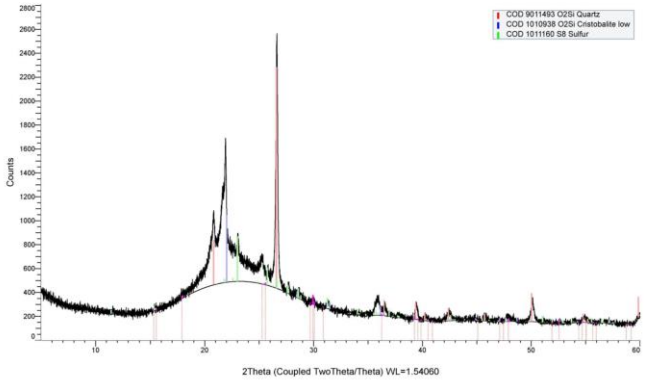

IW-18

- Translucent euhedral S crystals,
- S-isotope analysis

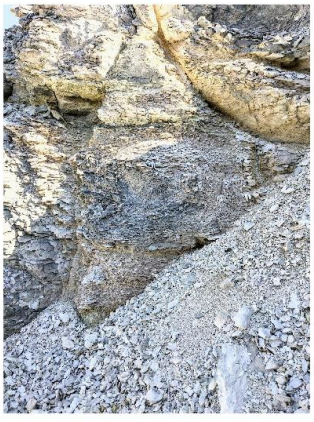
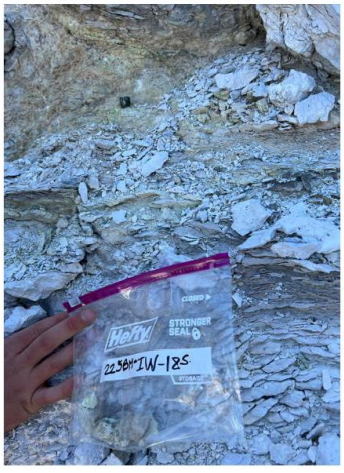

IW-20

- F

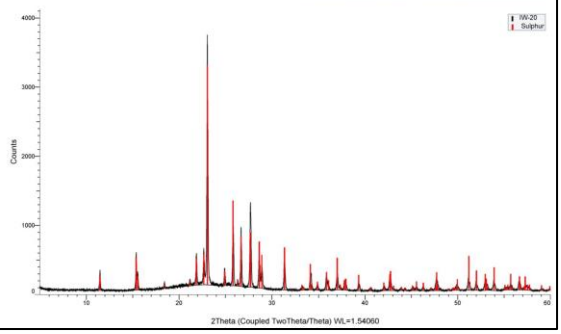

NEW-01

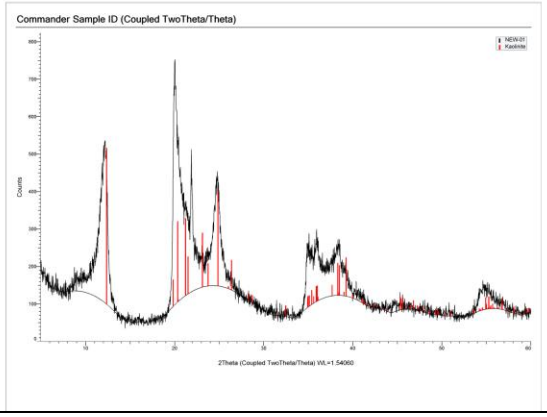

NEW-02

- EFLORVESCENT SALTS

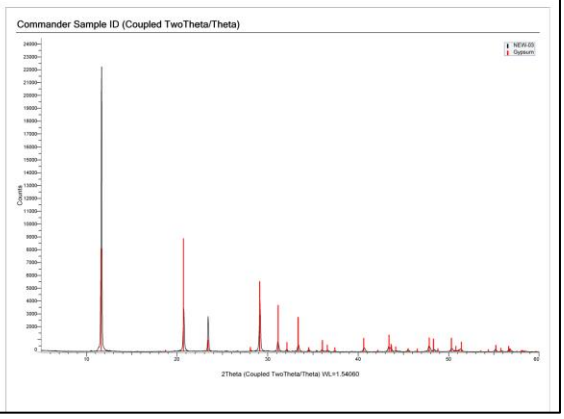

NEW-04

- red/brown/gray crumbly vein near salts (new-02)

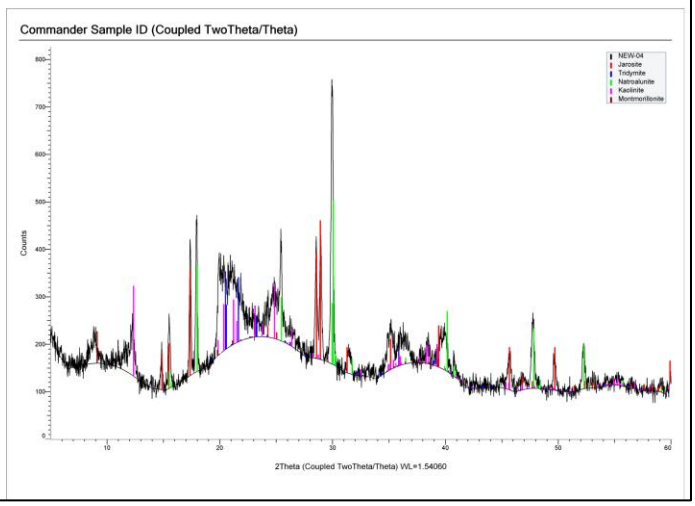

NEW-06

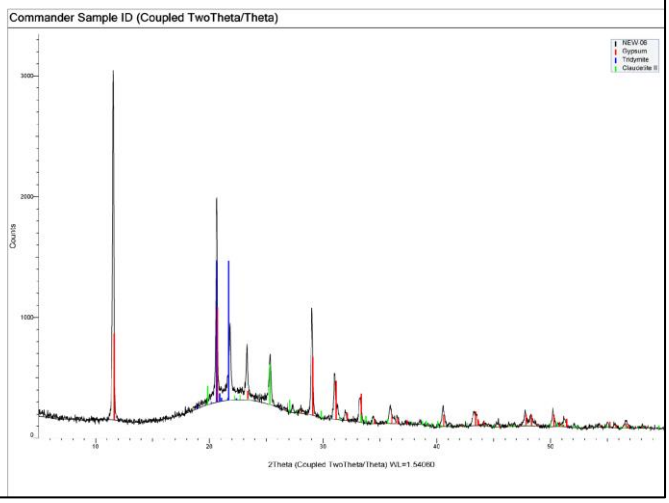

NEW-07

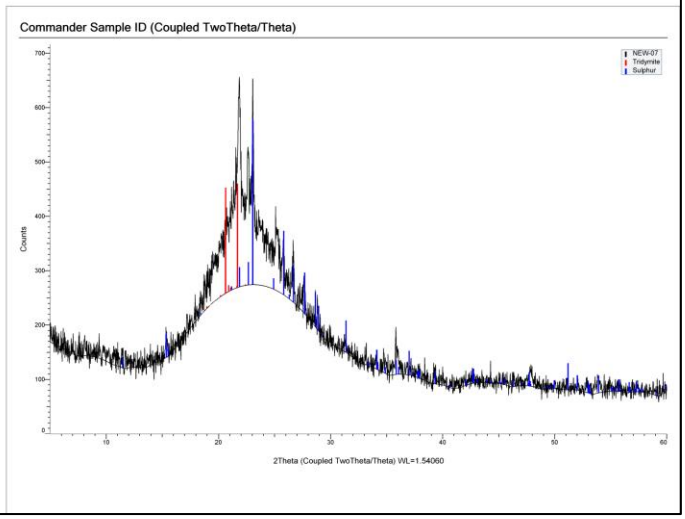

NEW-08

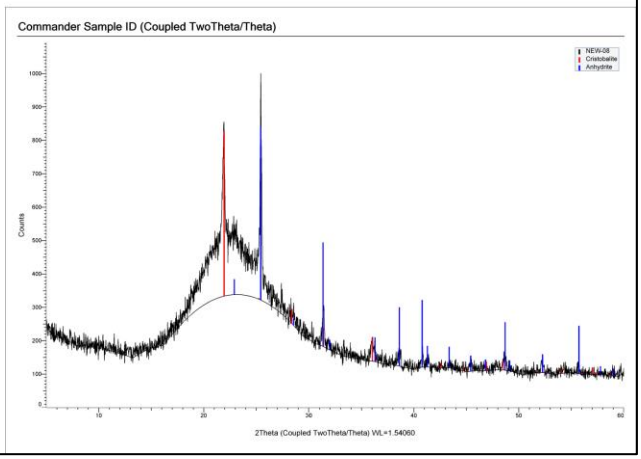

NEW-09

- Clay vein with lighter and darker zones

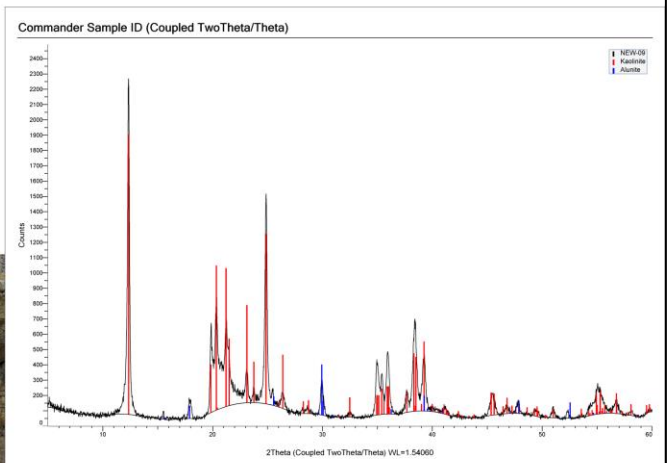

NEW-09L

- Lighter zone of clay vein

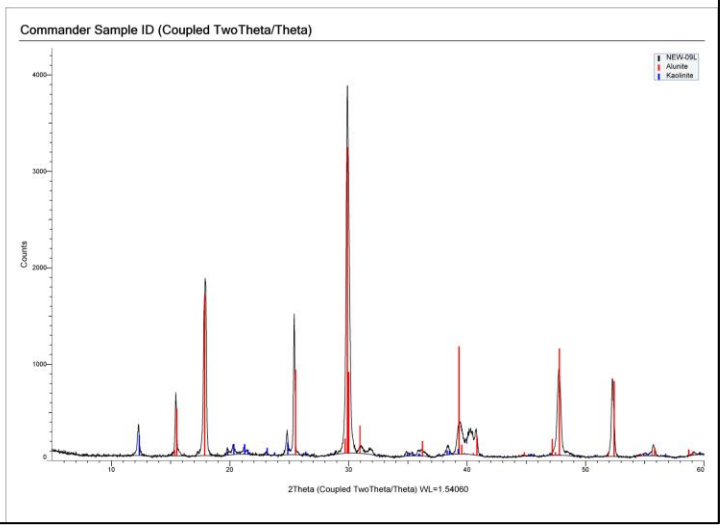

NEW-11

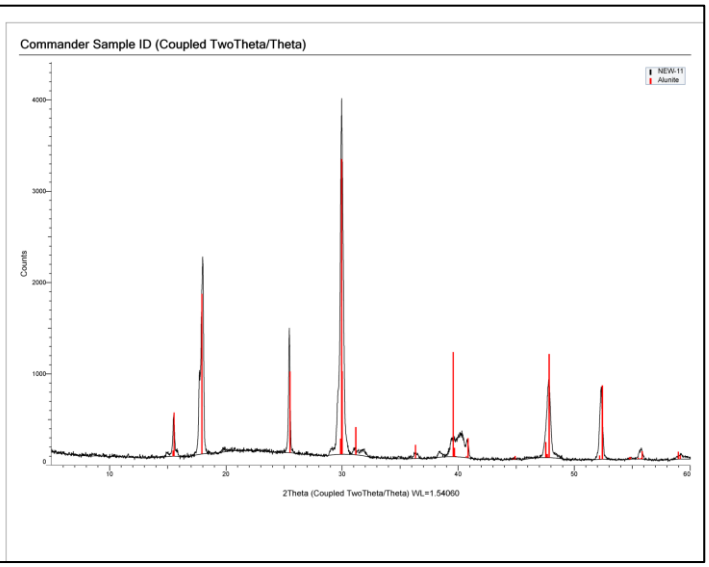

NEW-12

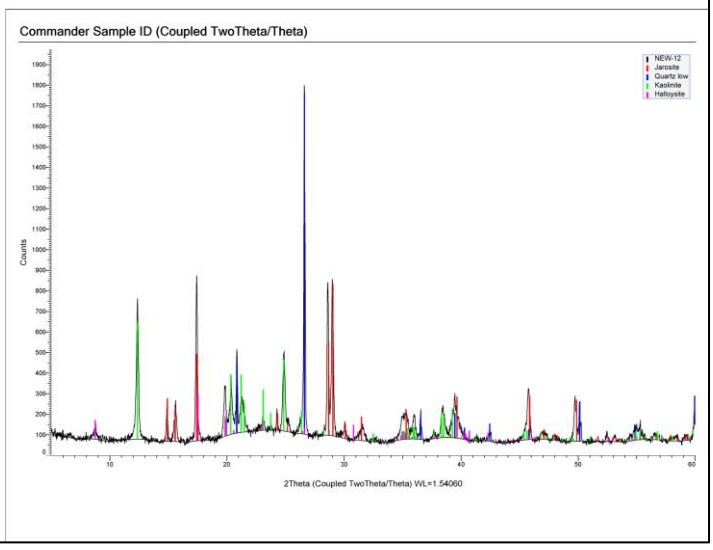

NEW-14

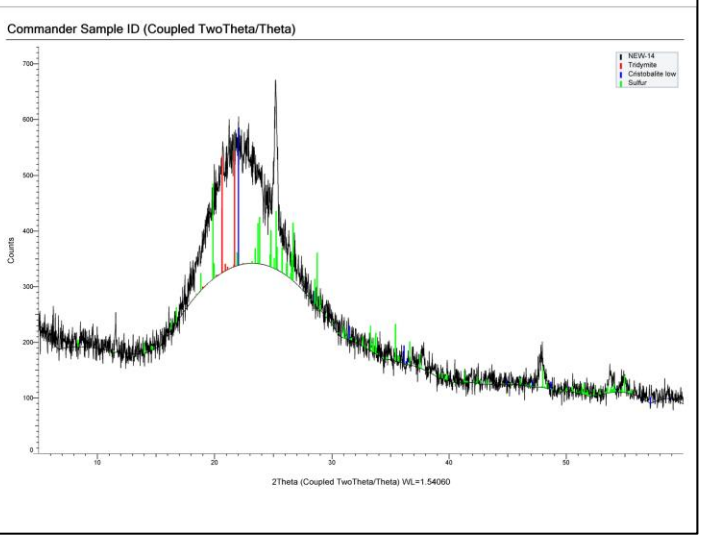

NP2

- df

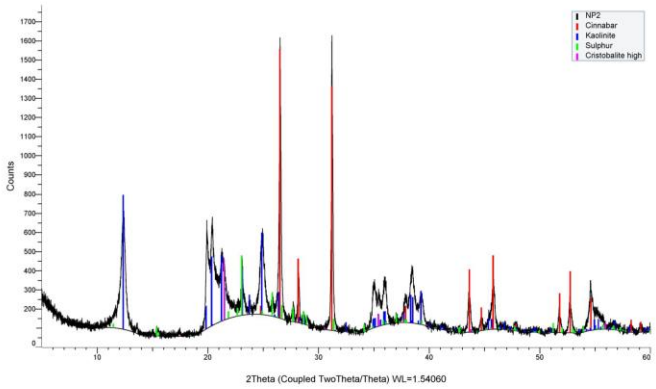

NWP-01

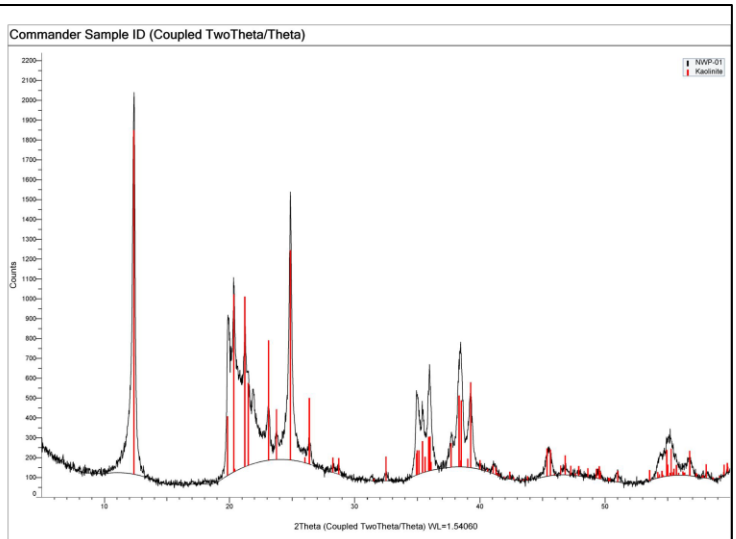

NWP-02

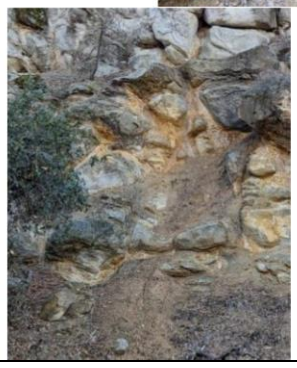

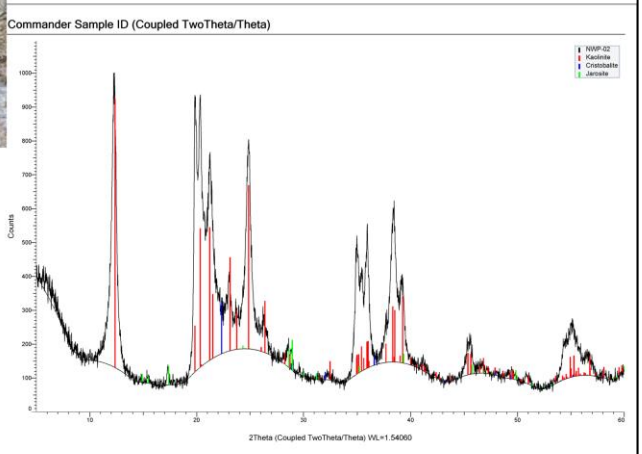

NWP-02B

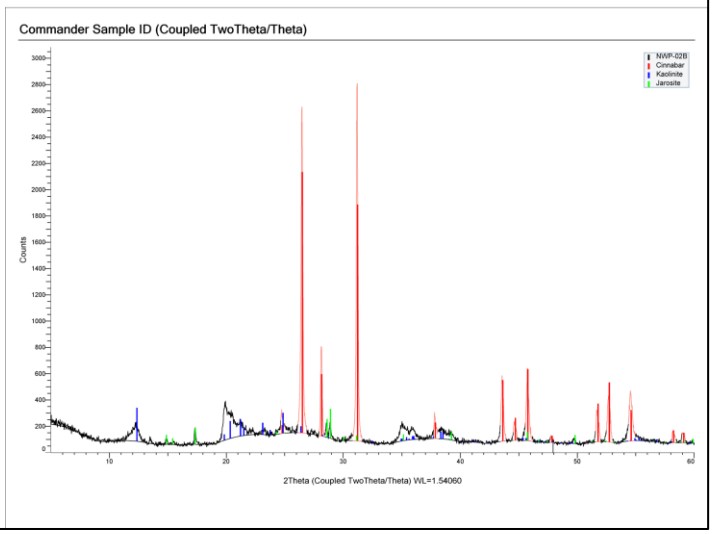

NWP-03

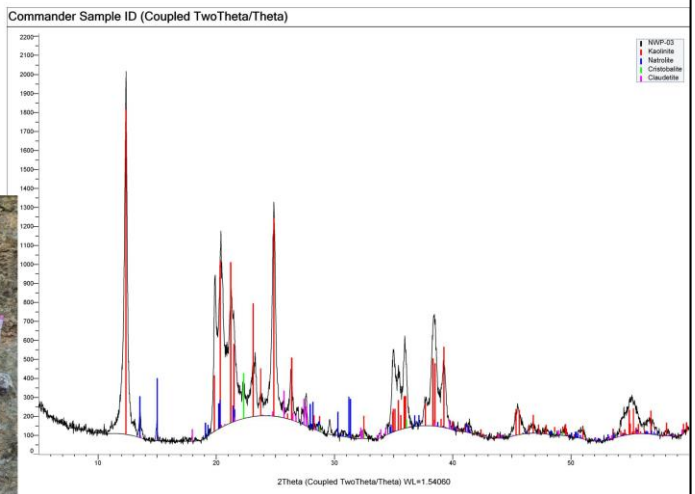

NWP-04

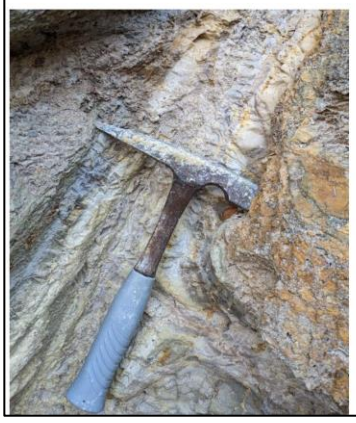

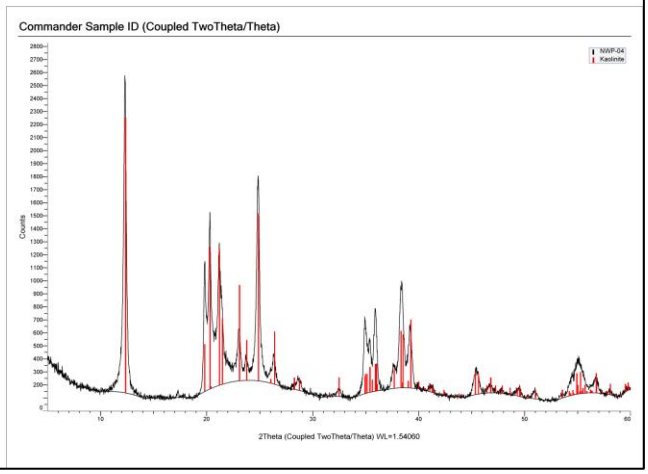

NWP-05

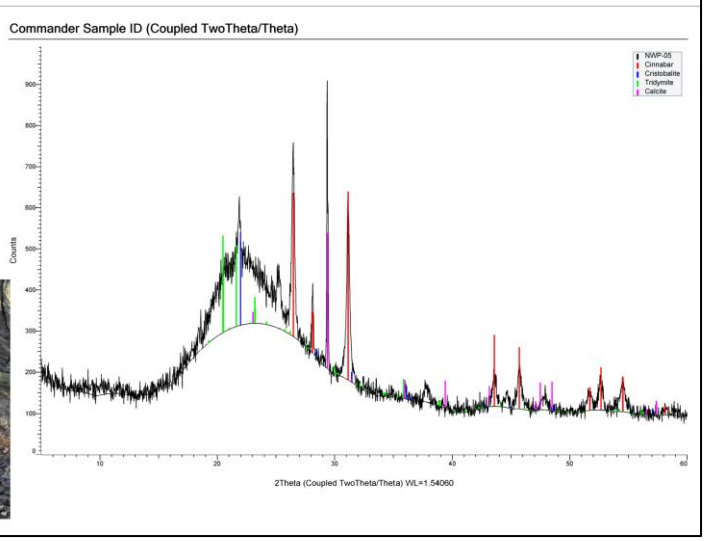

NWW-01

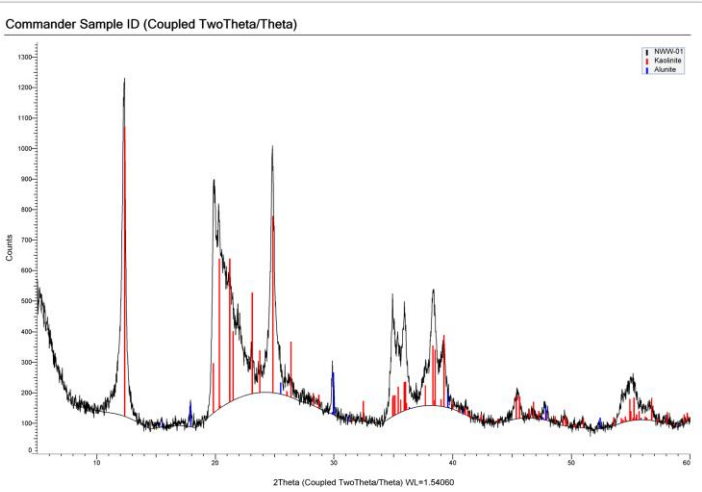

NWW-02

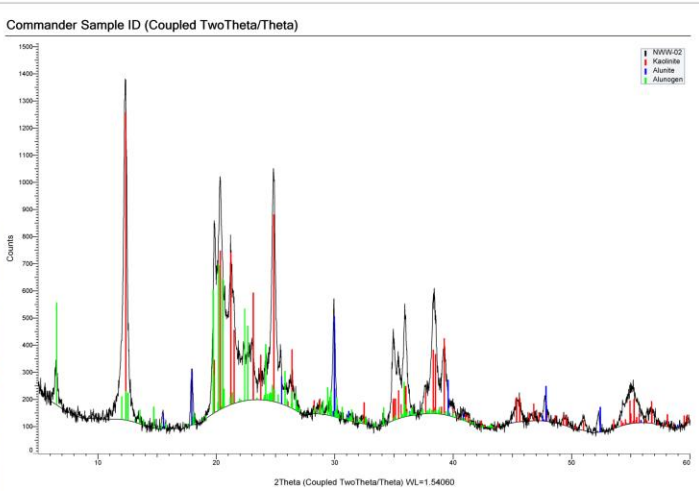

NWW-03

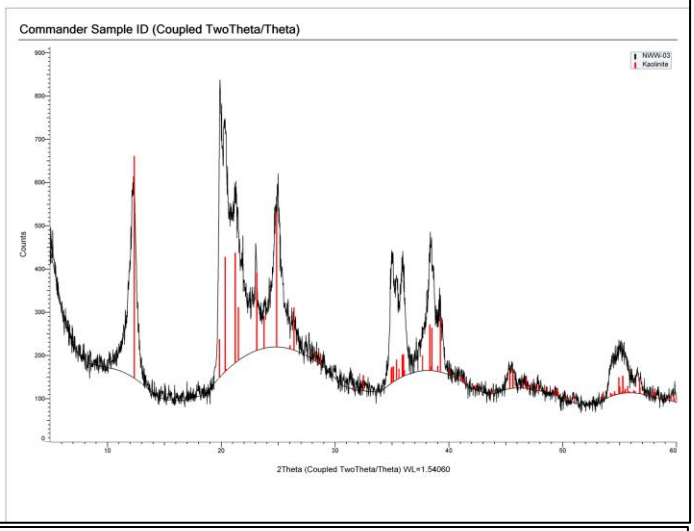

NWW-04

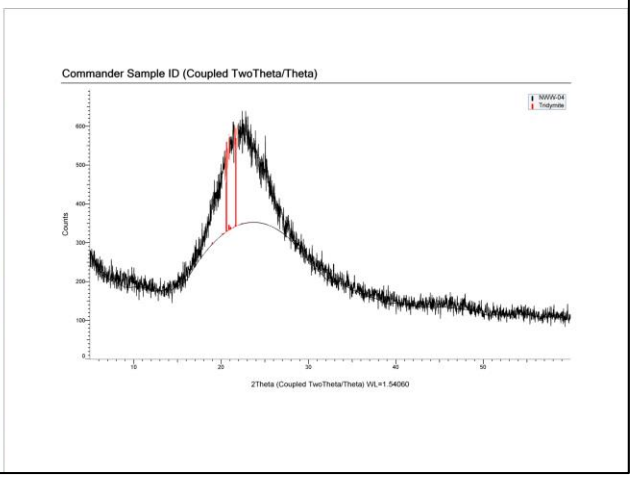

T-01

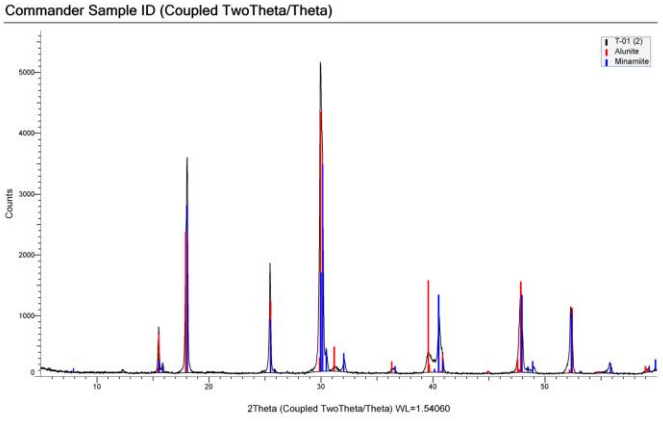

T-02

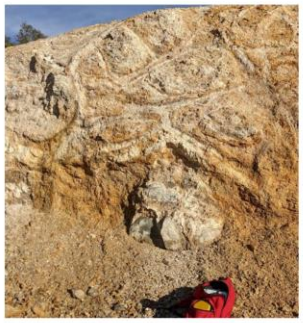

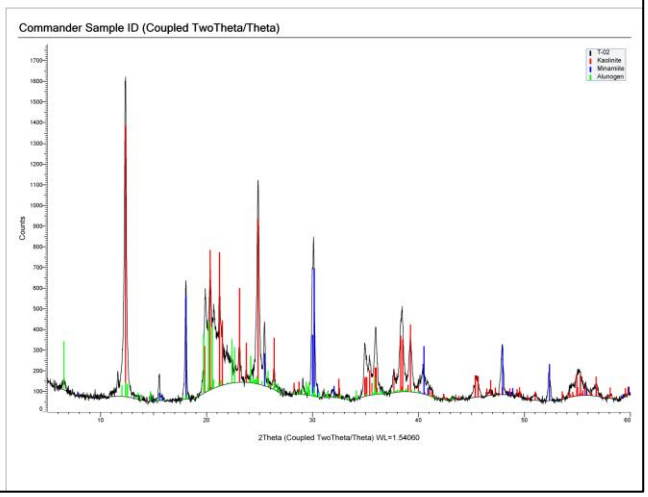
Commander Sample ID (Coupled TwoTheta/Theta)
T-02
Kaolinite
Minamite
Alunogen
Counts
2Theta (Coupled TwoTheta/Theta) WL=1.54060

T-03

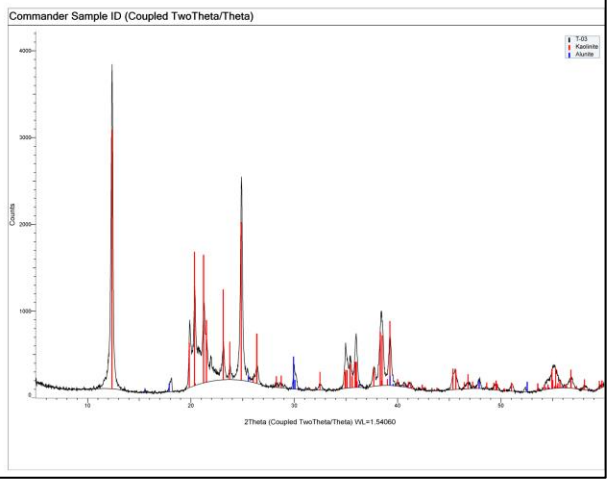
Commander Sample ID (Coupled TwoTheta/Theta)
T-03
Kaolinite
Alunite
Counts
2Theta (Coupled TwoTheta/Theta) WL=1.54060

T-04

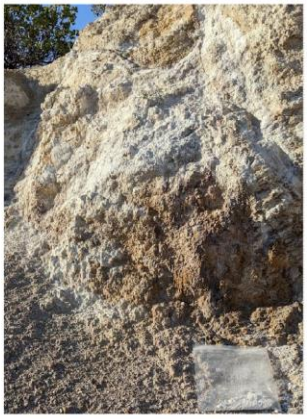

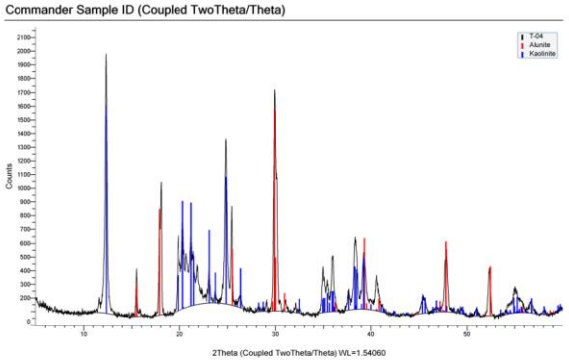
Commander Sample ID (Coupled TwoTheta/Theta)
T-04
Alunite
Kaolinite
Counts
2Theta (Coupled TwoTheta/Theta) WL=1.54060

T-05

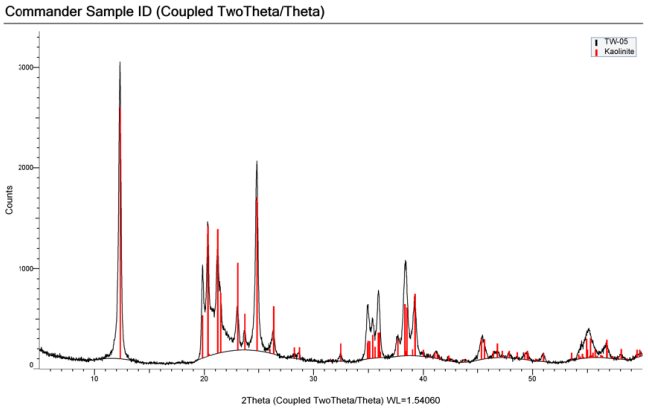
Commander Sample ID (Coupled TwoTheta/Theta)
TW-05
Kaolinite
Counts
2Theta (Coupled TwoTheta/Theta) WL=1.54060

T-06


T-06

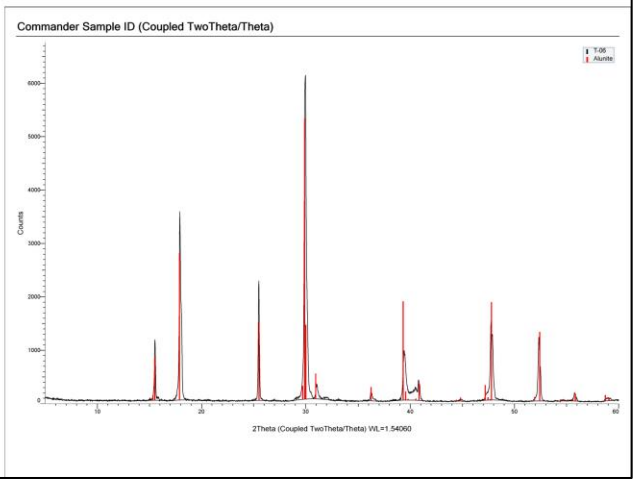
Commander Sample ID (Coupled TwoTheta/Theta)
T-06
Alunite
Counts
2Theta (Coupled TwoTheta/Theta) WL=1.54060

T-07

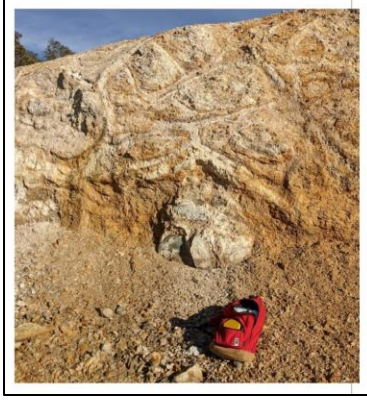

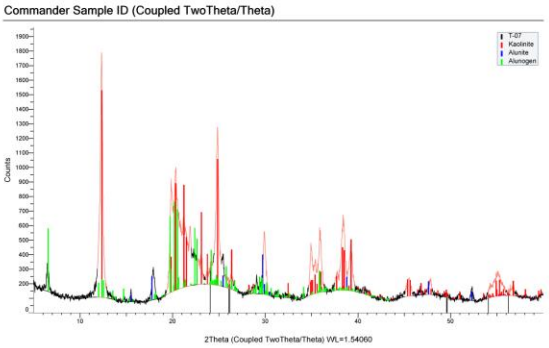
Commander Sample ID (Coupled TwoTheta/Theta)
T-07
Kaolinite
Alunite
Alunogen
Counts
2Theta (Coupled TwoTheta/Theta) WL=1.54060

T-08

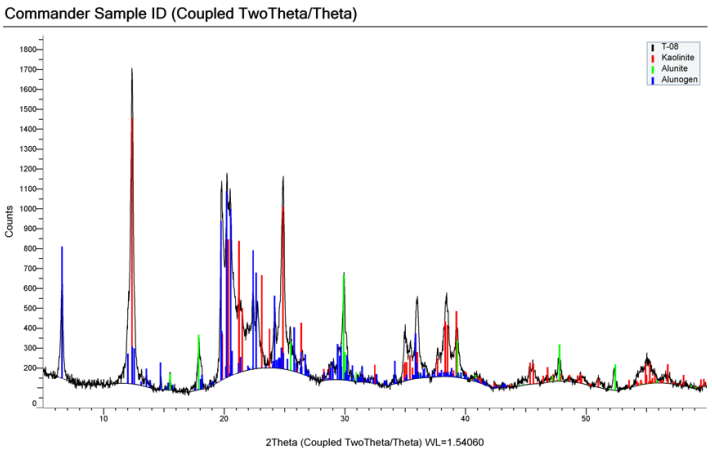
Commander Sample ID (Coupled TwoTheta/Theta)
T-08
Kaolinite
Alunite
Alunogen
Counts
2Theta (Coupled TwoTheta/Theta) WL=1.54060

T-10

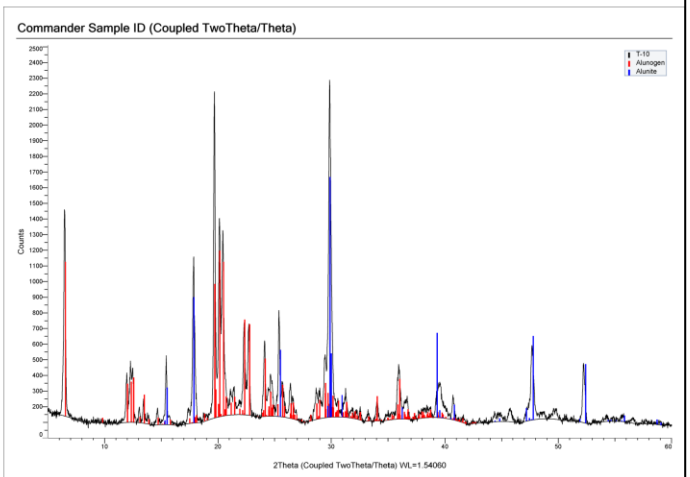
Commander Sample ID (Coupled TwoTheta/Theta)
T-10
Alunogen
Alunite
Counts
2Theta (Coupled TwoTheta/Theta) WL=1.54060

T-11

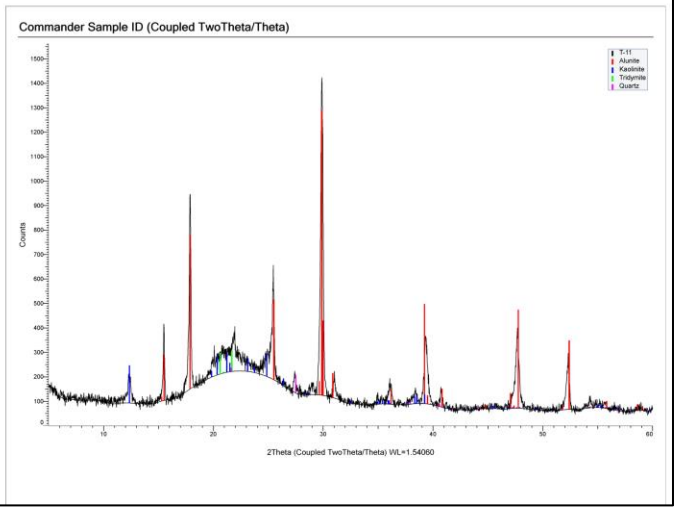
Commander Sample ID (Coupled TwoTheta/Theta)
T-11
Alunite
Kaolinite
Tridymite
Quartz
Counts
2Theta (Coupled TwoTheta/Theta) WL=1.54060

T-12

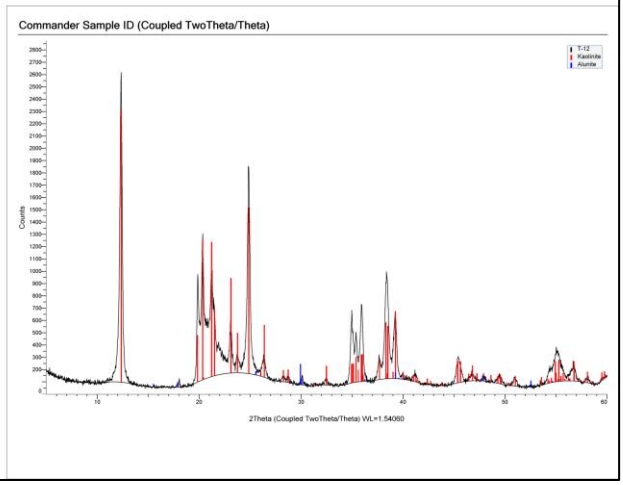
Commander Sample ID (Coupled TwoTheta/Theta)
T-12
Kaolinite
Alunite
Counts
2Theta (Coupled TwoTheta/Theta) WL=1.54060

WB-01

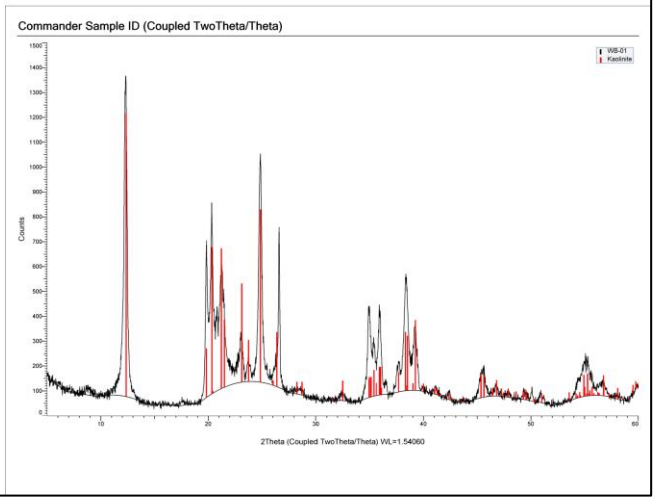
Commander Sample ID (Coupled TwoTheta/Theta)
WB-01
Kaolinite
Counts
2Theta (Coupled TwoTheta/Theta) WL=1.54060

WO-1

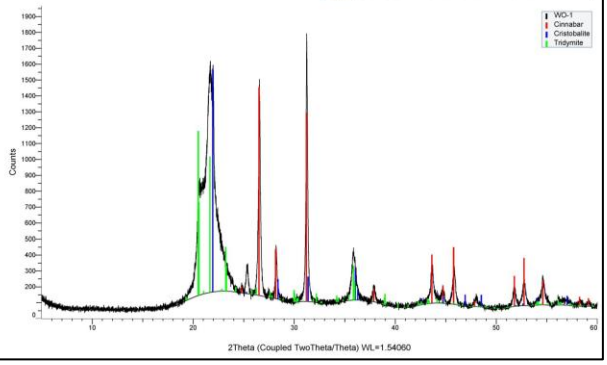
WO-1
Cinnabar
Cristobalite
Tridymite
Counts
2Theta (Coupled TwoTheta/Theta) WL=1.54060

WO-2

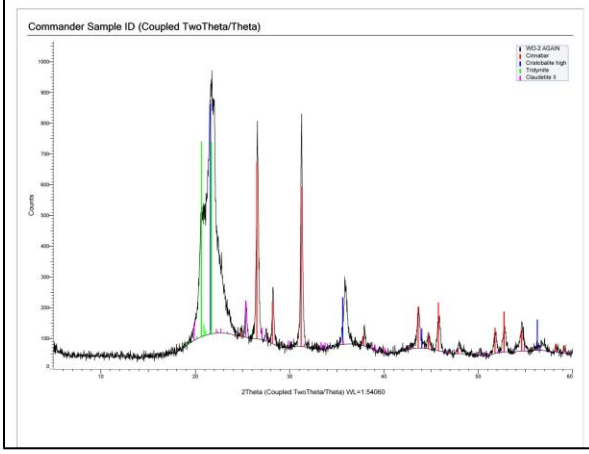
Commander Sample ID (Coupled TwoTheta/Theta)
WO-2 AGAIN
Cinnabar
Crednbaite high
Trdymite
Claudetite II
Counts
2Theta (Coupled TwoTheta/Theta) WL=1.54060

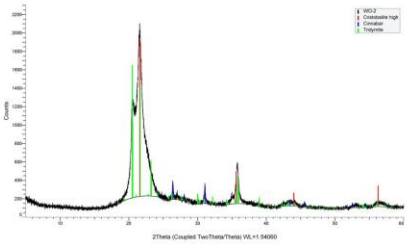
WO-2
Crednbaite high
Cinnabar
Trdymite
Counts
2Theta (Coupled TwoTheta/Theta) WL=1.54060

Appendix III: X-ray diffraction user manual

XRD USER MANUAL NOTES

A Guide to Using and Operating the Bruker D2 Phaser

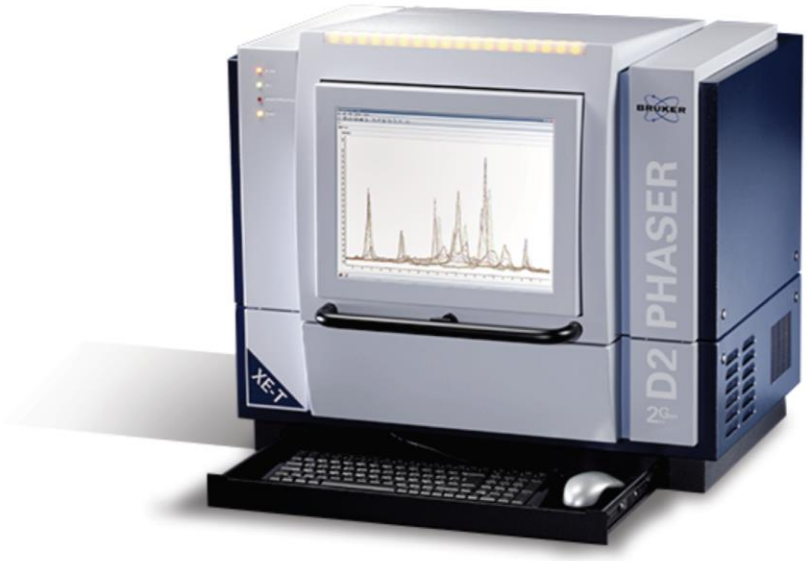

Table of Content (Page # and Contents)

University of Texas at El Paso
Department of Earth, Environmental, and Resource Science
David Muller

PART 1: Sample preparation

Remember: a) sample must be very well ground and homogenized
b) don't use acetone to clean these acrylic sample holders. Use ethanol.
c) training videos are available in "D2 Sample preparation" folder in USB thumb drive

Frontload or top-loading powder holder

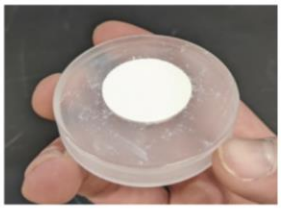

1. Make a little mound by filling the sample holder from the top
2. Use a glass slide to level off the sample and sweep the excess powder off, while turning the sample holder, to get a nice, smooth flat surface.
3. The goal is to get a top surface of the sample that is flush with the top surface of the sample holder. If the sample is too high, all the peaks will be shifted to a higher 2Θ angle ("*high to the right, low to the left*")

Back-loading powder holder (packed from behind so that there is less particle orientation in the top surface)

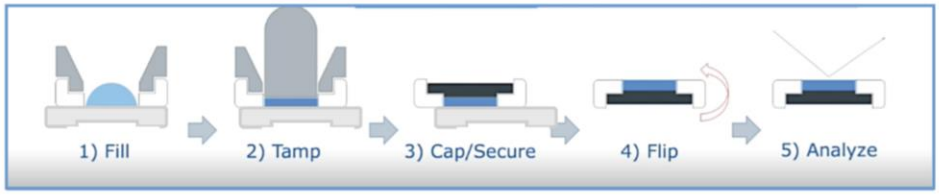

1. Use, e.g., the backside of a frontload holder to hold sample in place as it is filled from behind. Place the funnel in the back of the back-loading holder. Add sample powder through the funnel to make a little mound.
2. Very lightly*, press down on the sample mound using the tamp (*you don't want to force the material to orient itself). Carefully lift the tamp. Hold the bottom two pieces together and take the funnel off.
3. Cap and secure the sample by placing and pressing down on the black plastic backing (with teeth up).
4. Flip over and carefully remove the frontload holder backing.

Clay sample holder

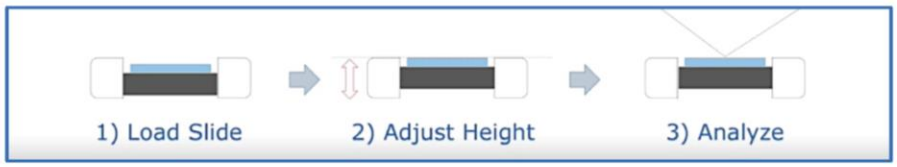

Deposit sample suspension onto glass slide and allow to dry.

1. Load slide with sample into the holder
2. Use one of the back-loading holders to adjust height. Sample should be level with top surface (remember, "*high to the right, low to the left*").

PART 2: Turning on D2 PHASER and Loading Samples

Power on and Login

- Turn key and flip power switch in back of instrument*

*Photo of key and switch, both "On" position

- Machine should boot up and turn on in 1-3 minutes
- Locate keyboard and mouse stored in tray (bottom front, a light tap will open tray)
- Login to 'USER' using password "password" (no caps or spaces)

Open and Load Sample

- TO OPEN: (1) place hand on black handle and gently pull the t-shape knob located directly below screen
- (2) machine door will lift itself up to full open position
- Pull black knob on metal lever downwards to lower the circular loading stage (3 and 4)
- Place prepped sample puck on loading stage and move metal lever back up so loading stage is in up position (5, 6, 7)
- Gently use both hands on black handle to lower door to closed position (8)
- A click will be heard when closed properly

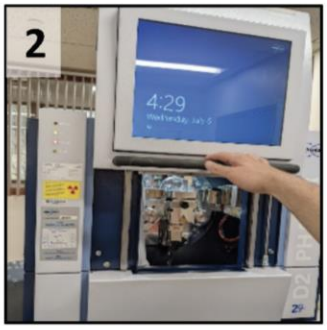

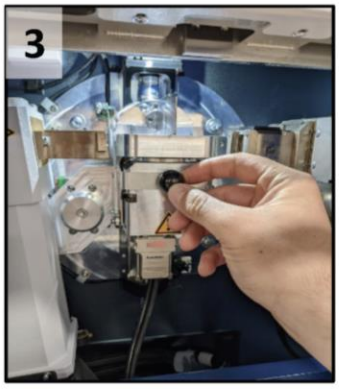

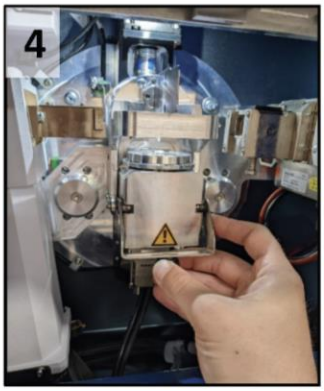

PART 3: Performing scans and using DIFFRAC.SUITE

- click on DIFFRAC.SUITE icon (see picture)
- "please login" pop up: just click "ok" you can leave password blank
- window will open up as shown below "DIFFRAC.COMMANDER"

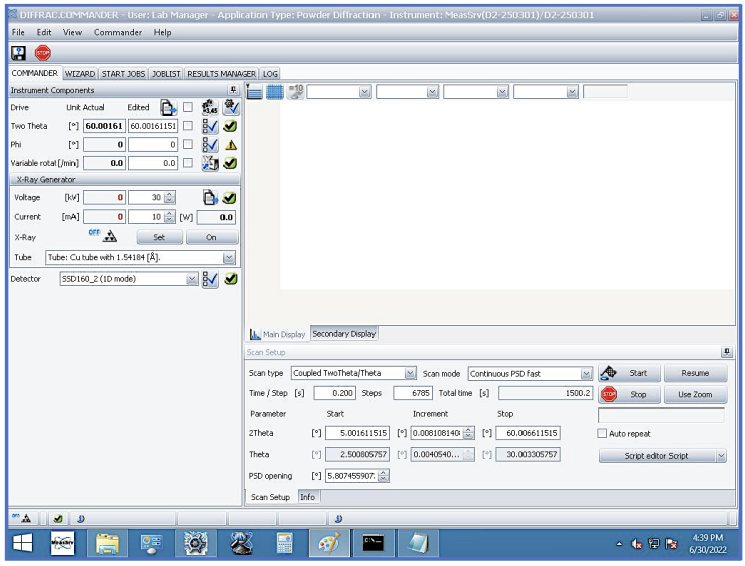

- (See next page for notes on scan adjustments)
- Run the scan by pressing "Start" (button with little checkered flag)
- Lights will turn on top of machine and next to "ready" "On" and "Busy"
- Scan will take place, after requisite time press "Stop" and "Off" next to "X-Ray" in left center of panel
- This will unlock the door and allow one to open the machine and remove the sample
- Go to "File" then "Save result" save to proper folder (and remember when you saved the file; e.g., inside a user folder in Desktop → Data)
- It will save as a ".brml" file, which is what is used to open the file in the DIFFRAC.EVA suite

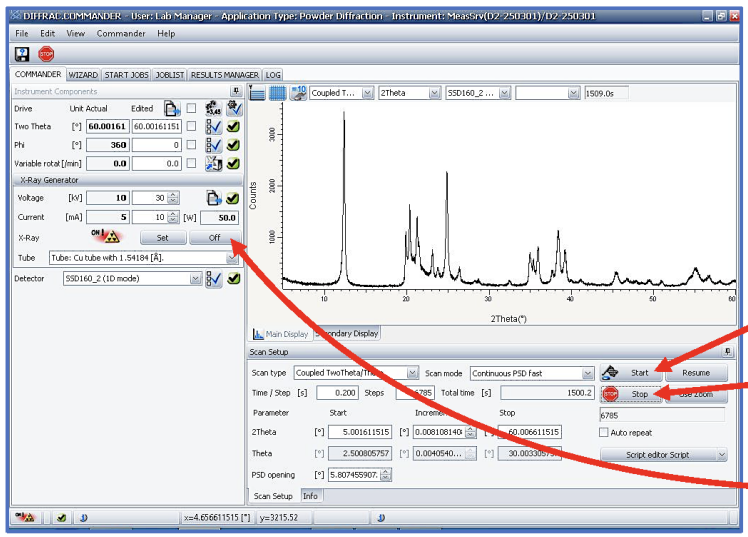

PART 3 Cont.: Notes on Scan Adjustments

Leave default settings and observe the options in the bottom right panel, total time in seconds is generally an indicator of how detailed the scan should be, most of my scans are about 5-50 minutes (300-3,000 seconds); more than that is most likely overkill and less than that might produce a very noisy image.

The only settings we are concerned with adjusting are:

- "Time / Step" (larger step will increase total time, and increase counts, more detail)
- "Start (2theta)" can adjust the display to start at a later 2theta
- "Increment", also called step size, smaller increment size will also increase total time. Note that total time and steps count will adjust automatically

Recommendation: I use the numbers shown in screenshots for most scans

- Time/step [s]: 0.02 to 0.5
- 2theta [°]: 5 to 60
- Increment [°]: 0.05 to 0.005

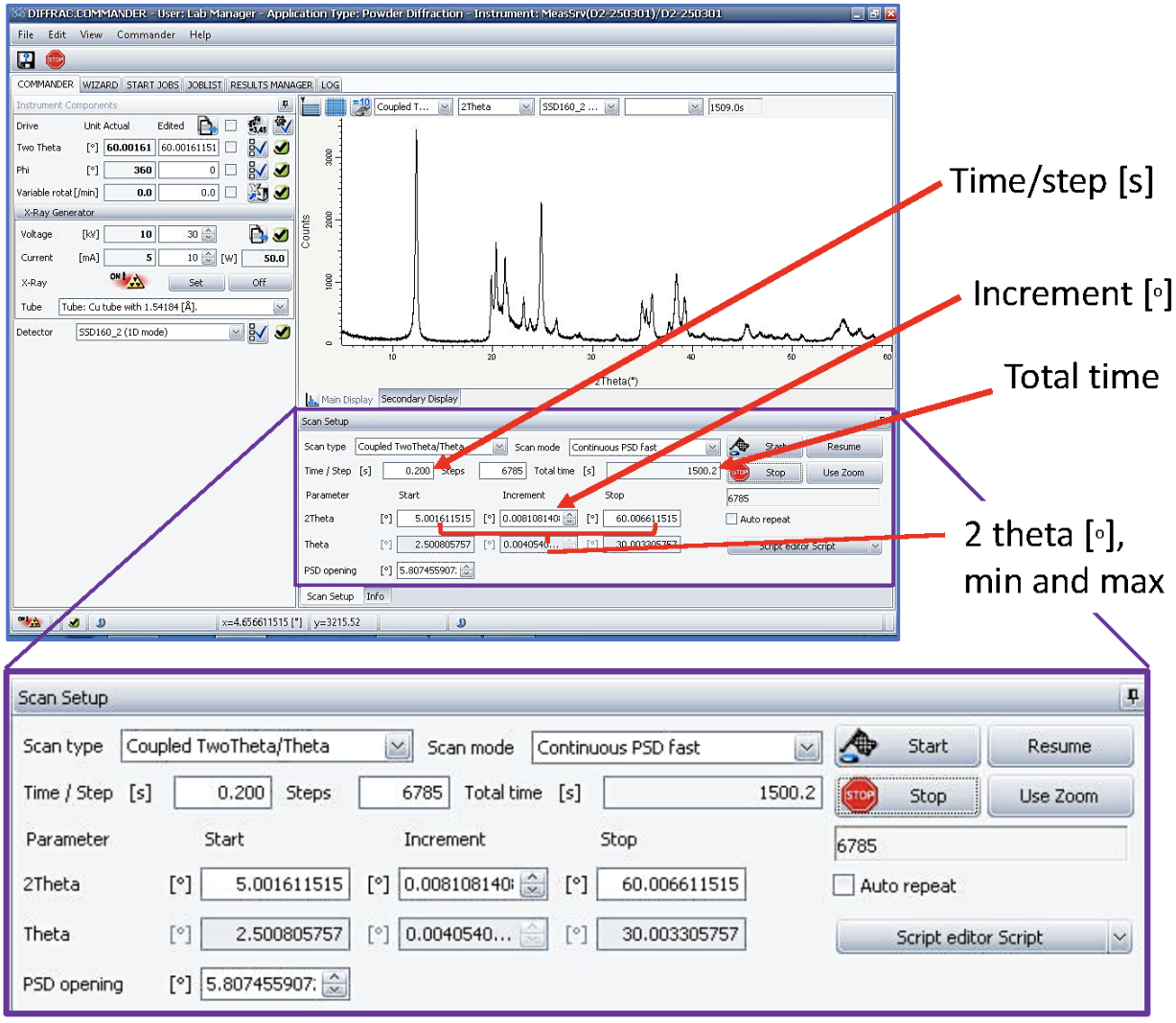

PART 4: Analysis with DIFFRAC.EVA

Step 1: Open suite with this icon. The following screen will appear:

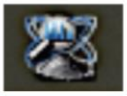

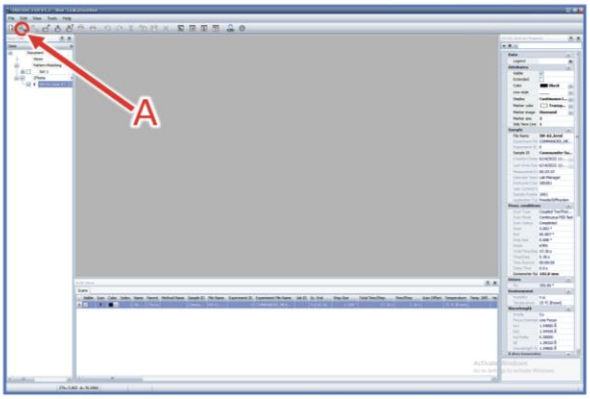

Step 2: Open .brml file you want to analyze with the button indicated on the above image (A)

Step 3: You will now see the peak displayed; your screen may look different depending on toolbar configuration. **Right click** on the file name in the data tree (B).

In the drop-down menu, click "**Tool**" (another drop down menu will appear) then click "**Search/Match (scan)**". The search match window will appear (below).

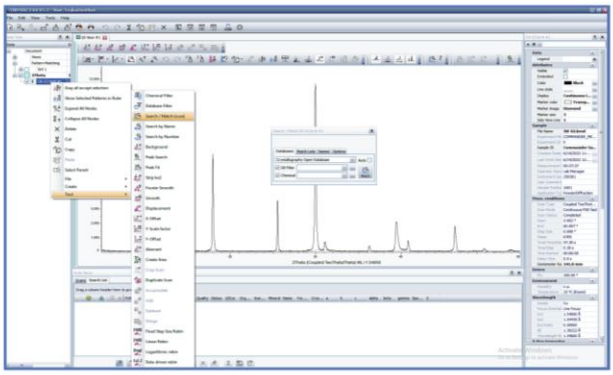

Step 4: In the Search/Match window, select Crystallography Open Database (COD; if not already selected), then change the DB Filter to "COD (Mineral related)", which should be the only option in the drop-down. When the window looks like the one pictured below, you can click the match button (C).

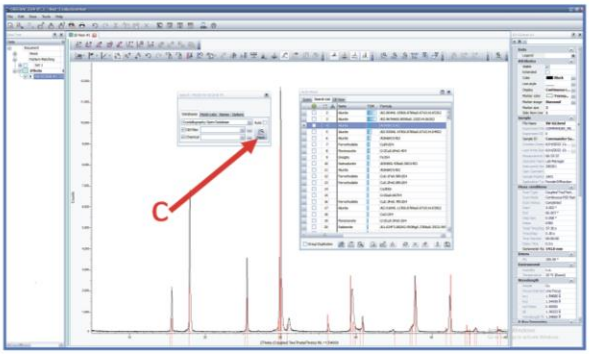

Step 5: The match function will bring up the "autoviews" window which will show possible matches from the database. Click on some of these matches and you will see the red sticks appear beneath your peaks, if you feel you see a good match and the mineral makes sense (a good match is not necessarily a true match if the mineral is nonsensical), then check the box and the mineral will be added to a legend on the side (see below).

Be sure to add a sample name to the legend at location (D), press enter to apply legend name, this sample was "IW-02"

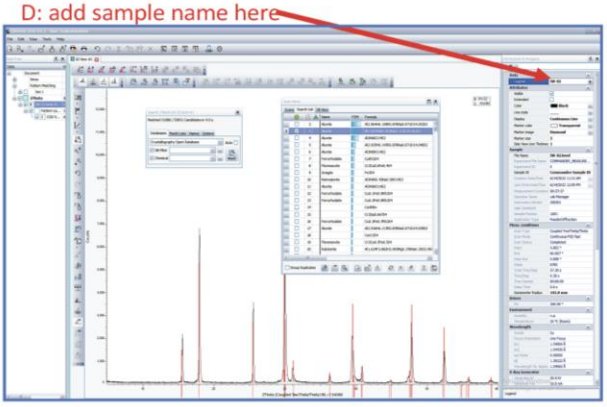

PART 4 Continued: Analysis with DIFFRAC.EVA

Step 1: The example on the previous page contained a relatively pure sample (alunite); this page will show a more complicated peak set that requires multiple mineral matches to match all of the peaks. Pictured below is sample IW-08, as one can see, the first scan only shows kaolinite and there are more peaks that need a match.

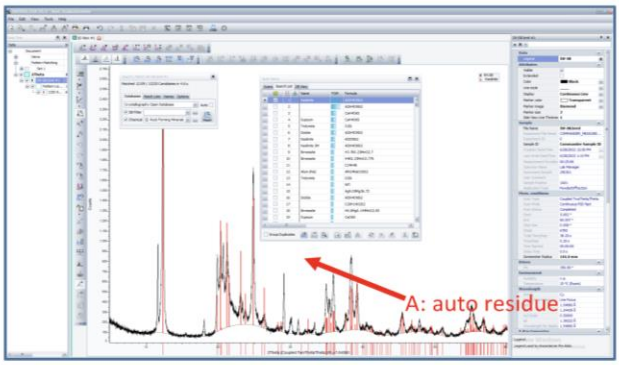

Step 2: Click on the auto residue button (A), this will cancel out the peaks that are already matched so one can autoscan again and the program will ignore the peaks that are highlighted in red. One can now click the scan button again. This time Gypsum comes up at the first match.

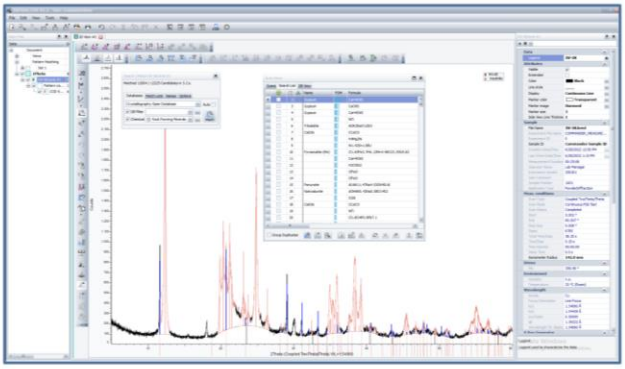

Step 3: Another auto residue and scan yields strange results in this case. The options shown below are strange minerals that are probably not present, now one can resort to manual matching.

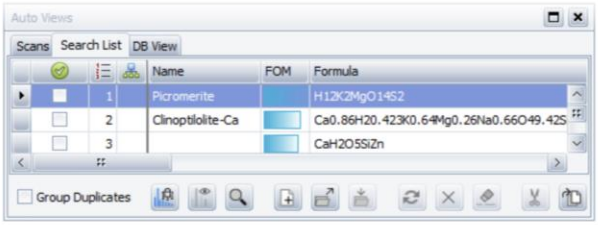

Step 4: Now one can go to the "Names" tab under the "Search/Match" window to manually search for minerals by name. Here I suspect alunite may be present because there is a peak at 17° 2theta.

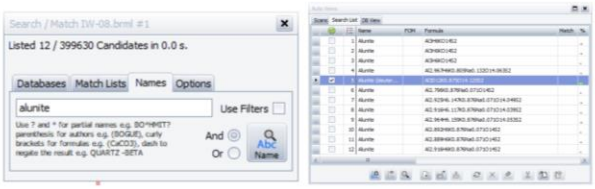

- Many options will come up for the mineral, it may not be the first, sort through the top options with the arrow keys to find the best match. In this case it was the 5th option (above)

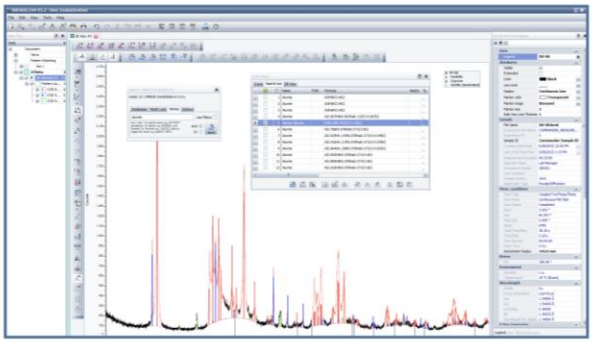

Another way to manually search is to go to "options" (B) in the "Search/Match" window and check "Match on subrange" (C). Then highlight the peak that you want to search by **click and drag** then click the **View** (D) button (the from/to will change to the highlighted view). Go back to the databases tab (E) and click "scan" button, and the scan will be restricted to the selected subrange

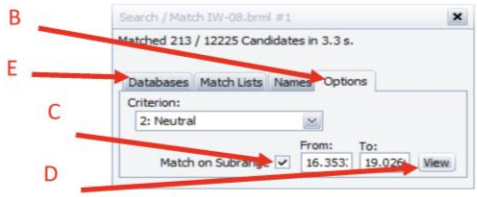

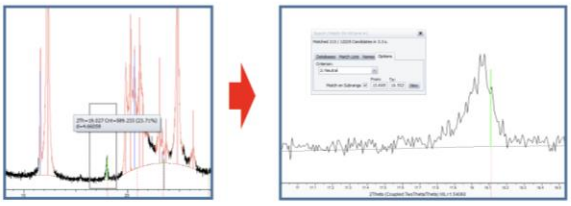

PART 4 Continued: DIFFRAC.EVA Export png/jpeg

- Before exporting to png/jpg be sure to restore all residue peaks with this button (A)

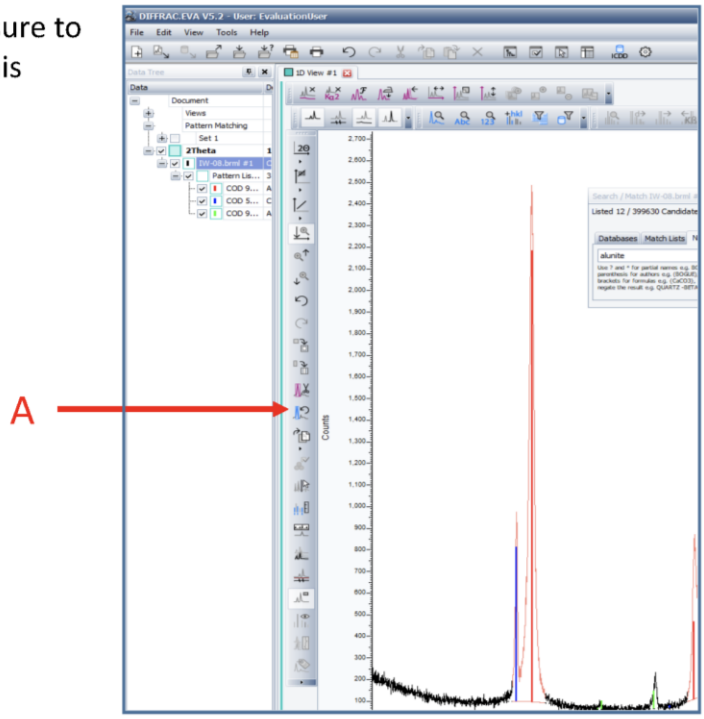

- Save the .eva file with file then save (B)
- Click the “Export image” button here (C)

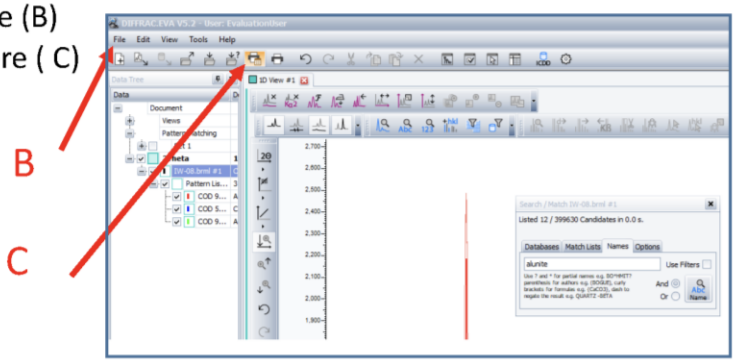

- When print preview window comes up, save as a png/jpg with this button (D)

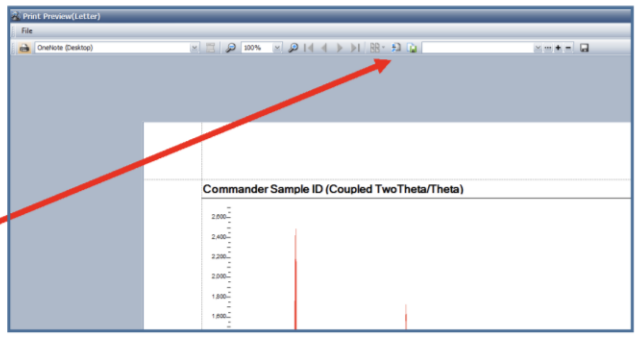

PART 5: Using remote desktop for alternative monitor

Using the additional monitor allows one to have a much better viewing screen.

- First log in to the XRD computer
- Once logged in, go to Applications and open up Command Prompt
- In Command Prompt type the following command ipconfig/all
- Press Enter
- This will bring up IP addresses for the computer, this changes daily. Find the “IPv4 address” which should be a 10-digit code punctuated by periods
- Use this code on the alternate monitor share screen remote access application
- On the alternate monitor open up “Remote Desktop” icon and type in the ip address described in the previous step
- Press ”Connect"
- You will have to go to "More choices" then ”Use a different account"
- Type the user code for the XRD computer:
  user: user
  password: password
- Click Connect, this should disable the XRD computer and allow remote screen sharing
- One should be able to seamlessly switch between computers on this monitor by using the minimize button at the top of the screen

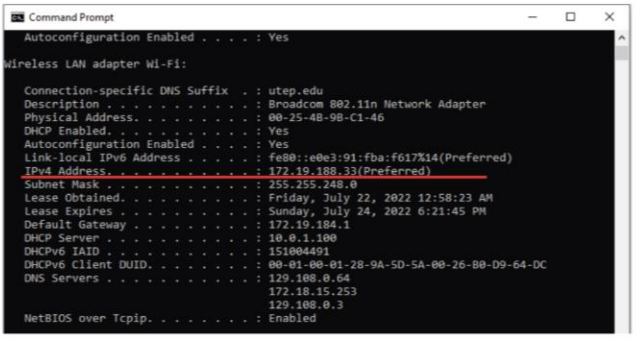

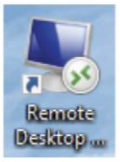

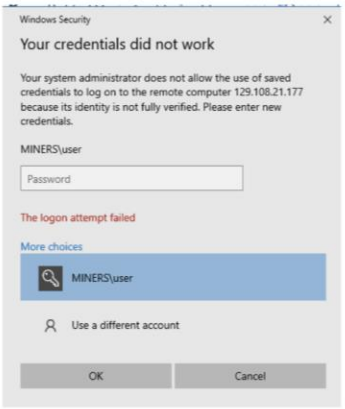

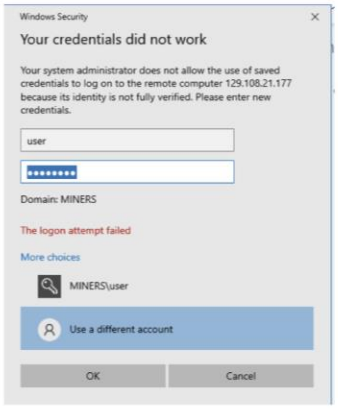

Vita

David E Muller was born in Doylestown Pennsylvania in December, 1995. After completing high school he completed a Bachelor of Science in Geology from Kutztown University of Pennsylvania graduating summa cum laude in May of 2020. He completed an exploration geology internship at the Doe Run Mining Company in Southeastern Missouri before enrolling in the graduate school at the University of Texas at El Paso (UTEP) working on a M. S in Geological Sciences working under Dr. Antonio Arribas. During his studies we worked as both a research assistant and teaching assistant as well as completing an internship as a student contractor working for the United States Geological Survey.

His research focused on economic geology focusing on the study of ore deposits and utilizing advanced technologies such as the Scanning Electron Microscope and X-ray Diffractometer to analyze and identify minerals for stable isotope analysis and better understand ore deposits.

David served as an officer in the Society of Economic Geologists UTEP student chapter and attended multiple short courses with the organization to Chile, Sweden, and Mexico. He graduated summa cum laude from UTEP in May 2022.

Email: dmuller1995@gmail.com